DISSERTATION

submitted to the

Combined Faculties of the Natural Sciences and for Mathematics

of the Ruperto-Carola University of Heidelberg

for the degree of

Doctor of Natural Sciences

presented by

Antonio Sorrentino, M.Sc.

born in Naples, Italy

Oral-examination:

……

A screening for novel immune modulators identifies SIK3 kinase as a regulator of tumor resistance to T cell attack

Referees: **Prof. Dr. Philipp Beckhove**

Prof. Dr. Viktor Umansky

The work described in this thesis was performed from 2013 to 2015 in the Department of Translational Immunology at the National Center for Tumour Diseases – NCT of the German Cancer Research Center - DKFZ in Heidelberg, Germany and from 2016 to 2017 in the department of Interventional Immunology at the Regensburg Center for Interventional Immunology – RCI in Regensburg under the supervision of Prof. Dr. Philipp Beckhove.

Declaration

I herewith declare that I have completed this thesis single-handedly without any unauthorized help of a second party. Any help that I have received in my research work or in the preparation of this thesis has been duly acknowledged.

Heidelberg, 15.05.2017

_____

Antonio Sorrentino

Parts of this thesis have been published in:

Sorrentino A, Menevse AN, Michels T, Khandelwal N, Breinig M, Poschke I, Werner-Klein M, Volpin V, Jeltsch K, Mikietyn D, Wagner S, Offringa R, Gebhard C, Rehli M, Boutros M, Beckhove P. A screening for next-generation immune checkpoints identifies AS1 as novel regulator of tumor resistance to T cell attack. *Cancer Immunotherapy and Immunomonitoring meeting - CITIM* 04/2017.

Sorrentino A, Menevse A, Michels T, Khandelwal N, Breinig M, Poschke I, Volpin V, Wagner S, Offringa R, Boutros M, Beckhove P. Discovering novel targets in a high-throughput fashion: RNAi screen for pancreatic ductal adenocarcinoma (PDAC) associated immune modulators. *Cancer Immunotherapy Meeting – CIMT* 05/2016. Poster Award.

Sorrentino A, Menevse A, Michels T, Khandelwal N, Breinig M, Poschke I, Volpin V, Wagner S, Offringa R, Boutros M, Beckhove P. RNAi discovery platform to identify novel genes that prevent immune surveillance in pancreatic ductal adenocarcinoma (PDAC). *American Association of Cancer Research annual meeting – AACR 04/2016*. Cancer Research 76 (14 Supplement): 2339-2339.

Sorrentino A, Menevse AN, Michels T, Khandelwal N, Breinig M, Poschke I, Offringa R, Boutros M, Beckhove P. Unraveling the “immune-modulatome” of pancreatic adenocarcinoma (PDAC): a RNAi screening with patient-derived tumor infiltrating lymphocytes (TILs). *Cancer Immunotherapy Meeting – CIMT 05/2015*. Oral Presentation.

Sorrentino A, Michels T, Menevse AN, Khandelwal N, Breinig M, Poschke I, Offringa R, Boutros M, Beckhove P. Identification of novel immune checkpoints as potential therapeutic targets in pancreatic ductal adenocarcinoma (PDAC) using RNAi screening. *American Association of Cancer Research annual meeting – AACR 04/2015.* Cancer Research 08/2015; 75 (15 Supplement): 245-245.

Khandelwal N, Breinig M, Speck T, Michels T, Kreutzer C,·**Sorrentino A**, Sharma AK, Umansky L, Conrad H, Poschke I, Offringa R,König R, Bernhard H, Machlenkin A, Boutros M, Beckhove P. A high-throughput RNAi screen for detection of immune-checkpoint molecules that mediate tumor resistance to cytotoxic T lymphocytes. *EMBO Molecular Medicine*. 02/2015. DOI:10.15252/emmm.201404414

Acknowledgments

When I first arrived in Germany more than four years ago, I could not imagine that I would have lived such a wonderful experience, and I would like to thank all the people who made this journey authentic.

First of all, I would like to thank Prof. Philipp Beckhove for his supervision. I am very glad to have conducted my PhD in his laboratory, as he gave me the opportunity to maximize my scientific development by giving me the independence to formulate novel hypothesis and the chance to make mistakes, which is the most effective learning method. A special thanks goes to my TAC members Prof. Adelheid Cerwenka and Prof. Karsten Mahnke for their constructive comments.

This experience would not have been the same without my wonderful colleagues. I would like to express my gratitude to Till for his constant help over these years, especially in getting familiar with the project and with my beloved bioinformatics. Thanks to Slava for always being there for any kind of problem, ranging from scientific issues to bike repair, and for having prevented me from starving during long working days. This thesis would not have been possible without the help of Ayse, an exemplary student, who often encouraged me during dark moments. A special thanks goes to Damian for his strong motivation and for his commitment in the project. I would like to express my gratitude to Vale for her constant help with experiments, for having reviewed my thesis and for her support with my complicated relationship with German bureaucracy. Thanks a lot to Kathy for having taken over some tricky parts of the project and for her constructive comments during the writing of this thesis. Thanks a lot to Chih-Yeh especially for being by my side during long FACS experiments. I would like to thank Heiko for his help in the lab and for being the best IT guy ever. Thanks a lot to Anchana for her constant moral support and for her precious advices. I would like to thank Maria and Noemi for their key suggestions during the thesis writing and submission process. My gratitude goes also to Mattea and Sabine for their efficient and professional administrative help at RCI. Thanks to Karin for always having helped me to find solutions using her vast net of contacts and to Birgitta for helping with the western blots.

This project would have been incomplete without the contibution of Dr. Marco Breinig who helped with the RNAi screening and Dr. Isabel Poschke who provided with the TILs. I would like to thank Prof. Michael Rehli and Dr. Claudia Gebhard for the essential help with the RNA sequencing. Thanks also to Nisit for having prepared the soil for this project by setting up this new method.

My settlement in Regensburg would not have been that pleasant without the support of the Immunology department. A special thanks goes to Doro for her essential support in the new lab and to Melanie for her help with in vivo experiments.

I would like to thank all my former colleagues in Heidelberg: Mudita, Jasmin, Anna Lena, Hans-Henning, Diane and Lora for their collaborative spirit and for the nice moments outside the lab, Ludmila, Simone, Sabrina and Mariana for their technical support and Miriam and Irmi for their administrative support.

I cannot imagine to have handled all the stress and the difficult moments without you, Chiara. You have always been by my side, giving me the strength to overcome the hard moments by always making me believe in myself.

A special thanks goes to my friends in Napoli on whom I can always rely on: Massimo, Claudio, Luciana, Veronica, Adelaide, Claudia, Paola and Roberta.

Last but not least, I would like to express my gratitude to my family for their support and their unconditional love.

“The only true wisdom is in knowing you know nothing”

Socrates

Dedicated to Lorenzo

Summary

Cancer is one of the leading causes of mortality worldwide. An important hallmark of cancer is its ability to escape immune surveillance by developing several immunological obstacles. These include a plethora of mechanisms that either dampen immune cell functionality, or foster tumor cell resistance towards immune attack. Immunotherapeutic strategies, such as immune checkpoint blockade, have emerged as promising therapeutic approaches for cancer treatment. However the majority of tumor patients are refractory to current immune therapeutic tools, emphasizing the need to identify more key players that could radically improve immunotherapy.

This study aimed to systematically identify novel tumor-associated immune modulators by performing a high-throughput RNAi screen and subsequently validate novel candidate genes whose blockade could potentially enhance anti-tumor immune response in tumor patients. Starting from a pancreatic ductal adenocarcinoma (PDAC) co-culture model, 2514 genes were knocked down in a luciferase-expressing tumor cell line using a siRNA library. Subsequently, the transfected tumor cells were co-cultured with HLA-A2.1^{+}- matched tumor infiltrating lymphocytes (TILs). TIL-mediated cytotoxicity was then assessed by measuring the remaining luciferase intensity of transfected tumor cells. In order to exclude genes whose knock-down affected cell viability per se, we cultivated tumor cells with the siRNA library in the absence of TILs.

The primary screening revealed 155 potential candidate genes (hits) whose downregulation increased T cell-mediated tumor lysis more efficiently than PD-L1 knockdown. The hit-list generated in the primary screen was narrowed down to 108 hits after performing a secondary screen. Among these candidate genes, salt-inducible kinase 3 (SIK3) was selected for extensive validation analysis, as this protein kinase is overexpressed in tumor biopsies and its role in immune escape mechanisms has not been reported so far. SIK3 impairment in tumor cells enhanced T cell mediated killing in several co-culture models derived from different cancer entities. We showed that SIK3 sustained intrinsic tumor resistance to immune cell attack, rather than modulating T cell functionality. We observed that T cells expressed TNF-α upon co-culture with tumor cells, and that this cytokine elicited tumor cell growth in SIK3-proficinent cells. On the contrary, SIK3 depletion sensitized tumor cells towards TNF-

α-induced apoptosis by regulating NF-κB activation via HDAC4. To prove the translational relevance of SIK3 blockade for cancer immunotherapy, we used a small molecule compound which recapitulated the effect of SIK3 genetic depletion. Additionally, stable knockdown of SIK3 in tumor cells resulted in retardation of tumor growth after adoptive cell transfer of TILs in a xenograft mouse model.

This study describes a robust method for a comprehensive identification of novel immune modulators in solid tumors. Furthermore, this work provides the rationale of SIK3 inhibition as a novel therapeutic strategy for cancer treatment.

Zusammenfassung

Krebs ist eine der Hauptursachen für die krankheitsbedingte Sterblichkeit weltweit. Ein wichtiges Merkmal von Krebs ist die Fähigkeit, der Immunüberwachung durch die Entwicklung mehrerer immunologischer „Hindernisse“ zu entkommen. Dazu gehören eine Vielzahl von Mechanismen, die entweder die Immunzellenfunktionalität abschwächen oder die Tumorzellresistenz gegen den Immunangriff erhöhen. Immuntherapeutische Strategien, wie die Immun-Checkpoint-Blockade, sind als vielversprechende therapeutische Ansätze für die Krebsbehandlung bekannt. Jedoch, profitiert die Mehrheit der Tumorpatienten nicht von den aktuellen immuntherapeutischen Ansätzen, was die Notwendigkeit neue wichtige immunologische „Key player“ zu identifizieren hervorbringt.

Diese Studie zielte darauf ab, neuartige Tumor-assoziierte Immunmodulatoren deren Blockade die Antitumor-Immunantwort bei Tumorpatienten verstärken könnten, systematisch zu identifizieren. Hierzu wurden Kandidaten mittels eines RNAi Hochdurchsatz-Screenings ermittelt und anschließend validiert. Ausgehend von einem Adenokarzinoms des Pankreas (Bauchspeicheldrüsenkrebs) Modell wurden 2514 Gene in einer Luziferase exprimierenden Tumorzelllinie unter Verwendung einer siRNA-Bibliothek supprimiert. Anschließend wurden die transfizierten Tumorzellen mit passenden HLA-A2.1^{+} Tumor infiltrierenden Lymphozyten (TILs) co-kultiviert. Die TIL-vermittelte Zytotoxizität wurde anhand der Messung der verbleibenden Luciferase-Intensität der überlebenden Tumorzellen bewertet. Um Gene auszuschließen, deren Supprimierung die Zelllebensfähigkeit beeinflussen, wurden siRNA-transfizierte Tumorzellen in Abwesenheit von TILs kultiviert.

Das primäre Screening zeigte 155 potentielle Genkandidaten (Hits), deren Knockdown die T-Zell-vermittelte Tumor-Lyse effizienter erhöhte als PD-L1. Die hieraus erzeugte Hit-Liste wurde nach einem zweiten Screening auf 108 Kandidaten eingegrenzt. Unter diesen Genkandidaten wurde „salt-inducible kinase 3“ (SIK3) für eine umfangreiche Validierungsanalyse ausgewählt, Diese Proteinkinase wird in Tumorbiopsien überexprimiert und ihre Rolle in der Abwehr einer TIL-vermittelnden Zerstörung des Tumors ist unbekannt. Eine Beeinträchtigung der SIK3 Funktionalität in Tumorzellen verstärkte die T-Zell-vermittelte Zerstörung in mehreren Co-Kulturmodellen

verschiedener Krebsentitäten. Wir konnten zeigen, dass SIK3 eine intrinsische Tumorresistenz gegen Immunzellenangriffe induziert, anstatt die T-Zell-Funktionalität direkt zu modulieren. Wir beobachteten, dass T-Zellen in einer Co-Kultur mit Tumorzellen TNF-α sekretieren und dass dieses Zytokin Tumorzellwachstum in SIK3-positiven Zellen hervorrufen kann. SIK3 Knockdown sensibilisierte die Tumorzellen gegenüber TNF-α induzierter Apoptose durch eine HDAC4-vermittelte NF-κB-Aktivierung. Um die translationale Relevanz einer SIK3-Blockade für die Krebs-Immuntherapie zu testen, inhibierten wir SIK3 mit einem niedermolekularen Inhibitor, dessen Wirkung die Ergebnisse der genetischen Assays bestätigte. Darüber hinaus führte ein stabiler Knockdown von SIK3 zu einer Verzögerung des Tumorwachstums nach adoptivem Zelltransfer von TILs in einem Xenograft-Mausmodell.

Diese Studie beschreibt eine robuste Methode für eine umfassende Identifizierung von neuartigen Immunmodulatoren in soliden Tumoren. Darüber hinaus bietet diese Arbeit eine experimentelle Grundlage zur Verwendung von SIK3 Inhibierung als ein neuartiger therapeutischer Ansatz für die Krebsbehandlung.

Table of Contents

1. Introduction

1.1 Hallmarks of cancer

Cancer is one of the leading causes of mortality worldwide, with approximately 14 million new cases and 8 million cancer-related deaths yearly [1]. Our perception of cancer biology has dramatically changed over the last two decades. For many years, tumors were considered as mere masses of aberrant cells [2]. Conversely, it is now believed that cancer is a multifactorial disease in which malignant cells form heterotypic interactions with benign stromal cells of the tumor microenvironment (TME) [3]. The essential elements in the stroma of a typical TME include fibroblasts, myofibroblasts, neuroendocrine cells, adipose cells, immune and inflammatory cells, the blood and lymphatic vascular networks, and the extracellular matrix (ECM) [3]. These cells orchestrate a series of processes that culminate in cancer progression and metastasis [4-6]. In the year 2011, Hanahan D. and Weinberg R.A. systematically schematized the major characteristics endowed both by tumor cells and the TME in the review: “Hallmarks of Cancer: The Next Generation” [7]. The hallmarks of cancer consist of 8 biological capabilities acquired during tumor formation, namely:

- *Sustaining proliferative signaling:* tumors can either intrinsically sustain their proliferation by activating molecular regulators of the cell cycle or extrinsically promote cell growth by paracrine secretion of growth factors [8, 9].
- *Evading growth suppressors:* impairment of mechanisms that serve to constrain inappropriate replication of cells, such as dysregulation of the tumor suppressors p53 and retinoblastoma-associated proteins (Rb) [10, 11]. Alternatively, cancer cells can become insensitive to mechanisms of cell contact inhibition and therefore grow uncontrolled [12].
- *Resisting cell death:* aberrant neoplastic cells often show upregulation of anti-apoptotic genes and down-regulation of pro-apoptotic factors [13]. Furthermore, necrosis, which spontaneously occurs in tumors, exacerbates inflammation and results in tumor proliferation [14].

- *Enabling replicative immortality:* ectopic expression of telomerase is found in many types of cancer.This RNA-dependent polymerase sustains telomeres elongation thus preventing cell senescence and promoting cell immortalization [15].
- *Inducing Angiogenesis:* during tumor progression an angiogenic switch is frequently activated, causing sprouting of new vessels that provide neoplastic cells with nutrients for their growth [16].
- *Reprogramming energy metabolism:* even in the presence of oxygen, cancer cells utilize glycolysis as main source of energy production. Although less efficient in producing ATP molecules compared to the oxidative phosphorylation, glycolysis allows the diversion of its intermediate metabolites into different pathways which are involved in the biosynthesis of new organelles for proliferating cells [17].
- *Evading immune destruction:* an emerging hallmark is the ability of tumors to evade the immune system [7]. Aberrant cells are constantly recognized and eliminated by immune cells. Nevertheless, malignant cells can use several mechanism to evade immune cell recognition.

The interplay between tumor and immune cells will be described in more details in the next paragraph.

1.2 Cancer immunoediting

The first evidence that the immune system plays a role in tumor progression appeared in the 1890s when Dr. William Coley observed tumor regression in patients whose immune system was activated after bacterial infection [18]. During the 20th century, these observations were partially neglected due to the dogma that cancer cells are presenting self-antigens and therefore the immune system is incapable of recognizing them as aberrant cells [19]. However, new discoveries from the last two decades shed new light on cancer immunology. The current theory is referred to as cancer immunoediting and is based on a multitude of studies on genetically modified mouse models with altered immune system [20]. Additionally, there are several proofs that cancer immunoediting occurs in humans as well. The most convincing evidence is the

correlation among the quantity, the quality and the spatial distribution of tumor-infiltrating lymphocytes (TILs) and patient survival [21]. Galon et al., showed that high infiltration of T cells, especially with memory and effector phenotype, correlates with improved overall survival in colorectal cancer patients [22]. Furthermore, other groups demonstrated that the ratio and the distribution patterns of $CD8^+$ T cells and regulatory T cells (T_{reg}), predict patient prognosis in several tumor entities [18, 23-25]. Another evidence hinting to the occurrence of cancer immunoediting in humans, is the observation that immunodeficiency is associated with a higher risk of cancer [26]. As an example, patients with acquired immunodeficiency syndrome (AIDS) or individuals under chronic immunosuppressive therapy, develop tumors with higher frequency compared to healthy individuals [20]. The complex interplay between aberrant cells and immune cells can be schematized into three main phases: elimination, equilibrium, and escape [26].

1.2.1 Elimination

The immune system can prevent tumor formation and progression using at least three different mechanisms. First, immune cells are able to clear viral infections, thus protecting the host from virus-associated tumors. Second, elimination of pathogens by the immune system prevents the establishment of a pro-inflammatory milieu, which promotes tumorigenesis. Finally, immune cells are able to directly build up an efficient response against tumor cells [20]. The latter mechanism is also referred to as immune surveillance, and is mainly mediated by two cell subsets: natural killer (NK) cells and $CD8^+$ T cells, also called cytotoxic T lymphocytes (CTLs). NK cells are able to kill tumor cells either via exocytosis of cytotoxic granules containing perforin and granzymes or alternatively via the engagement of tumor necrosis factor (TNF) receptor superfamily (TNFRSF) members, such as TNFR-I, FAS and TRAIL receptors on tumor cells [27, 28]. NK cells can recognize altered patterns on tumor cells such as the lack of MHC-I molecules on the surface of aberrant cells [29]. However, this cell subset lacks the capability to build up an adaptive immune response against cancer. On the contrary, $CD8^+$ T cells, although sharing common effector mechanisms with NK cells, are able to elicit a tumor-specific immune response. CTLs can recognize a plethora of tumor antigens which are presented on MHC-I molecules of cancer cells. These antigens derive either from oncofetal, oncoviral or tissue-restricted proteins, which are

ectopically expressed by tumor cells, or from proteins that are mutated or post-translationally altered (e.g. glycosylated or phosphorylated) in tumors [30].

An optimal anti-cancer immune response is a complex and iterative process which is also referred to as “Cancer-Immunity Cycle” [31]. In order to obtain an effective anti-cancer response, a series of stepwise events must be initiated. First, tumor associated antigens must be released by tumor cells. This process occurs upon cancer cell death [32, 33]. Hence, APCs capture tumor-derived neo-antigens and present them on class I and class II MHC molecules. In this step, several stimuli from the tumor microenvironment are required to switch from a tolerogenic to an immunogenic environment. Such stimuli include factors released by necrotic cells or the gut microbiota as well as pro-inflammatory cytokines [34, 35]. Next, APCs migrate to the lymph node and prime naïve T cells whose T cell receptor (TCR) is specific for the presented antigens [36]. After their activation, effector T cells enter blood vessel and infiltrate into tumors. There, $CD8^+$ T cells recognize tumor cells via TCR-MHC-I interaction and release cytotoxic granules and cytokines that induce tumor cell death. Killing of cancer cells results in additional release of tumor antigens, which in turn sustains the cancer-immunity cycle [31].

In most cancer patients, anti-tumor immunity is imbalanced and immune cells are incapable of complete tumor eradication. The processes and mechanisms leading to this phenomenon will be clarified in the next two subsections.

1.2.2 Equilibrium

Cancer immune equilibrium is conceived as a period during which tumor cells and immune cells reach a steady state [26]. In this phase, immune cells arrest cancer progression without eliminating the tumor. The concept of immune equilibrium derives from the observation that tumors can reach a dormant stage in the body [37]. Cancer dormancy is a phase in tumor progression where cells undergo quiescence because of unfavorable conditions from the tumor microenvironment such as lack of appropriate growth factors [38, 39]. The phenomenon of tumor relapse, often observed in cancer patients, supports the theory that malignant cells are able to persist for decades in the body in a quiescent state, and eventually harbor tumors when tumor-suppressive

mechanisms are overtaken. The equilibrium phase involves the continuous elimination of tumor cells which is compensated by a moderate cell proliferation [40].

1.2.3 Escape

The persistency of the immune system, together with the genomic instability of cancer cells, ultimately results in the formation of resistant malignant cell variants. In the later stage of equilibrium, the accumulation of selected malignant clones with molecular abnormalities renders the tumor less immunogenic, thus preparing the soil for the tumor immune escape phase [41, 42]. Cancer immune escape is the ultimate phase of cancer immunoediting. This phase consists in the establishment of multiple resistance mechanisms, developed by the tumor and its microenvironment, to elude both the innate and the adaptive anti-tumor immune responses [43]. As a result, the tumor progresses uncontrolled, thus leading to a clinically apparent disease [44].

1.3 Immune escape mechanisms

Several studies have been conducted with the purpose of characterizing the mechanisms that interfere with the ability of the immune system to develop effective immunological responses against tumor cells. Tumor escape mechanisms have been classified in different ways, depending on the aspect that is taken into consideration (e.g. cellular versus molecular mechanisms) [45]. Despite canonical classifications, the ultimate causes that are responsible for tumor evasion, converge into two major groups: i) mechanisms that impair effector immune cell functionality, or ii) mechanisms that confer tumor cell resistance towards immune attack (Figure I). These mechanisms can be either direct or indirect and are mediated by the tumor itself and/or its microenvironment. However, this classification is just a simplification of the complex net of molecular and cellular events in the TME, and some factors can have a dual role in modulating immunity while contemporarily promoting tumor cell aggressiveness.

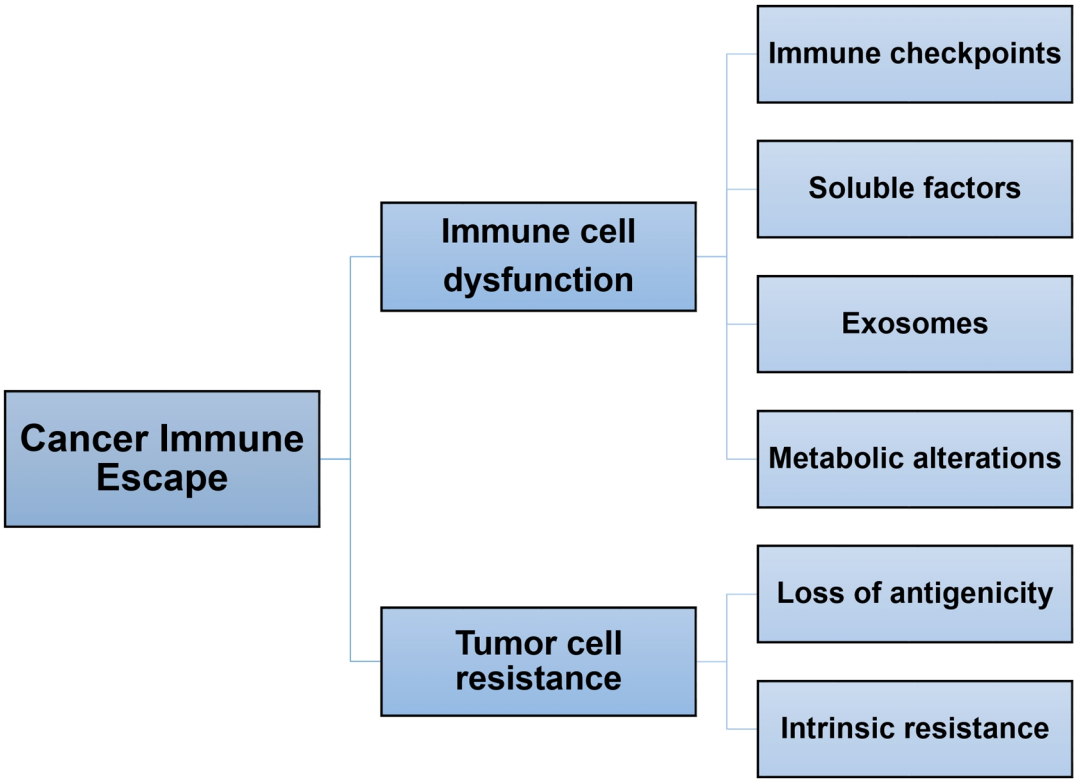

Figure I. Cancer immune escape mechanisms. Cancer immune escape mechanisms are divided into two major groups by virtue of their action either on immune cells or on tumor cells. Escape mechanism that modulate effector immune cell functionality include: immune checkpoint molecules, soluble factors (e.g. cytokines), exosomes and factors that induce metabolic dysfunction. Tumor cells can mediate immune resistance by either becoming invisible to immune cell attack (loss of antigenicity) or by altering molecular pathways that confer intrinsic resistance to immunity.

1.3.1 Impaired immune cell functionality

In ideal conditions, cancer immune eradication is mediated by specialized subsets of immune cells, such as NK cells and $CD8^+$ T cells, which are endowed with several cytotoxic mechanisms against cancer (section 1.2.1). During tumor immune evasion, different factors can act on effector immune cells, thus reducing their functionality and/or survival. As T cells are considered the epicenter of adaptive anti-tumor immunity [46], this section mainly focuses on the mechanisms that modulate this immune cell subtype.

1.3.1.1 Immune checkpoint molecules

Immune checkpoints are a plethora of receptors and ligands that are canonically expressed on the surface of T cells and APCs [47]. Immune checkpoint molecules are

classified as co-stimulatory or co-inhibitory, in virtue of their action on the TCR signaling [48]. In healthy tissues, inhibitory immune checkpoint signaling is essential to prevent autoimmunity and tissue damage, whereas stimulatory signaling is required for T cell activation and differentiation [48].

On a structural point of view, the majority of these molecules belongs to the immunoglobulin super family (IgSF) and the TNFRSF [48]. Within the IgSF, the most characterized members are included in the CD28 family, which mainly interact with the B7 family. Members of the IgSF comprise:.CD28, programmed death 1 (PD-1), programmed death ligand 1 (PD-L1), cytotoxic T lymphocyte antigen 4 (CTLA-4), lymphocyte activation gene 3 (LAG-3), T cell immunoglobulin mucin 3 (TIM-3), T cell immunoreceptor with Ig and ITIM domains (TIGIT), V-domain Ig suppressor of T cell activation (VISTA), carcinoembryonic antigen related cell adhesion molecule 6 (CEACAM6) [48]. Members of TNFRSF include several receptors that contain one or more extracellular cysteine-rich domains (CRDs), whereas their ligands contain a conserved extracellular TNF homology domain (THD). Members of this family include: TNFRSF9 (4-1BB), TNFRSF4 (OX40), and TNFRSF18 (GITR) and CD40 [48].

Recent studies demonstrate that tumor cells can exploit co-inhibitory immune modulatory pathways to shut down immune cell responses. For instance, PD-L1 was identified on the plasma membrane of melanoma and pancreatic cancer cells [49, 50]. The current theory proposes that two major mechanisms can lead to immune checkpoint expression on tumor cells. In the first model, also referred to as “cancer innate immune resistance”, altered oncogenic pathways in the tumor cells induce the ectopic expression of immune checkpoints (Figure IIA) [47]. In the second scenario, tumor cells can develop an “adaptive immune resistance”. This phenomenon occurs when the expression of immune modulatory molecules on tumor cells is triggered by the encounter with immune cells in the microenvironment. For instance, the interaction of tumor cells with T cells via the TCR:MHC recognition, leads to interferon-γ secretion by T cells, which in turn stimulates PD-L1 expression in tumor cells (Figure IIB) [47].

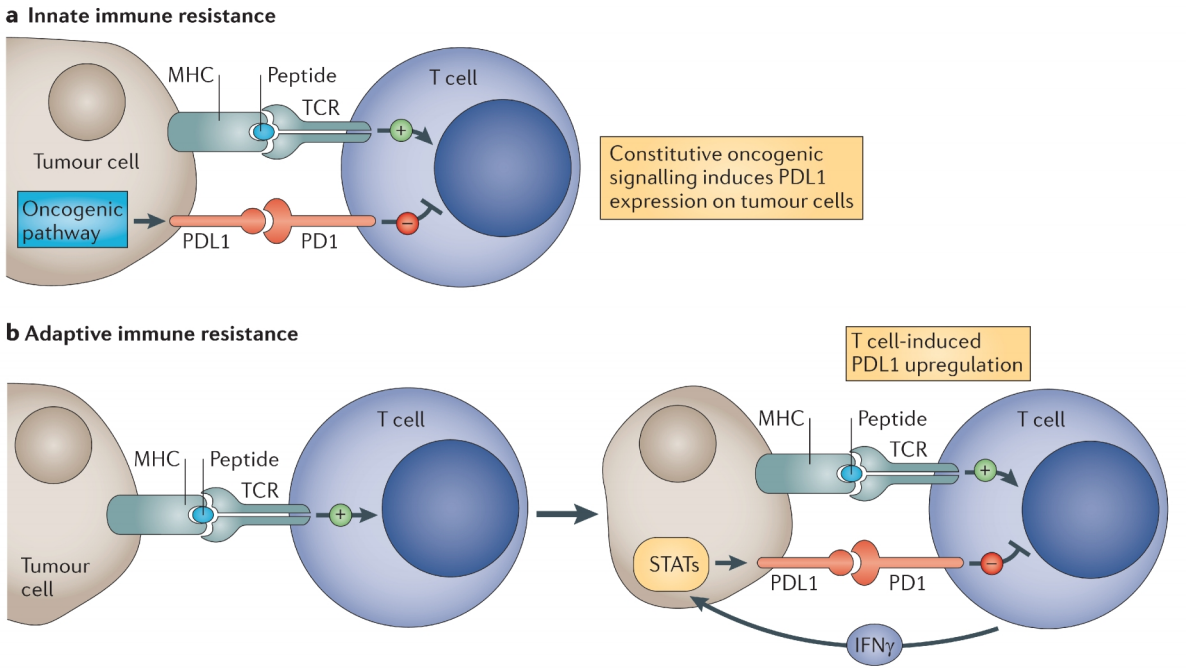

Figure II. Mechanisms of immune checkpoints´ expression on tumor cells. **(A) Innate immune resistance**. The genomic instability of cancer cells results in alteration of several molecular pathways, which lead in turn to expression of inhibitory immune checkpoints, such as PD-L1. **(B) Adaptive immune resistance**. Expression of PD-L1 is induced upon interaction of T cells with tumor cells via TCR:MHC recognition. TCR engagement results in IFN-γ secretion by T cells. This cytokine acts in a paracrine manner on tumor cells, by activating the signal transducer and activator of transcription (STAT) signaling. STAT activation promotes PD-L1 expression on the surface of tumor cells. Pardoll D., Nature Reviews Cancer, 2012 [47].

Co-inhibitory immune checkpoints

The *PD-1/PD-L1 axis* is one of the most characterized cancer immune escape mechanisms. PD-1 is expressed on several immune cells after activation, such as T and B cells, NK cells and NK T cells [51]. In T cells, PD-1 expression is sustained by persistent antigen presentation [52]. After the binding with its ligands (PD-L1 or PD-L2), the cytosolic part of this receptor activates two inhibitory motifs: the tyrosine-based inhibitory motif (ITIM) and the immunoreceptor tyrosine-based switch motif (ITSM). In particular, the activation of ITSM leads to the recruitment SH2-domain containing tyrosine phosphatase 2 (SHP-2), which shuts down the phosphatidylinositol-4,5-bisphosphate 3-kinase (PI3K)/ protein kinase B (AKT) pathway [53]. Additionally, PD-1 activation can shut down the TCR signaling by preventing the phosphorylation of its downstream molecular interactors [53]. As a result, T cells reduce the production of

cytokines such as, IFN-γ, interleukin (IL) 2 and TNF-α. Furthermore, PD-1 activation affects T cell proliferation and promote apoptosis [54].

CTLA-4 plays an essential role in controlling T cell hyperactivation and homeostasis. Studies in mice lacking the *Ctla4* gene, show uncontrolled lymphocyte proliferation and multi-organ destruction [55]. CTLA-4 is expressed after activation of naïve T cells and it competes with the co-activator molecule CD28 for the binding to CD80 and CD86 on APCs. Because of its higher affinity to its ligands compared to CD28, the expression of this molecule on effector T cells leads to a series of signaling cascade events resulting in decreased IFN-γ secretion and T cell anergy [56]. Beside its role on activated T cells, CTLA-4 promotes the activation of T_{regs}, thus exacerbating the immunosuppressive tumor microenvironment [57, 58].

LAG-3 and TIM-3 are emerging co-inhibitory molecules that are expressed on several T cell subsets. The exact molecular mechanism by which LAG-3 negatively regulates T cell function is not completely understood yet. However, it was shown that activated $CD8^+$ T cells express high levels of this receptor and that adoptive transfer of LAG-3-deficient $CD8^+$ T cells into mice presenting their cognate antigens attenuates the effector function and the proliferative capacity of this cell subset [59, 60]. Furthermore, LAG-3 plays an essential role in sustaining the functionality of a subset of regulatory $CD8^+$ T cells, suggesting its role in orchestrating several immunosuppressive mechanisms in cancer [59, 61]. TIM-3 is a receptor that negative regulates Th1 responses against viruses and plays a role in peripheral tolerance [62]. In several tumors, such as human hepatocellular, cervical, colorectal and ovarian carcinoma, TIM3 is upregulated on $CD4^+$ infiltrating T cells, and this cell subtype shows suppressive activity towards $CD8^+$ T cells [63] . Due to these properties, LAG-3 and TIM-3 are used as markers of T cell exhaustion [64].

CEACAM6 is an adhesion molecule that plays a role in exacerbating tumor progression and metastasis [65]. In a study conducted in this laboratory, it has been shown that CEACAM6 is expressed by multiple myeloma malignant cells and it shuts down $CD8^+$ T cell responses against cancer cells. Depletion of CEACAM6 using RNA interference or monoclonal antibodies, restored T cell activation towards multiple myeloma cells [66].

Besides these mechanisms, which mostly act on the suppression of immune cell functionality, tumor cells can directly mediate cytotoxicity of proximal immune cells using the *FAS/FAS ligand (FASL)* axis. During the phase of cancer immune elimination, activated T cells express FASL, which induces apoptosis in cancer cells upon the interaction with the receptor FAS [67] . However, aberrant cells can induce a "counterattack" by upregulating the FASL, thus leading to effector T cell death [68, 69].

1.3.1.2 Soluble factors mediating immune suppression

In the tumor microenvironment, a considerable amount of soluble factors is secreted by the tumor itself, the stroma and the immune system. Soluble factors play a pivotal role in orchestrating cancer immune evasion mechanisms by acting on different cell types. These factors, which include cytokines and chemokines, may directly modulate effector cell functionality or act indirectly, on stroma cells, thereby creating a fertile microenvironment for cancer progression (e.g. promoting angiogenesis or recruiting pro-inflammatory immune cells). In addition to these effects, soluble factors can promote tumor proliferation, plasticity and resistance to cell death [45].

It has been shown that the presence of T helper (Th) cells with Th1 phenotype, induces local production of type 1 cytokines like IFN-γ, IL-2 and TNF-α, which are associated with effective anti-tumor immunity [70]. However, in many cancer patients, T helper cell differentiation is skewed towards the Th2 and the T_{reg} phenotype [71, 72], which are characterized by the secretion of several immune modulatory cytokines, such as:

- *IL-10*. Beside the aforementioned cells, this cytokine is produced by several immune cells with immunoregulatory functions, such as M2 tumor associated macrophages (TAMs) [73]. IL-10 can directly reduce the proliferation, cytokine production and migratory capacities of effector T cells [74]. It has been shown that IL-10 can contribute to sustains the T_{reg} phenotype, by inducing STAT3 signaling and activating the forkhead Box O1 (Foxo1) transcription factor [75]. Furthermore, IL-10 can down-regulate the expression of MHC class II and of co-stimulatory molecules, thus leading to defective antigen presentation and T cell anergy [76].
- *Transforming growth factor beta (TGF-β).* This cytokine is commonly overexpressed in many tumor types, where it plays a role in inhibiting T cell

proliferation and development into mature effector cells [77]. Of note, TGF-β overexpression correlates with an aggressive tumor phenotype [78]. Besides its role in immunity, TGF-β regulates a series of processes that can exacerbate cancer progression, such as cells growth, angiogenesis and cell plasticity [78] .

Besides T helper cells, a plethora of myeloid immune cell subsets, stoma cells and eventually tumor cells release other cytokines such as *IL-6, IL-8* and *vascular endothelial growth factor (VEGF),* which induce impairment of NK and T cell activation and sustain angiogenesis and tumor proliferation [45].

In addition to cytokines, some soluble factors are released by tumors cells and can directly mediate apoptosis of immune cells. For instance, *receptor-binding cancer antigen expressed on SiSo cells (RCAS-1)* was found in 15 different malignancies and it can induce apoptosis in effector immune cells via molecular mechanisms that remain undiscovered [79-81].

1.3.1.3 Metabolic alterations in the tumor microenvironment

Metabolic changes in the TME can lead to immune suppression because of depletion of essential metabolites for immune cell survival. As described in section 1.1, tumor cells utilize glycolysis as main source of energy production. This process results in high production of lactic acid, which is responsible of a decreased pH in the TME. It has been reported that a pH lower than 6.0, is sufficient to impair cytolytic activity and cytokine secretion in $CD8^+$ T cells [82].

Alteration of the tryptophan (Trp) biosynthesis has also emerged as an important immune escape mechanism. It was shown that tumor cells, as well as dendritic cells (DCs) and myeloid-derived suppressor cells (MDSCs), can upregulate the *indoleamine 2,3-dioxygenase (IDO)*, an enzyme involved in the conversion of tryptophan to kynurenine. The resulting Trp starvation and the increase of kynurenine metabolites induce profound dysfunction of several immune cells such as T cells [83, 84].

1.3.1.4 Exosomes

Tumor cells from different cancer entities can release nanovesicles with the size ranging from 30 to 100 nm, also referred to as exosomes. Exosomes contain a variety

of factors, such as heat shock proteins (HSPs), shed FASL, TGF-β and TNF-α that can act in a paracrine manner towards stroma and immune cells. Two major mechanisms of immune suppression have been attributed to tumor-released exosomes: i) direct impairment of NK and T cell mediated antitumor immunity, ii) expansion of suppressive immune cells, such as MDSCs and T_{regs}. In addition, these nanovescicles contain mRNAs and microRNAs (miRNAs), which can induce tumor growth and metastasis and might regulate immune cell functionality as well [45, 85].

1.3.2 Increased tumor cell resistance

The continuous interaction between the immune system and the tumor induces a "Darwinian selection", which leads to the generation of resistant tumor mutants. Tumor cell resistance occurs either when cancer cells become invisible to the immune system, or when they lose sensitivity to the arsenal of cytotoxic factors from immune cells.

1.3.2.1 Loss of antigenicity

The ability of the immune system to discriminate tumor cells from normal cells is a pillar in tumor immune biology and it is based on the antigenicity of tumor cells [86]. It has been recently shown that tumors with high mutation load, such as melanoma, are more immunogenic than tumors characterized by low mutations, such as pancreatic cancer [87-89]. This phenomenon can be attributed to the theory that higher presence of mutated proteins leads to the presentation of neo-antigens, which can be presented on MHC molecules and be recognized as non-self by T cells. Supporting this theory, recent studies demonstrated that intratumoral $CD4^+$ and $CD8^+$ T cells possess TCRs that specifically recognize neo-antigens, and that their *ex vivo* expansion and adoptive cell transfer induces tumor regression [90-93].

However, some tumors may lose their antigens, either incorporating them via endocytosis or by shedding them into the extracellular matrix. As an example, it was observed that loss of *mucin 1 (MUC1)* in breast cancer cells, is responsible of resistance to T cell response, and MUC1 cDNA transfection restores the cytotoxic ability of autologous $CD8^+$ T cells [94].

Besides mechanisms affecting antigen expression, loss of antigenicity can arise from alteration in the antigen-presenting machinery. For instance, aberrant epigenetic

events, such as DNA methylation, can modulate the expression of the human leukocyte antigen (HLA) gene in tumor cells, resulting in down modulation of MHC-I molecules [95]. Alternative mechanisms include: i) alteration *of β-2 microglobulin (β2m)* expression, which results in defective MHC-I folding or, ii) defects in intracellular antigen processing, such as dysfunction of *transporter associated with antigen processing (TAP)* or proteasomal subunits (Figure III) [96].

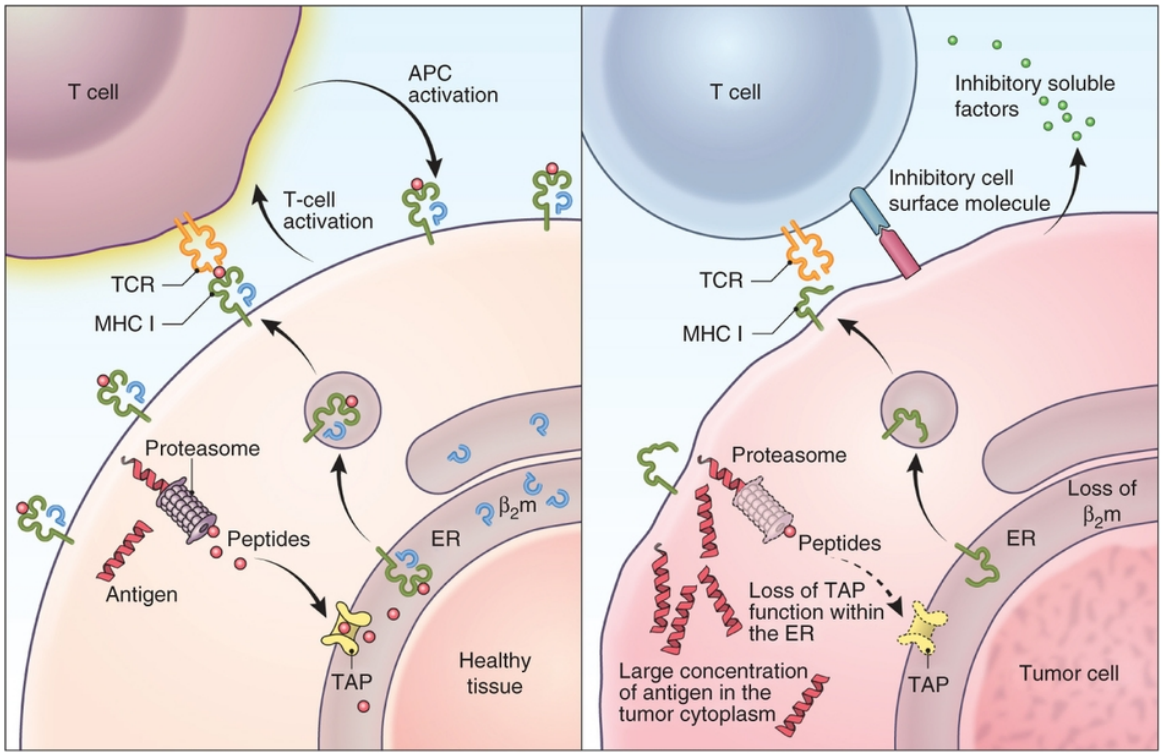

Figure III. Alterations in the antigen-presenting machinery that render tumor cells invisible to the attack of T cells. **Left panel**. Healthy cells possess intact antigen processing and presentation machinery and are highly susceptible to the attack of CTLs. **Right panel**. Aberrant cells may show one or more defects in antigen presentation, such as downregulation of MHC-I molecules or β2m, or alterations in antigen processing, such as dysfunction of TAP and proteasomal subunits. Hinrichs, C.S., Nature Biotechnology, 2013 [96].

1.3.2.2 Intrinsic tumor resistance to immunity

Even in the case of normal antigen presentation, tumor cells can exploit several mechanisms to become refractory to the attack of immune cells.

Regulation of apoptosis

The majority of cytotoxic effector molecules released by CTLs and NK cells, acts via apoptosis induction in tumor cells. However, aberrant cells can alter the balance between pro-death and anti-death signals, thus becoming resistant to immunity. On an etiological point of view, an increase of anti-apoptotic factors can arise either from the oncogenic pathways activated in tumor cells, or it can be triggered by the TME. For example, several cytokines from the TME, such as IL-4, IL-10 and TGF-β can upregulate the expression of anti-apoptotic molecules, such as the caspase-like apoptosis regulatory protein (c-FLIP), and the B-cell lymphoma-extra large (BCL-xL) [45].

Apoptosis resistance can directly involve the blockade of cytotoxic effector molecules, such as granzyme B. The *serpin family B member 9 (PI-9)* is a protease inhibitor that is physiologically expressed by T cells and DCs, where it prevents deleterious effects of granyzme B. In fact, this enzyme can directly inhibit granyzme B proteolytic activity. It has been shown that PI-9 is overexpressed in a variety of malignancies such as lung adenocarcinoma and prostate cancer [97, 98]. In tumor cells, PI-9 expression can be induced by exposure to estrogens and it can prevent the activation of the extrinsic apoptosis pathway that can be triggered by other effector molecules from the CTL/NK cells, such as FASL, TRAIL and TNF-α [99] (Figure IV) .

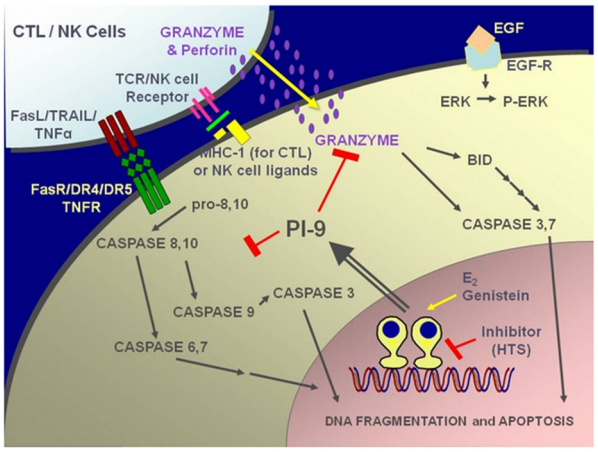

Figure IV. PI-9 prevents immune cell-mediated apoptosis of tumor cells. PI-9 can be expressed by tumor cells, as result of genomic alterations or upon estrogen stimulation (such as estradiol (E_2). PI-9 acts by both blocking granzyme B proteolytic activity and caspase 8/caspase 10 cleavage, thus inhibiting immune cell-mediated apoptosis at multiple levels [99].

Alteration of FAS expression is another mechanism that tumor cells can use to evade apoptosis. Decreased levels of this receptor were found in several tumor such as hepatocellular carcinoma and adult T cell leukemia [100, 101]. Alternatively, tumor cells can release the *decoy receptor 3 (DcR3)*, which binds to FASL, thus preventing FAS/FASL interaction [102].

Increased tumor cell survival

Resistance to immune cell attack can be the result of the upregulation of pro-survival signals that can directly or indirectly contrast apoptosis by inducing cell cycle, tumor cell plasticity, autophagy and expression of anti-apoptotic factors.

One of the best characterized examples of molecular mechanisms that sustain tumor cell survival is the alteration of the *nuclear factor kappa B (NF-κB)* activation. NF-κB is an important transcription factor orchestrating several physiological processes, such as stress response and inflammation [103]. Elevated levels of NF-κB were identified in different tumors (e.g. Hodgkin lymphoma and T cell lymphoma), as result of genetic alterations [104, 105] . NF-κB activation results in the trans-activation of genes that promote tumor progression in several manners. These genes include pro-mitogenic factors such as cyclin D, which sustain cell proliferation, and anti-apoptotic genes, such as B-cell lymphoma-2 (BCL-2), BCL-xL, x-linked inhibitor of apoptosis (XIAP) and c-IAP1/2. A comprehensive overview of NF-κB-induced effects in cancer is depicted in Figure V [106]. Activation of NF-κB in tumor cells can be triggered by the TME as well. Cytokines such as TNF-α and IL-1 can bind to their respective receptors on tumor cells and activate NF-κB [107]. Importantly, NF-κB activation prevents TNF-α-mediated apoptosis in tumor cells [108-110] .

STAT3 and PI3K/AKT signaling pathways in tumor cells can lead to resistance to immunity as well [111, 112]. In particular, STAT3 signaling induces, on the one hand, unrestrained cancer cell proliferation and resistance to apoptosis, and on the other hand, to the production of immunosuppressive cytokines that impair immune responses in the TME [111, 113, 114].

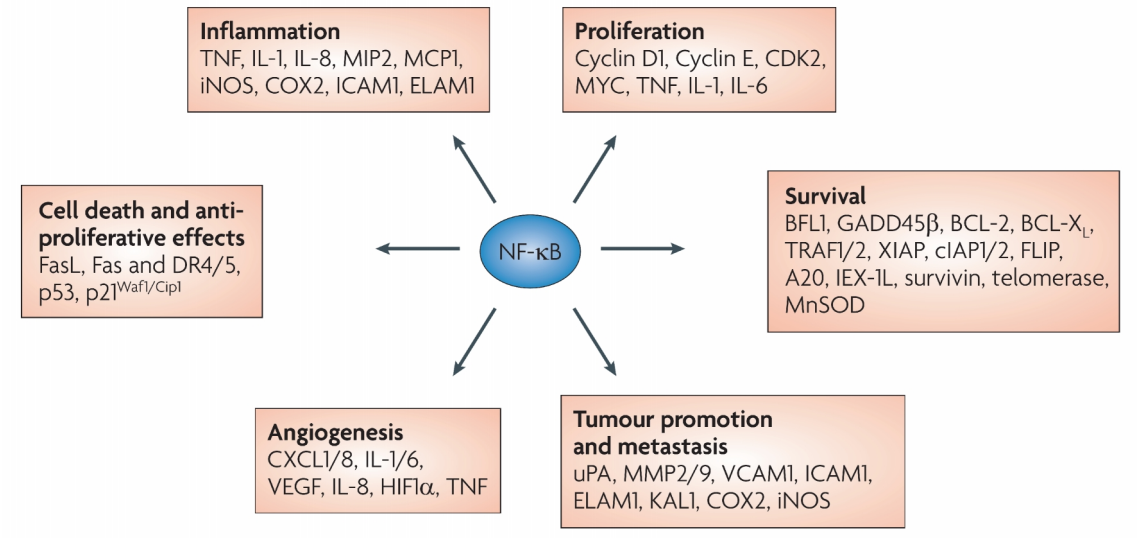

Figure V. NF-κB activation induces immune evasion by regulating tumor progression and invasiveness. NF-κB leads to the transcription of genes involved in cell proliferation, angiogenesis, metastasis, inflammation and suppression of apoptosis. Baud V., Nature Review Drug Discovery, 2009 [106]

1.4 Cancer immunotherapy

The intricate mechanisms that tumor cells use to evade the immune system have led to a strong interest in discovering novel ways to overcome these pathways and restore effective anti-tumor response of host immune cells. In the last years, major advances in the field of immunotherapy have been achieved and a number of novel therapeutic strategies have emerged.

Cancer vaccines

Therapeutic cancer vaccination has been the first exploited approach in cancer immunotherapy. This approach is based on the ability of APCs, such as DCs, to induce an antigen-specific response in $CD8^+$ and $CD4^+$ T cells [115]. One of the main challenging aspects in cancer vaccination is the choice of appropriate antigens. An ideal antigen should be specifically expressed at the tumor site and should be essential for tumor survival in order to avoid the possibility of immune escape events, such as downregulation of antigen expression [116]. Disappointing results were obtained using short peptides antigens due to their poor pharmacokinetic properties, whereas whole irradiated tumor cells have more recently been used as an efficacious antigen source

[115]. As an example, the granulocyte macrophage colony-stimulating factor (GM-CSF)-transduced autologous tumor cell vaccine GVAX showed effective DC recruitment, maturation, and $CD8^+$ T cell priming in a variety of pre-clinical studies [117]. However, advanced Phase III clinical studies showed lack of efficacy of this vaccine [117].

So far, only a few therapeutics reached clinical approval. The first clinically approved therapeutic cancer vaccine was the DC-based vaccine sipuleucet-T. This therapeutic agent is based on the isolation of DCs from peripheral blood of the tumor patient, *ex vivo* stimulation with cancer antigens, and subsequent reinfusion into the patient [118]. Treatment with sipuleucet-T led to increased survival in patients with prostatic cancer [119].

Despite recent advances, cancer vaccination remains a challenging approach and further research needs to be conducted in order to: i) find more specific tumor-associated antigens, ii) define appropriate route of administration, and iii) improve commercial scale up.

Adoptive cell transfer (ACT)

Adoptive cell transfer (ACT) has recently emerged as a promising immunotherapeutic strategy for cancer. ACT consists in the production of antitumor lymphocytes that are expanded *ex vivo* and subsequently transferred into the patient [120]. The advantage of this strategy over vaccination is that anti-tumor T cells are cultivated with cytokine cocktails that restore T cell activity, thus overcoming immune tolerance [115]. The injection of expanded T cells is often preceded by lymphodepletion [120]. Lymphodepletion allows eliminating immunosppressive immune cells populations in the TME that would eventually inhibit the activity of adoptively transferred T cells [120]. Expanded lymphocytes can derive from patients´ peripheral blood, draining lymph node or tumor tissues [115]. In particular, the usage of TILs has shown durable clinical response in several patients with metastatic melanoma refractory to standard therapy [121]. However, TIL-based therapy is only limited to resectable tumors, and in some patients, TILs are unable to expand *ex vivo* [120].

ACT can be coupled with genetic T cell engineering approaches that aim to generate T cell clones with high selectivity against tumors. In this regard, two major strategies have been used thus far. The first approach consists in the expression of tumor-antigen specific TCRs from peripheral blood-derived T cells. However, this strategy has shown little clinical applicability because the generated highly avid TCRs can provoke severe immune responses in healthy tissues as well [115]. The second approach involves the usage of chimeric antigen receptors (CARs) that are recombinant constructs with an Ig variable domain fused to a TCR constant domain. CARs recognize tumor antigens that are directly expressed on the surface of tumor cells, thus bypassing the involvement of MHC-I molecules [120]. The most promising results from CAR-based therapy have been observed in hematological tumors such as B-cell malignancies [122]. However, this approach showed little clinical benefit in solid tumors, because of the poor infiltration of engineered T cells in the tumor site and paucity of potential cancer-specific targets [123].

ACT is a promising approach for cancer immunotherapy. However, further improvements need to be made to reduce adverse effects, prolong clinical responses and reduce costs.

Immune checkpoint blockade

As described in section 1.3.1.1, immune checkpoints are surface molecules that can modulate T cell responses by boosting or dampening the TCR signaling. Current available therapeutic tools act either as antagonists of co-inhibitory molecules or as agonist of co-stimulatory checkpoints. However, the former reached the most clinical success in recent years. In particular, ipilimumab, a human monoclonal antibody (mAb) blocking CTLA-4, restored anti-cancer immune response in a number of pre-clinical tumor models and it currently represents the first-in-line treatment for patients with metastatic melanoma [115, 124, 125].

The success of CTLA-4 blockade was followed by pembrolizumab and nivolumab, two PD-1 blocking antibodies that reached the market in 2015 [126]. PD-1 blockade increases T cell proliferation, cytokine release and cytotoxicity in several pre-clinical models [127]. Furthermore, PD-1 knockout mice exhibit more favorable toxicity profile

over CTLA-4 knockout [128]. This effect is attributed to the role of PD-1 in regulating peripheral tolerance rather than modulating the general activation status of T cells. Current clinical applications of PD-1 blockade include melanoma, non-small cell lung carcinoma (NSCLC) and renal carcinoma [129, 130] .

Blockade of CTLA-4 and PD-1/PD-L1 axis is only the tip of the iceberg in the field of potential molecules that can be targeted to improve anti-tumor responses. Pre-clinical and clinical studies have recently shown encouraging results with LAG-3,TIM-3 and VISTA targeted therapy [115], as well as with co-stimulatory molecules including OX40 [131] , 4-1BB [132] and CD40 [133].

Combination therapy is currently in use with the aim of synergizing the effects of immune checkpoint blockade. Association of anti-CTLA-4 and anti-PD-1, significantly improved objective response in patients with metastatic melanoma compared to monotherapy [134], suggesting that the simultaneous blockade of different immune modulatory nodes might represent a more effective strategy to treat cancer.

1.4.1 Limitations

Immunotherapy, and in particular immune checkpoint inhibition has inaugurated a new era for cancer immunotherapy; however a large number of patients still exhibit lack of response to this therapeutic approach.

Variability of response to immunotherapy can occur across different tumor entities. The reason of this heterogeneous response is not completely elucidated. However, it was observed that tumors characterized by a higher mutation load, such as melanoma and lung cancer, respond more effectively to immunotherapy compared to patients with a low mutation rate [135-137]. It is speculated that a higher mutation load can harbor higher numbers of neo-antigens presented on MHC-I molecules, thereby leading to an influx of greater numbers of tumor-reactive T cell [136, 138]. Conversely, in some malignancies, such as pancreatic adenocarcinoma (PDAC), the amount of mutation load negatively correlates with immune cell activation [138]. PDAC is unique from an immunological perspective [139]. Infiltration of effector T cells is rarely observed, whereas several immunosuppressive immune subsets can infiltrate the tumor [140, 141]. Additionally, the rat sarcoma oncogene (RAS) triggers an inflammatory program

that exacerbates tumor progression [142]. As a result, several clinical trials using immune checkpoint blockade failed in this disease. For instance, ipilimumab was ineffective as monotherapy for the treatment of PDAC in a Phase 2 clinical trial [143]. These disappointing results emphasize the need to discover additional therapeutic targets that could show clinical efficacy in a wider range of tumor entities.

Another critical issue that limits the success of immunotherapy is the heterogeneity of response within patients affected by the same malignancy. For instance, less than 40% of melanoma patients benefit from anti-PD-1 therapy [144]. Many efforts have been made to stratify patients to predict responders versus non responders [145]. In particular, Hugo et al., showed that melanoma tumors refractory to anti-PD-1 treatment exhibit a specific signature of genes, also referred to as innate anti-PD-1 resistance signature, or IPRES [146]. Furthermore, some tumors may develop an adaptive resistance to immunotherapy [147]. In a recent study, approximately 25% of melanoma patients who exhibited an objective response to PD-1 blockade therapy, developed disease progression at a median follow-up of 21 months [148]. Zaretsky et al., demonstrated that melanoma patients who develop resistance to anti-PD-1 blockade, often exhibit loss-of-function mutations of Janus kinases 1 and 2 (JAK1/2) genes [149]. Additionally, PD-1 blockade may induce the expression of alternative immune checkpoint molecules, such as TIM3, thus abrogating the effect of anti-PD-1 antibodies [150].

These studies suggest that additional efforts must be made to identify novel therapeutic targets whose blockade overcomes innate and adaptive resistance to immunotherapy.

1.5 High-throughput (HT) RNAi-based screens for novel immune modulators

RNA interference (RNAi)-based genetic screens have emerged as powerful approach to study gene function in a high-throughput (HT) fashion. In recent years, a few studies exploited this technique to identify novel immune modulators in disparate tumor models. In 2014, Zhou et al., performed an elegant study for the discovery of novel immune modulators *in vivo* [151]. Mouse $CD8^+$ T cells were transduced with a pooled short hairpin RNA (shRNA) library, and subsequently injected into tumor-bearing mice.

Afterwards, next-generation sequencing was conducted to identify genes whose depletion increased proliferation and activation of T cells. Despite its relevance, this work showed two major limitations: i) it was conducted in mouse rather than in human, and ii) the final readout was the measurement of T cell proliferation rather than their cytotoxic potential.

To overcome these limitations, a novel approach was developed in this laboratory by Dr. Nisit Khandelwal [152]. In this *proof-of-concept* study, human breast cancer cells, MCF7 were transfected with an arrayed small interfering RNA (siRNA) library targeting 500 genes and subsequently challenged with CTLs. CTLs derived from peripheral mononuclear blood cells (PBMCs) of healthy donors, and tumor recognition was induced using a bispecific antibody. In addition, the screen was conducted using tumor antigen-specific T cells as well. In this study, luciferase-based killing assay was used as final readout to directly measure T cell mediated killing.

The successful identification of the C-C chemokine receptor type 9 (CCR9) as novel immune modulator, suggested that this approach could be applied to different human tumor cell models using a broader library.

2. Aims of the study

Immunotherapy has inaugurated a new era for the treatment of cancer, however the majority of tumor patients does not benefit from this therapeutic approach. Despite the numerous efforts to dissect the mechanisms underlying resistance to immunotherapy, a comprehensive understanding of this phenomenon is still missing. It is currently conceived that a plethora of immunological obstacles may simultaneously concur to the establishment of an immunotherapy-resistant tumor microenvironment [45, 145].

Given these considerations, we hypothesized that the majority of these immunosuppressive mechanisms remained undiscovered, and we aimed to unravel novel immune modulatory molecules expressed by tumor cells.

Starting from a *proof-of-concept* approach developed in this laboratory [152], we sought to:

- Develop a high-throughput RNAi screening for the identification of novel immune modulators in the immunotherapy-resistant PDAC.
- Validate the role of selected hits in mediating immune modulation in several cancer entities.
- Unravel the molecular mechanism underlying the immune suppressive function of selected hits.
- Provide the rationale for the applicability of selected candidate genes as novel targets for cancer immunotherapy.

3. Results

3.1 Set-up of a HT-screen for novel immune modulators in pancreatic cancer

In order to identify novel genes involved in escape mechanisms of cancer immune surveillance, pancreatic ductal adenocarcinoma (PDAC) was used as tumor model for this thesis. PDAC is the fourth most common cause of cancer-related death across the world [153] and it is characterized by its ability to escape immune surveillance by developing many immunological obstacles [154]. Immunotherapeutic strategies, such as immune checkpoint blockade, have proven clinical success in many cancer entities [125, 155-157], but showed little clinical benefit in PDAC patients [143], emphasizing the need to identify more key players that could radically improve immunotherapy in this particular cancer disease.

To discover novel potential immune checkpoint molecules in PDAC, a high-throughput (HT) screening approach was utilized. This method was previously established in this laboratory by Dr. Nisit Khandelwal et al. [152], and subsequently expanded and improved in this work. Briefly, firefly luciferase-expressing tumor cells are reverse transfected with a siRNA library for 72h. Afterwards T cells (*cytotoxicity setting*) or culture medium (*viability setting*) are added. After 20h the supernatant (containing T cells and dead tumor cells) is removed, remaining tumor cells are lysed and luciferase intensity is measured. Luciferase activity is proportional to the amount of living cells in each sample. The *cytotoxicity setting* allows identifying genes whose knockdown increases T cell-mediated killing of tumor cells. In order to exclude genes whose knockdown affects cell viability *per se*, the *viability setting* is used, where tumor cells are cultivated with the siRNA library in the absence of T cells. For this project, the following modifications and implementations were applied to this method:

- Use of PDAC as tumor model, instead of breast cancer.
- Use of patient-derived tumor infiltrating lymphocytes (TILs) from PDAC patients, as T cell source, instead of PBMC-derived T cells.

- siRNA library extension, from 516 genes used in the previous screening to a 2514-gene siRNA library containing G-protein coupled receptors, protein kinases and 1117 genes encoding for cell surface proteins.

A schematic description of the method is depicted in Figure 1.

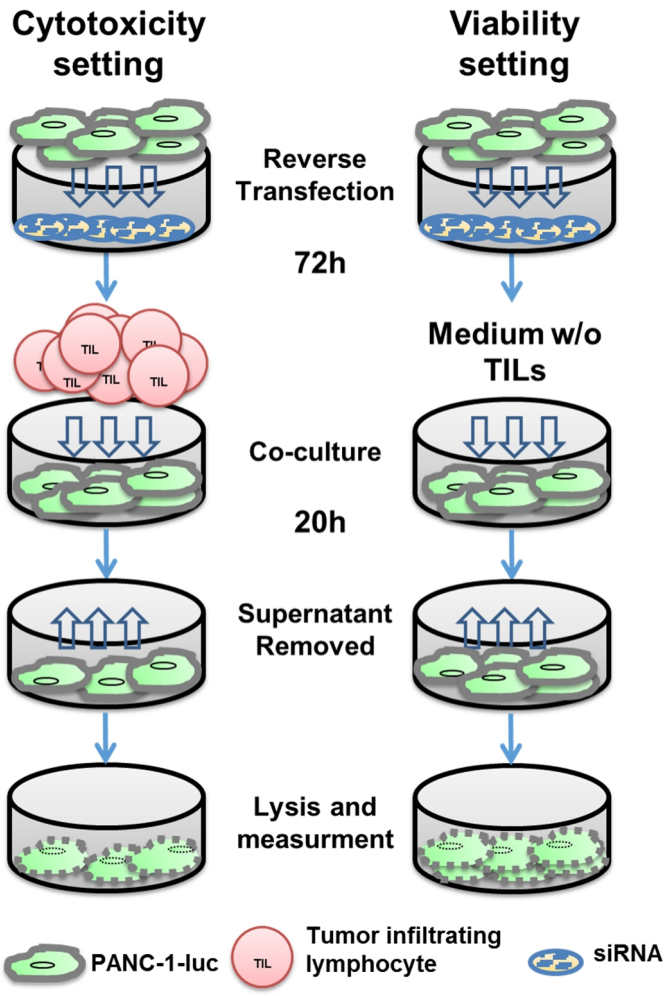

Figure 1. Principle of the HT-screening for novel immune checkpoints in PDAC. A siRNA library of 2514 genes is distributed in several 384-well plates. Each well contains a pool of 4 siRNAs targeting the same gene. Stable luciferase-expressing PANC-1 (PANC-1-luc) tumor cells are seeded in each well (reverse transfection). 72h after transfection, patient-derived TILs are added and co-cultured with transfected tumor cells for 20h. Supernatant is removed and luciferase activity of remaining tumor cells is measured after cell lysis.

Before performing the HT-screening, a series of adaption and optimization procedures were necessary, in order to ensure reliability and robustness of the methods. These procedures are schematized in Figure 2 and described in further details in next paragraphs.

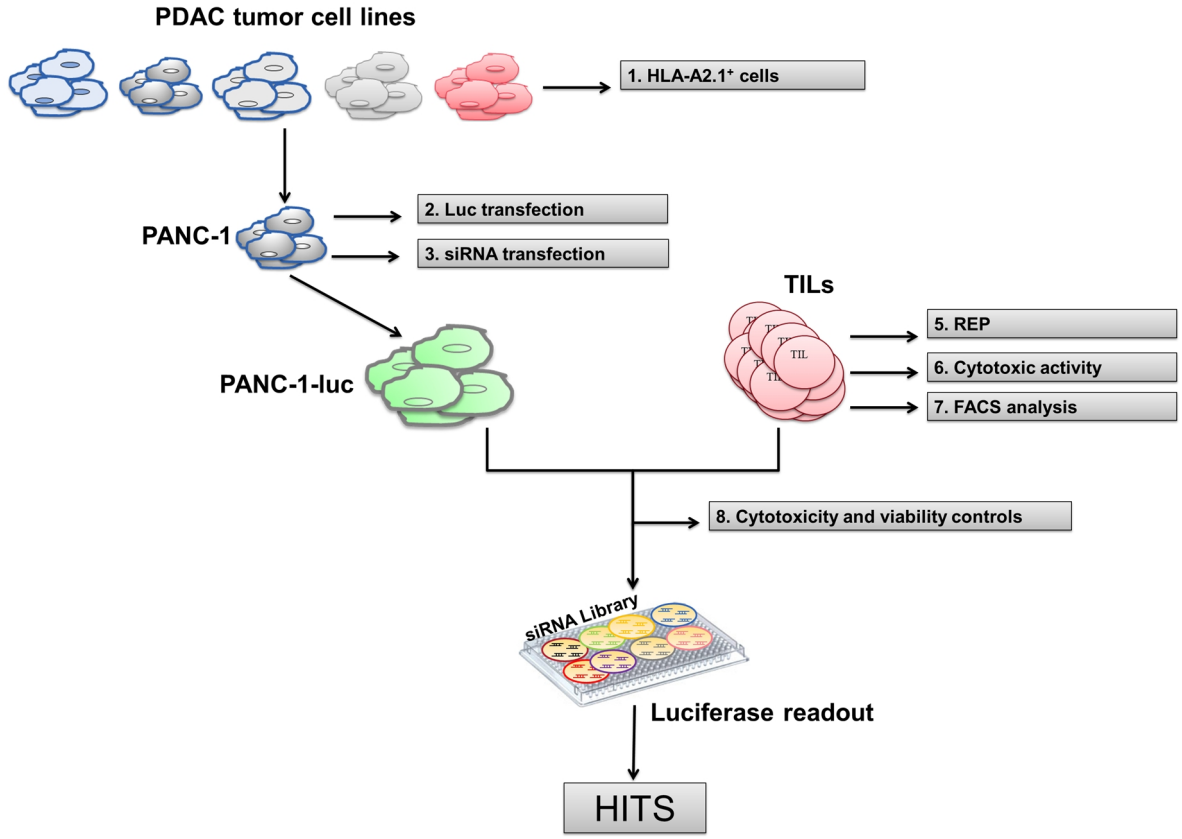

Figure 2. Screening set-up workflow. Several PDAC cell lines were tested for their expression of HLA-A2.1 allele. PANC-1 cell line was chosen for further validation due to its HLA-A2.1 expression. Firefly luciferase gene and siRNA transfection efficacy were optimized in PANC-1 cells. HLA-A2.1$^+$ (TILs) were tested for their ability to expand using the rapid expansion protocol (REP) [158], and for their capacity to kill PANC-1 cells. Appropriate siRNA controls for the cytotoxicity and the viability setting were established.

3.1.1 Selection of HLA-A2.1$^+$ tumor cell lines

As the HT-screen is based on the co-culture of tumor cells and TILs, HLA-2.1$^+$ PDAC cell line had to be identified to match with HLA-2.1$^+$ TILs. To this purpose, flow cytometry analysis (FACS) was performed to assess HLA-2.1$^+$ expression in four PDAC cell lines. ASPC-1, BxPC-3 and Capan-1 cell lines were HLA-A2.1$^-$, while PANC-1 cells showed positive staining for HLA-A2.1 antibody (Figure 3). For this reason, PANC-1 cells were selected for further optimization experiments.

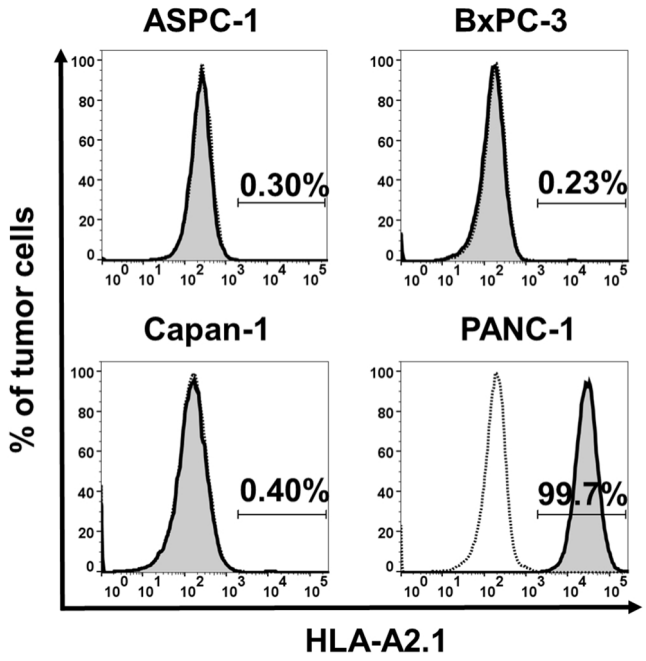

Figure 3. Expression of HLA2.1 in tumor cell lines. Flow cytometry analysis of HLA-A2.1 expression on several PDAC-derived cell lines. Dotted line: Isotype control; solid line: HLA-A2.1 staining. Gate shows percentage (%) of HLA-A2.1$^+$ cells. Representative data of two independent experiments.

3.1.2 Generation of luciferase-expressing PANC-1 cells (PANC-1-luc)

The final readout of the HT-screening is the measurement of luciferase activity from tumor cells. To this end, stably transfected PANC-1 expressing the luciferase gene (PANC-1-luc) were generated. PANC-1 cells were transfected with a vector containing the firefly-luciferase reporter gene fused with the green fluorescent protein (GFP). 14 days after antibiotic selection, transfection efficacy was evaluated by determining GFP expression by FACS. Only 6,1% of PANC-1 cells showed GFP expression.

Therefore, FACS sorting was used to enrich GFP$^+$ population. After 2 rounds of cell sorting, 96% of cells were positive for GFP (Figure 4A) and efficiently expressed the firefly-luciferase gene (Figure 4B).

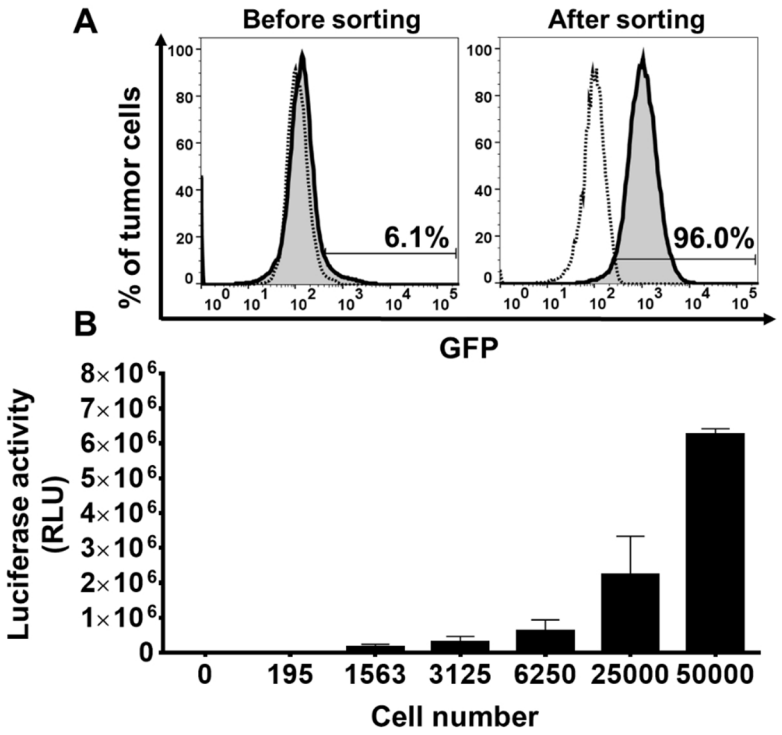

Figure 4. Generation of PANC-1-luc cell line. (A) FACS analysis of GFP expression in PANC-1 tumor cells. Left panel: GFP expression after 14 days of tumor cells selection with G418. Right panel: GFP expression after two rounds of FACS cell sorting. Dotted line: PANC-1 wild type (WT) cell; solid line: PANC-1-luc cells. **(B)** Detection of luciferase activity (relative light units = RLU) in PANC-1-luc cells after cell sorting. Representative data of at least two independent experiments. Columns show mean +/- standard error of the mean (SEM).

3.1.3 Optimization of siRNA transfection

Optimizing siRNA transfection efficacy is an important step to ensure robustness and validity of the RNAi screen. The following transfection reagents on PANC-1 cell lines: RNAiMAX, HiPerfect, Altogen1 and Altogen1 mixed to a liposome condenser (Altogen2). The ability of these reagents to deliver siRNA sequences into PANC-1 cells was evaluated by comparing PD-L1 expression between tumor cells transfected with scrambled (siCtrl1) or PD-L1 pool siRNA. The transfection reagent RNAiMAX showed the highest transfection efficacy in PANC-1 cells (Figure 5A). To confirm these observations, additional genes were knocked down in tumor cells using RNAiMAX. Transfection of siRNA sequences, targeting Galectin-3, CEACAM6 and RCAS-1, resulted in efficient gene knockdown (Figure 5B). Furthermore, significant reduction of PD-L1 (Figure 5C and 5D left panel) or CEACAM6 knockdown (Figure 5D right panel) was observed at transcriprtional level as well.

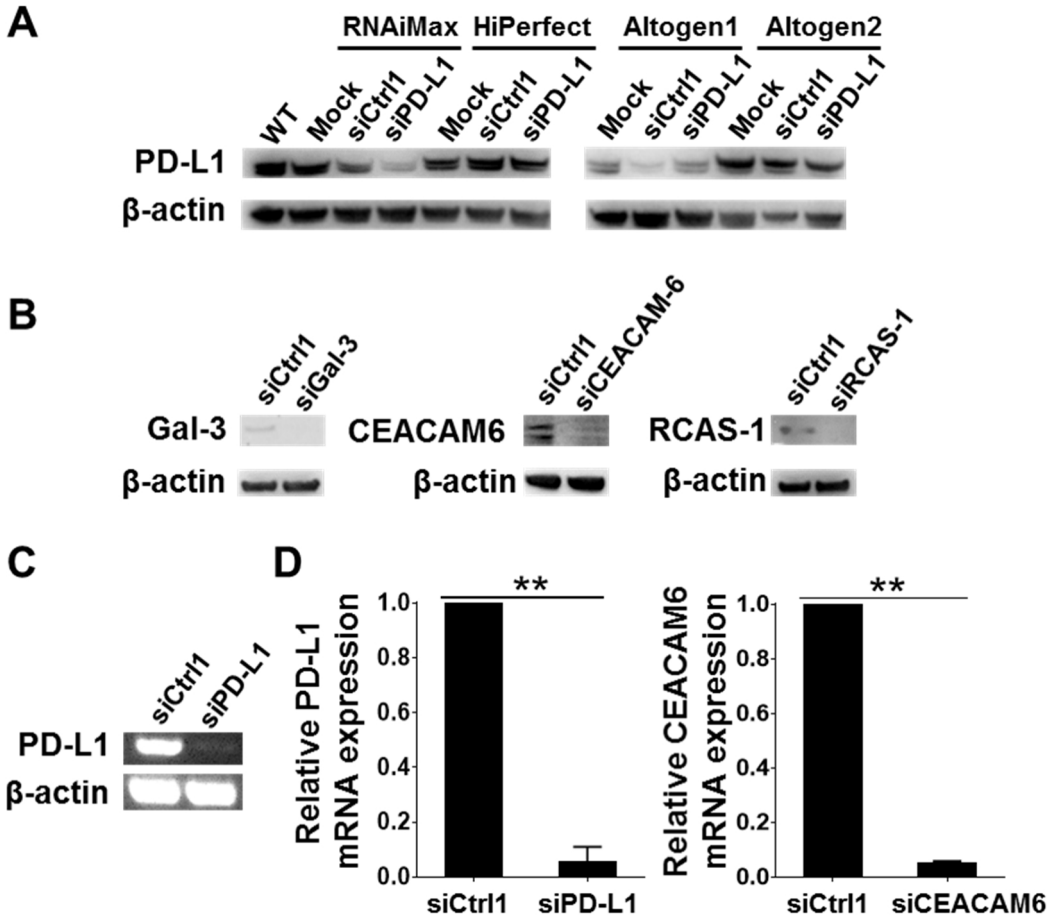

Figure 5. Optimization of siRNA delivery into PANC-1 cells. (A) Western blot assay for the detection of PD-L1 in PANC-1 cells. PANC-1 cells were reverse-transfected either with scrambled (siCtrl1) or PD-L1 pool (siPD-L1) siRNAs, with the indicated transfection reagents for 72h. As additional control, tumor cells were treated with transfection reagents in the absence of siRNA (Mock). β-actin was used as loading control . **(B)** Western blot assay for detection of Galectin-3 (Gal-3), CEACAM6 and RCAS-1 in PANC-1 cells. Tumor cells were transfected with the indicated siRNA for 72h. **(C)** End-point polymerase chain reaction (PCR) assay for detection of PD-L1 mRNA abundance in PANC-1 cells, after siRNA transfection for 72h. **(D)** Quantitative PCR (qPCR) analysis of PD-L1 (left panel) or CEACAM6 (right panel) mRNA expression in PANC-1 cells after siRNA transfection. Results are presented in terms of a fold change after normalizing with β-actin mRNA. Representative data of at least two independent experiments. Columns show mean +/- SEM. P-values were calculated using two-tailed student´s t-test. * $p < 0.05$, ** $p < 0.01$.

3.1.4 Selection of a suitable T cell source for the HT-screen

High-throughput RNAi screens require a large number of cells. As PANC-1-luc cells are immortalized tumor cells, the necessary target cell number for the screening was easily achieved. On the contrary, TILs are primary cells with limited proliferation

potential. In order to reach an appropriate number of T cells, the rapid expansion protocol (REP) established by Rosenberg et al., was used [158]. Five HLA-A2.1^{+} TIL cultures, derived from PDAC patients, were expanded: TIL#1, TIL#2, TIL#3, TIL#4 and TIL#5. TIL growth was regularly monitored for a period of 15 days. Efficient cell growth was achieved in each tested TIL culture. T cell number increased from about 400x to 800x at day 15 of REP (Figure 6A). Next, the killing ability of the above mentioned TIL cultures towards PANC-1-luc target cells was assessed. The HLA-A2.1^{-} cell line ASPC-1 was used as a negative control. Co-culture of TIL#1 and TIL#2 with tumor cells, elicited specific lysis of PANC-1-luc cells but not of ASPC-1 cells (Figure 6B-C). TIL#3, TIL#4 and TIL#5 were unable to kill the tested PDAC cell lines (Figure 6D-F). Hence, TIL#1 and TIL#2 cultures were selected for further experiments.

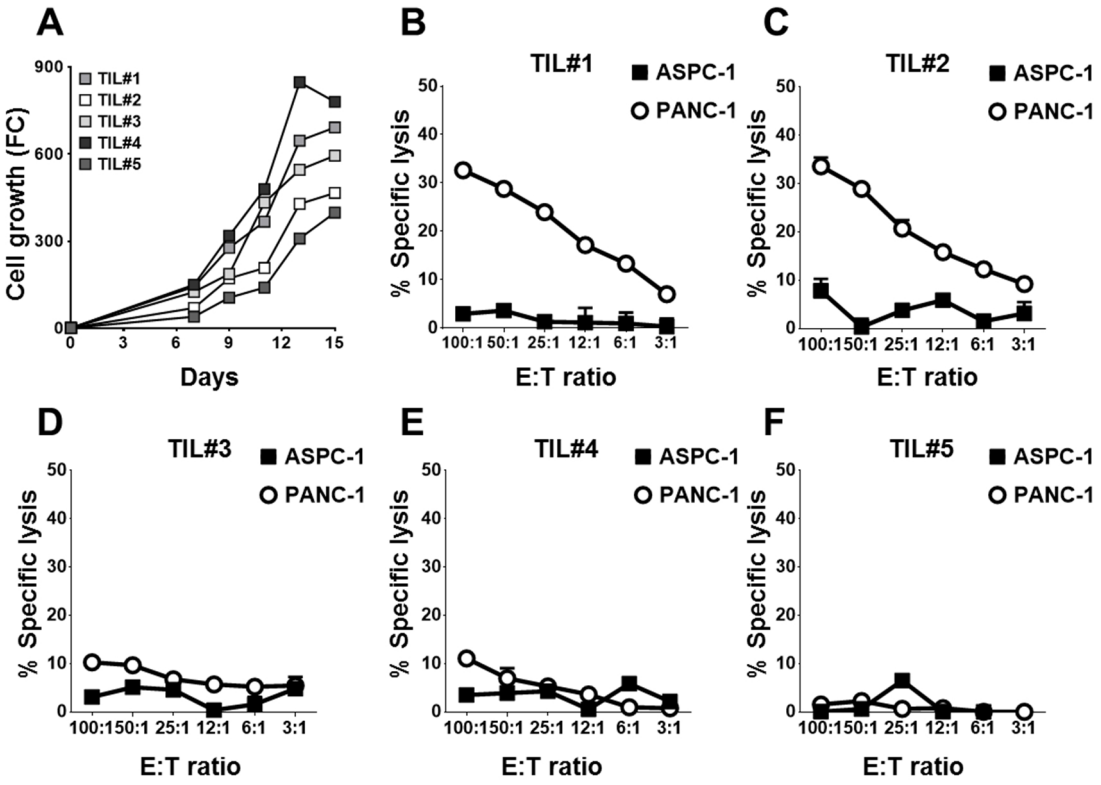

Figure 6. TILs selection for the HT-screening. (A) Cell growth (fold change) of several patient-derived TIL cultures during REP. T cell number was measured every two days from day 7 until day 15. **(B-F)** Chromium release assay after 6h co-culture of PANC-1 or ASPC-1 target cells with the indicated TIL culture, using different E:T ratios. Data show mean +/- SEM.

3.1.5 Phenotypical and functional characterization of TIL#1 and TIL#2

In order to choose between the two potential TIL cultures that showed cytotoxicity towards PANC-1 target cells (TIL#1 and TIL#2), a phenotypical characterization of these T cells was conducted. Flow cytometry analysis showed higher abundance of the $CD8^+$ subset in TIL#1 (84.4%) compared to TIL#2 (21.7%) (Figure 7A and 7B, left panel). Based on the evidence that both TIL#1 and TIL#2 showed a modest cytotoxic activity towards PANC-1 cells even at high E:T ratios (Figure 6A-B), we hypothesized that this effect was attributed to T cell exhaustion [64]. Several studies demonstrate that TILs from different tumor entities have impaired T cell effector activity and upregulate several receptors associated with T cell dysfunction [159-162]. Both TIL#1 and TIL#2 upregulate exhaustion markers such as PD-1, LAG-3, and TIM-3 [64, 161, 162]. In particular, TIM-3 expression was detected in about 90% and LAG-3 in about 58% of $CD8^+$ T-cells in both tested TIL cultures. Only a minor $CD8^+$ T cell population expressed PD-1 exhaustion marker: 11.5% in TIL#1 and 22.4% in TIL#2 (Figure 7A-B, right panels). The two tested TIL cultures did not show major differences in their cytotoxic potential and exhaustion phenotype. Hence, TIL#1 sample was selected as T cell source for the HT-screening due to its higher proliferation rate during REP (Figure 6A) and its higher abundance of $CD8^+$ T cells, compared to TIL#2.

Next, the modality by which TIL#1 killed PANC-1 target cells was investigated. Both TIL#1 and PANC-1 cells expressed the HLA-A2.1 haplotype. Nevertheless, the two cultures derived from two different individuals. Therefore, the observed cytotoxicity could be caused either by TCR engagement or by TCR-independent mechanisms, such as unspecific secretion of cytotoxic molecules or tumor apoptosis induction by members of the TNF-α superfamily (e.g. FASL or TNF-α) [27]. In order to prove TCR engagement in this system, TIL#1 were co-cultured with PANC-1 cells in the presence of a MHC-I blocking antibody. A dose-dependent reduction of TIL-mediated killing was observed using MHC-I blocking antibody (Figure 7C). One marker of TCR activation is IFN-γ production by T cells [70]. TIL#1 and PANC-1 cells were co-cultured at different E:T ratios and IFN-γ secretion was measured by enzyme-linked immunosorbent assay (ELISA). Significant increase of IFN- γ production by T cells was observed in the co-culture compared to unstimulated T cells (Figure 7D).

These data suggest that TIL#1 cells recognize and kill PANC-1 cells after TCR activation.

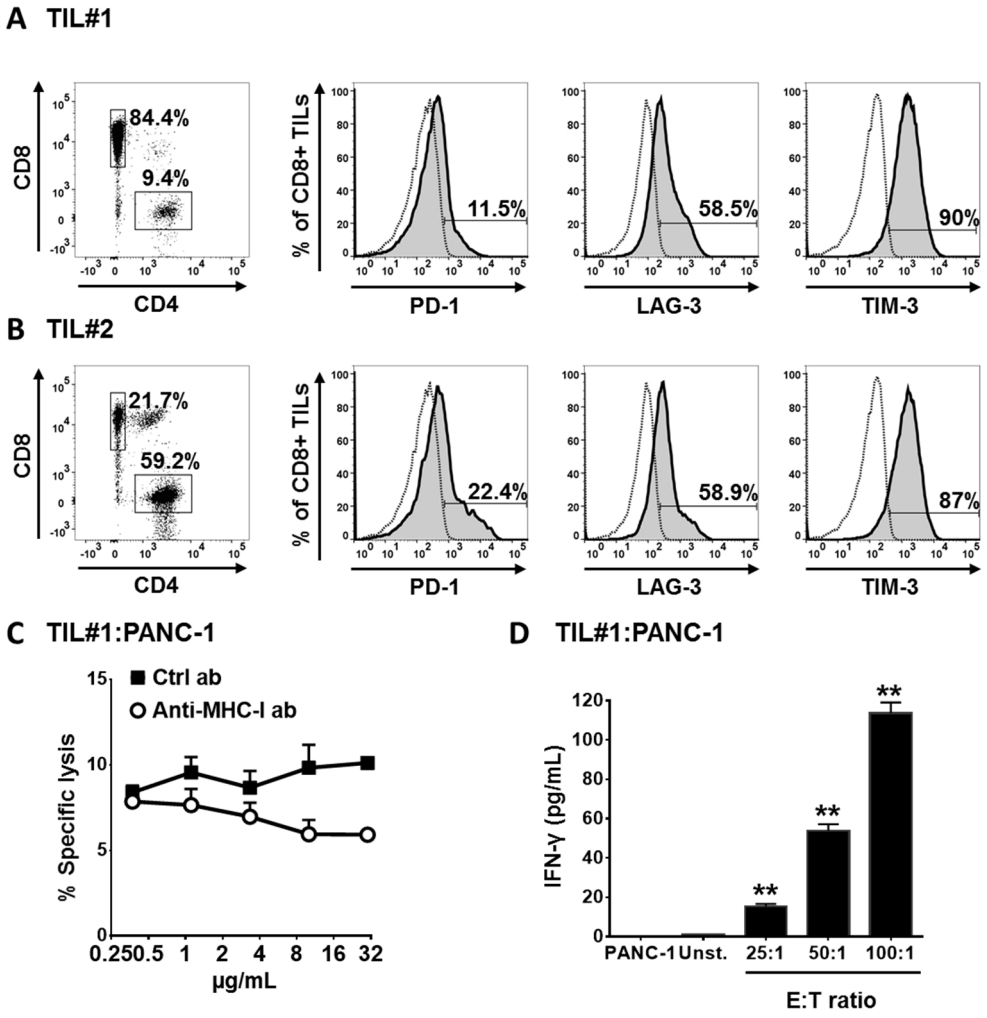

Figure 7. Phenotypical and functional characterization of TIL#1 and TIL#2. (A-B) Left panel: CD4 and CD8 expression in $CD3^+$ T cells from TIL#1 **(A)** and TIL#2 **(B)** by flow cytometry. TILs were isolated from two PDAC biopsies, enriched in CD8+ subset and subjected to REP. **Right panel:** Flow cytometry analysis for the exhaustion markers PD-1, LAG-3 and TIM-3 in $CD3^+CD8^+$ subpopulation of TIL#1 **(A)** and TIL#2 **(B)**. Dotted line: isotype control, solid line: anti-PD-1, anti-LAG-3, anti-TIM-3 staining. **(C)** Chromium release assay for detection of T cell mediated cytotoxicity in the presence of the indicated concentrations of anti-MHC-I antibody (white symbols) or IgG2a isotype control (black symbols). TIL#1 and PANC-1 cells were co-cultured for 6h at E:T ratio = 50:1. **(D)** TIL#1 and PANC-1 cells were co-cultured for 24h at the indicated E:T ratios. IFN-γ secretion was measured by ELISA: As negative control, T cells were cultured in the absence of tumor cells (Unst.). Data information: **(A-D)** Graphs show representative data of at least two independent experiments. **(C-D)** Graphs show mean +/- SEM. (D) P-values were calculated using two-tailed student´s t-test. * $p < 0.05$, ** $p < 0.01$.

3.1.6 Selection of appropriate controls for the HT-screen

Positive and negative controls give important information on the reproducibility, robustness and ease of HT-screens [163]. In order to determine appropriate negative controls for the assay, the impact of two different siRNA scrambled sequences (siCtrl1 and siCtrl2) on PANC-1-luc cell viability was tested using luciferase-based viability assay. Both siCtrl1 and siCtrl2 transfection did not alter cell viability compared to mock transfected PANC-1-luc cells (Figure 8A). Therefore, both sequences were included in the HT-screening. Next, we aimed to identify appropriate positive controls both for the viability and for the cytotoxicity setting (scheme in Figure 1). The viability setting is performed to exclude genes whose knockdown intrinsically impairs tumor cell survival. To identify proper viability controls, we knocked down several genes that are essential for cell survival: ubiquitin C (UBC) [164], checkpoint kinase 1 (CHK1) [165], polo-like kinase 1 (PLK1) [166], coatomer protein complex subunit beta 2 (COPB2) [167, 168] and “cell death” (CD), a mixture of several siRNAs targeting ubiquitously expressed human genes. Using a luciferase-based readout, we found that siUBC and siCD transfection elicited efficient cell death in PANC-1-luc cells, PLK1 knockdown showed modest reduction of tumor cell viability (about 25%) while knockdown of CHK1 and COPB2 did not significantly affect cell survival. Firefly-luciferase (Fluc) knockdown was used as transfection control for the assay (Figure 2B). We selected siUBC and siCD as viability controls for the screening because of their strong phenotype. For the cytotoxicity setting, we tested T cell-mediated cytotoxicity after knockdown of several known immune modulatory molecules, such as programmed death ligand 1 (PD-L1) [169], carcinoembryonic antigen related cell adhesion molecule 6 (CEACAM6) [66], receptor binding cancer antigen expressed on SiSo cells (RCAS-1) [79] and galectin-3 (GAL-3) [170, 171]. Using luciferase-based killing assay, we detected increased T cell-mediated cytotoxicity after PD-L1 and CEACAM6 knockdown, while transfection with RCAS-1- and GAL-3- specific siRNAs did not increase T cell mediated cytotoxicity (Figure 8C). Without the addition of TIL#1, knockdown of PD-L1 or CEACAM6 elicited a weak or moderate effect on tumor cell viability, respectively. We corroborated these results using chromium release assay. TIL#1 co-culture with PD-L1- or CEACAM6-depleted PANC-1 cells, resulted in increased T-cell mediated specific lysis (Figure 8C-D).

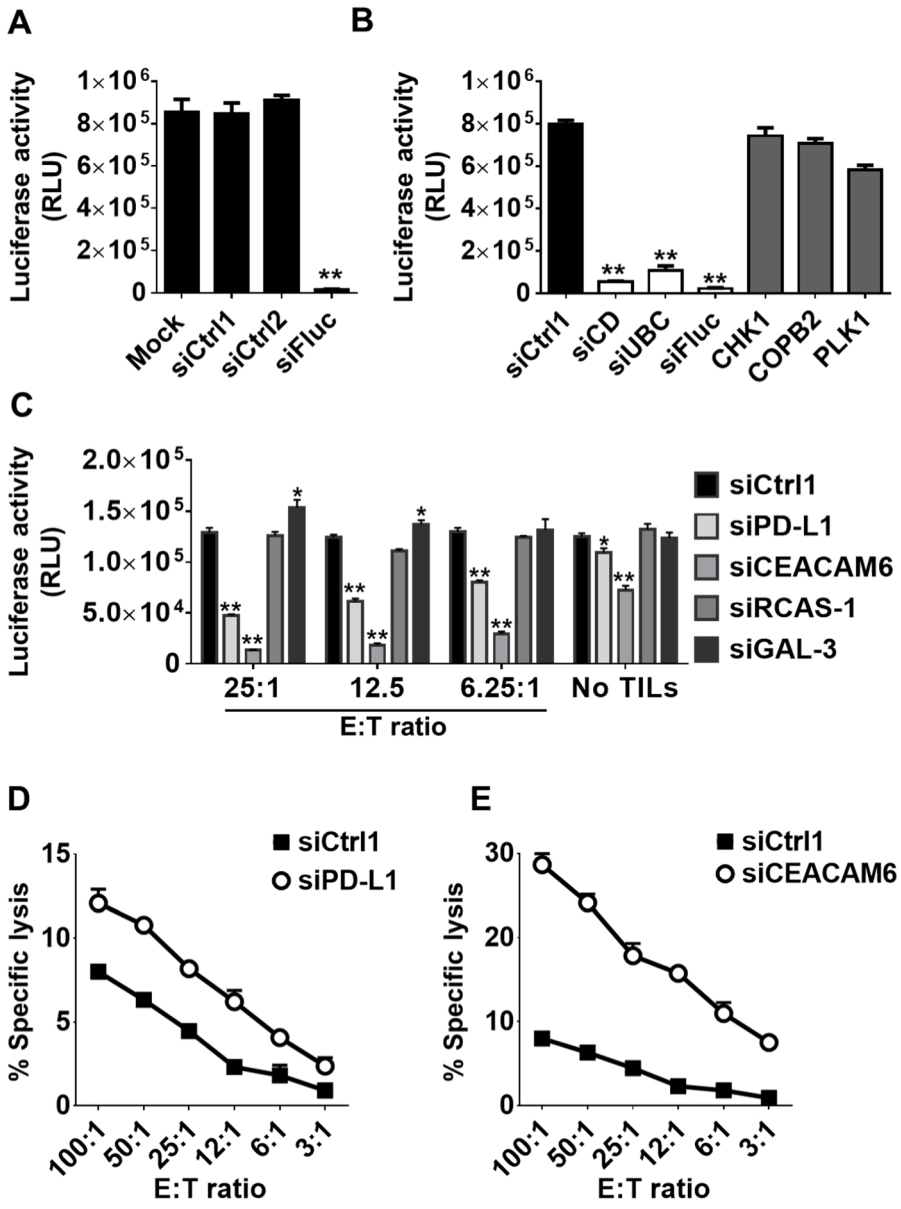

Figure 8. Assessment of appropriate controls for the HT-screen. (A) Selection of negative controls. PANC-1-luc cells were transfected with the indicated siRNA sequences for 72h. Afterwards, luciferase-based viability assay was performed. **(B)** Selection of viability controls. PANC-1-luc cells were transfected as is **(A)** and luciferase-based viability assay was conducted **(C)** Selection of cytotoxicity controls. PANC-1-luc cells were transfected as in **(A)** and subsequently co-cultured with TIL#1 at the indicated E:T ratios. Cell survival was determined by measuring the remaining luciferase activity of tumor cells after 20h co-culture with TIL#1 or culture medium (No TILs). **(D)** Chromium release assay for the detection of TIL#1-mediated lysis after 6h co-culture with siPD-L1 or siCtrl-transfected PANC-1 cells. **(D)** Chromium release assay for the detection of TIL#1-mediated lysis after 6h co-culture with siCEACAM6 or siCtrl-transfected PANC-1 cells. Data information: **(A-E)** Graphs show representative data of at least two independent experiments. **(A-C)** Graphs show mean +/- SEM. P-values were calculated using two-tailed student´s t-test. * $p < 0.05$, ** $p < 0.01$.

3.2 Performance of the HT-screen

After having completed the necessary adaption and optimization procedures, we performed the arrayed RNAi screening in a 384-well format, using TIL#1 as T cells source and PANC-1-luc as target cells. PANC-1-luc cells were transfected with a siRNA library of 2514 genes for 72h and RNAiMAX was used as transfecting reagent. TIL#1 were added to transfected cells at E:T ratio of 25:1 for 20h (cytotoxicity setting). As viability control, transfected tumor cells were cultured in the absence of TIL#1 (viability setting). Afterwards, supernatant was removed and the remaining luciferase intensity (RLU) was measured (Schematic representation in Figure 1). The assay was conducted using technical duplicates both for the cytotoxicity and for the viability setting.

3.2.1 Performance of controls

As first step, plate normalization was conducted to compare RLUs from transfected tumor cells residing in different plates (Figure 9A). This step was necessary because of the relatively short signal half-life of the assay, which causes inter-plate variability. Next, the performance of control genes, which were loaded in each plate, was assessed.

As shown in Figure 9B, siRNA transfection with negative control sequences (siCtrl1 and siCtrl2) did not affect tumor cell viability in both settings. Knockdown with UBC or “cell death” (CD) siRNAs, elicited strong cell death independently of the addition of TIL#1. Depletion of CEACAM6 or PD-L1 resulted in enhanced tumor cell killing in the cytotoxicity setting while it showed a minor effect in the viability setting. Knockdown efficiency was confirmed after firefly-luciferase siRNA transfection.

To evaluate the technical quality and reproducibility of the assay, Pearson correlation coefficient (r^2) was calculated for both settings. We observed an $r^2 = 0.92$ in the cytotoxicity setting and $r^2 = 0.90$ in the viability setting, confirming the technical robustness of the assay.

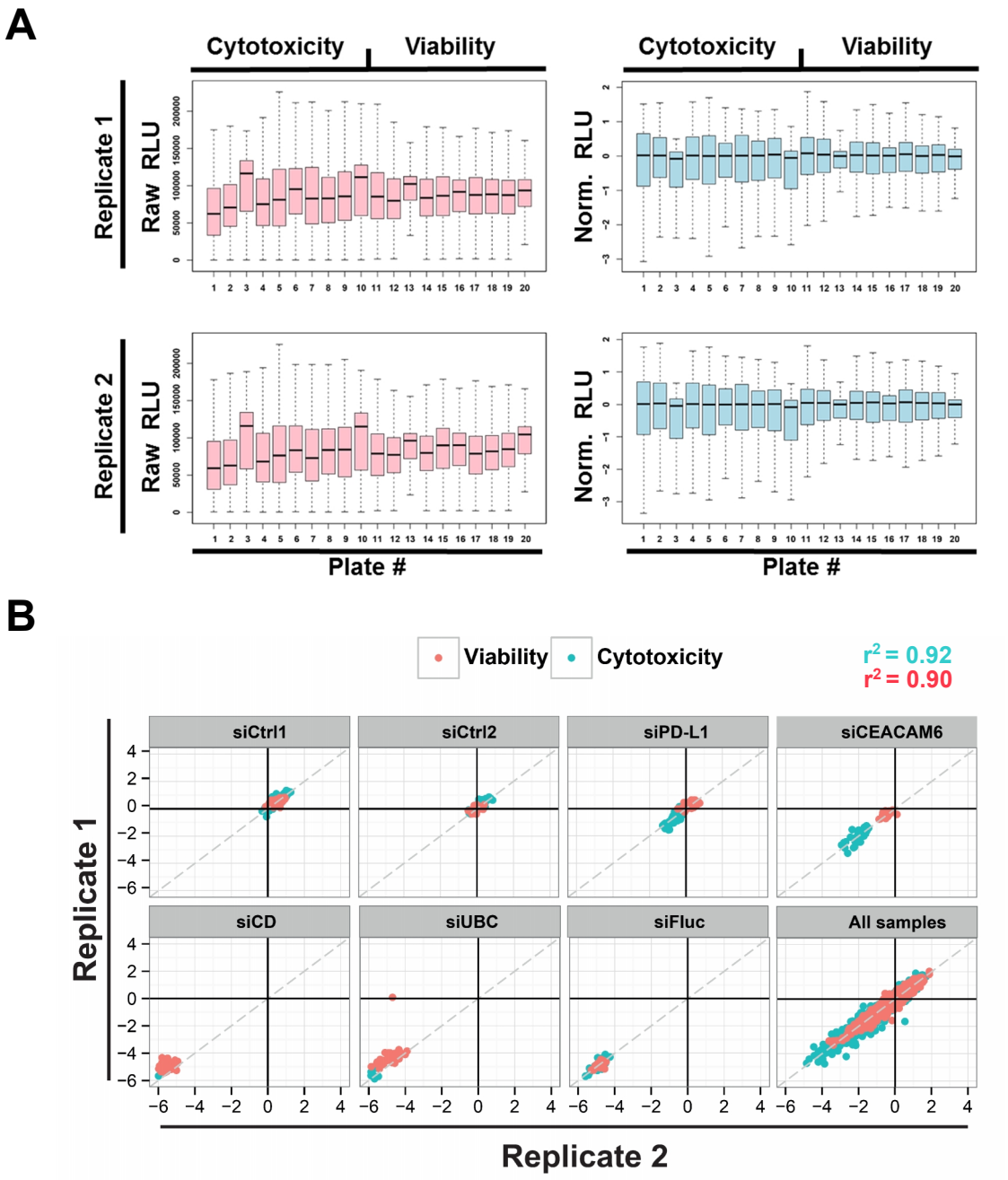

Figure 9. Performance of controls. (A) Raw luciferase activity (RLU) was measured for each well of 40 x 384-well plates (upper and lower left panels). To exclude inter-plate variability, RLUs were normalized using the following formula: Normalized RLU =$\log_2 x/M$, where x is the raw RLU from each well and M is the median RLU value in each plate. For each replicate set, plates from 1 to 10 were co-cultured with TIL#1 at E:T = 25:1 (Cytotoxicity), while plates from 11 to 20 were cultured in the absence of TIL#1 (Viability) **(B)** Controls performance in the HT-screening. Dot plot shows normalized RLUs after transfection of PANC-1-luc cells with several control siRNAs. Technical replicates were plotted against each other. Blue dots: cytotoxicity setting (with TIL#1). Red dots: viability setting (without TIL#1). Pearson correlation (r^2) among the 2 replicate values was calculated for each setting (cytotoxicity setting: r^2 = 0.92; viability setting: r^2 = 0.90).

3.2.2 Gating strategy for hits´ identification

The goal of the screen was to identify potential genes with undescribed role in modulating T cell mediated cytotoxicity. In principle, the screen can unravel both negative and positive modulators of T cell killing. Yet, our analysis was focused on the discovery of novel negative regulators of the immune system, as blockade of this class of proteins has shown improved clinical benefits in several tumor entities [35, 155, 172-174].

To find these potential targets, we first transformed RLU from each gene knockdown in *–z* scores. We then compared the effect of each gene depletion in modulating tumor cell viability versus its capacity in regulating T cell killing. First, genes whose knockdown markedly affected tumor cell viability *per se,* were excluded. Then, only genes showing enhanced TIL-mediated cytotoxicity after knockdown were selected. Our gating strategy is represented in Figure 10A. For the viability setting, we arbitrarily excluded genes showing a –z > 2,0 or –z < 1,0. For the cytotoxicity setting, we considered as potential immune checkpoints only genes whose cytotoxicity score was higher than PD-L1 knockdown. To rank our hits, local regression (LOESS) score for each gene was calculated. LOESS score correlates with the difference between the cytotoxicity and the viability (*–z*) scores and therefore it allows to identify hits whose knockdown show the strongest phenotype (Figure 2B). Based on the LOESS score, we excluded genes with a weaker phenotype than PD-L1 knockdown (Figure 2B).

Before obtaining the final hit-list, a luciferase-independent viability assay, based on the measurement of ATP levels in tumor cells, was used to further exclude genes which are intrinsically affecting cell survival.

Our analysis revealed 155 potential negative regulators of T cell cytotoxicity. Supporting the reliability of our analysis, the hit-list contained several genes with known cancer immune regulatory function such as Interleukin 17 receptor A (IL17RA) [175], interleukin 1 receptor accessory protein (IL1RAP) [176-178], and JAK2 [179]. (Further details are given under section 4.1.2).

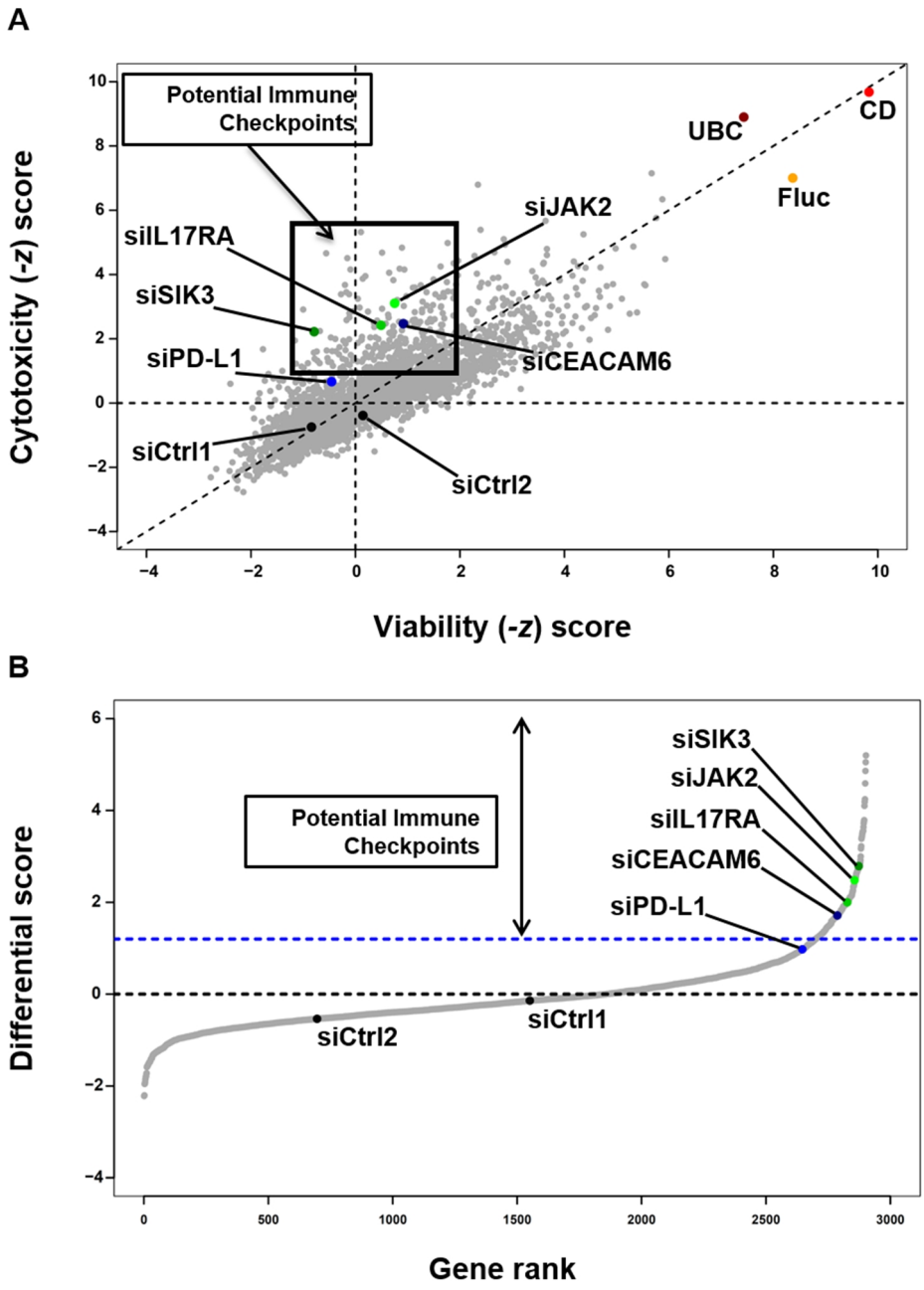

Figure 10. Screening results. (A) Dot plot showing -z scores of plate-normalized RLUs from transfected PANC-1-luc cells after co-culture with TILs (cytotoxicity -*z* score) or with culture medium (viability -*z* score), using a siRNA library of 2514 genes plus controls. Cytotoxicity -*z* score: influence of gene knock-down on TIL-mediated killing. Positive values: decreased cell viability. The black box shows genes which were considered as potential negative immune modulators. **(B)** Differential score between cytotoxicity and viability –z scores using local regression (LOESS) rank. Genes with differential score higher than PD-L1 knockdown were selected as potential negative immune modulators.

3.2.3 Secondary screening

In order to narrow down the generated hit-list, we performed a luciferase-based secondary screening using a library of genes from the primary hit-list. In addition to TIL#1, we used survivin-specific T cell clones to test hits´ performance in an antigen-specific setting (Figure 2D). We confirmed that about 70% of the hits showed the same phenotype as in the primary screening. Notably, we detected high correlation between the two used T cell sources (Pearson correlation = 0.85). Based on the secondary screening results, we refined our hit-list considering only genes whose down-regulation improved T cell mediated cytotoxicity over siCtrl1 transfection, in both the TIL#1 and the survivin TCs-based screens. At the end of this analysis, a hit-list of 108 potential immune modulators was generated (Table 1).

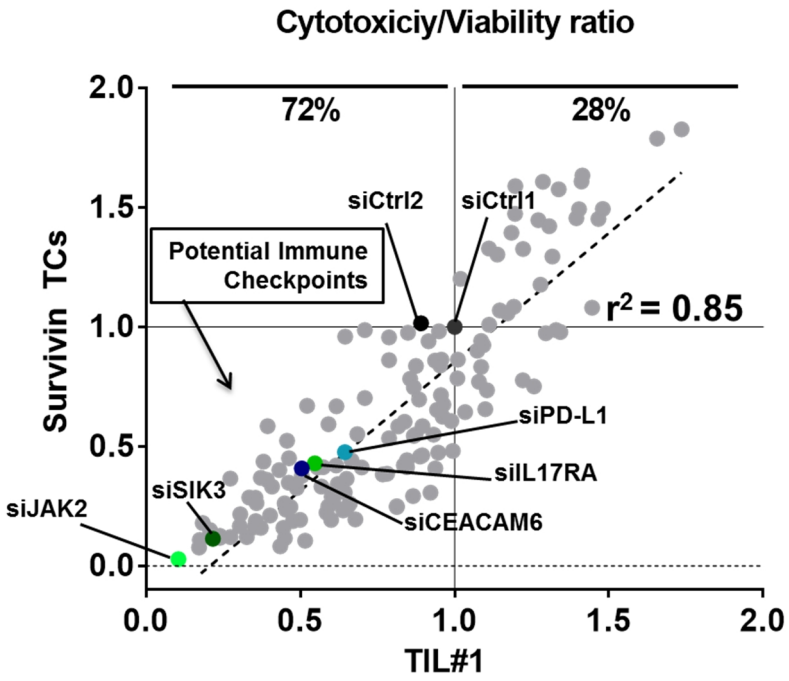

Figure 11. Secondary screening. Luciferase-based secondary screening was performed using the hits obtained from the primary screening. Survivin-specific T cell clones (TCs) were used as an additional T cell source. RLUs were normalized to siCtrl1 and cytotoxicity/viability ratio was calculated (see section 6.2.8.4). R^2: Pearson correlation of cytotoxicity/viability ratios between survivin-specific T cell clones and TIL#1-based screens.

Rank	Hit	Score	Rank	Hit	Score	Rank	Hit	Score
1	JAK2	0,104	37	SCNN1G	0,468	73	AK5	0,787
2	CDC42BPA	0,171	38	IL10RB	0,476	74	GPRC5B	0,788
3	PTPN6	0,174	39	IL36G	0,488	75	PSPH	0,788
4	C16orf87	0,184	40	FAT1	0,499	76	DAPK1	0,813
5	RPS6KC1	0,207	41	ASTL	0,505	77	CCL7	0,813
6	SIK3	0,216	42	OR10H1	0,516	78	LBP	0,817
7	PMVK	0,239	43	LIMK2	0,522	79	PLXNA3	0,836
8	PPP2CB	0,239	44	IL17RA	0,547	80	CDADC1	0,837
9	CD4	0,273	45	HTR1F	0,556	81	OPRK1	0,846
10	AKAP11	0,274	46	GPR78	0,568	82	MAPK8IP3	0,846
11	EDAR	0,303	47	AKAP10	0,574	83	PXK	0,849
12	PRY2	0,305	48	ICAM3	0,585	84	OR7A5	0,856
13	NEK1	0,327	49	SORT1	0,590	85	PIGR	0,866
14	GUCY2D	0,334	50	ULK1	0,591	86	STK16	0,868
15	FGFR3	0,352	51	TLK1	0,600	87	RIPK4	0,868
16	DVL2	0,354	52	NTSR2	0,602	88	SLC2A8	0,873
17	PRPF4B	0,354	53	UCK2	0,606	89	SQSTM1	0,875
18	NEK11	0,355	54	OR5F1	0,617	90	TRHR	0,885
19	TRPM1	0,355	55	CDK5R1	0,617	91	LRP1	0,888
20	DMPK	0,358	56	CASK	0,621	92	GPR3	0,896
21	BEST1	0,372	57	GPR31	0,621	93	XCR1	0,896
22	TNFRSF21	0,372	58	NEK3	0,630	94	GALK1	0,916
23	PLK4	0,381	59	NCOA1	0,639	95	FAS	0,922
24	MLN	0,392	60	WASF2	0,644	96	CCL4L2	0,932
25	KIF1B	0,394	61	PPEF2	0,646	97	OR1C1	0,937
26	TTN	0,402	62	YWHAH	0,650	98	RGS7	0,938
27	SLC5A5	0,408	63	CCR8	0,653	99	NPY5R	0,943
28	ALPK3	0,432	64	HDGF	0,661	100	IFNAR1	0,947
29	FAM195A	0,434	65	CCL4	0,666	101	SNRK	0,950
30	MPL	0,445	66	LGALS3BP	0,679	102	AKAP1	0,953
31	COPB2	0,449	67	SHC3	0,684	103	HCK	0,956
32	CINP	0,449	68	ANGPT4	0,698	104	CTDSP1	0,957
33	LMNA	0,454	69	GDF15	0,709	105	TTBK2	0,961
34	GRB2	0,457	70	PEX13	0,709	106	MED1	0,964
35	MAP4K5	0,462	71	PAPSS2	0,767	107	ULK4	0,990
36	MAST3	0,463	72	GRIN2B	0,781	108	MERTK	0,994

Table 1. Hit-list from the secondary screen. Hits are ranked according to their score in the TIL#1-based screen. Color code: green = hits with stronger phenotype, red = hits with weaker phenotype.

3.3 Hit selection

As the hit-list contained a large number of potential immune checkpoints, we applied the following criteria to select hits for further validation:

- *Undescribed hit´s involvement in tumor immune escape mechanisms*: as mentioned in section 3.2.2, the generated hit-list contained many genes with described immune regulatory function in cancer. These genes were not considered for further validation, whereas genes with undefined roles in cancer immune surveillance were preferred.

- *Differential expression in cancer versus heathy tissues:* we retrieved information on hits´ expression using databases containing transcriptome array and RNA sequencing (RNA-seq) experiments, namely the gene expression database of normal and tumor tissues (GENT) [180], the portal for the genotype-tissue expression (GTEx) [181], and the Oncomine ™ database [182]. Additionally we interrogated the Human Protein Atlas database to assess hits´expression in immunohistochemical sections of cancer and healthy tissues [183]. We selected hits showing higher expression in tumor biopsies over healthy tissues, or proteins that are ectopically expressed in tumors and are not present in the majority of healthy tissues.

- *Hit´s druggability*: as the long-term aim of this project was to identify novel targets for cancer immunotherapy, we prioritized genes encoding for proteins associated with the plasma membrane, which could be easily targeted with biological drugs; alternatively we selected specific classes of intracellular proteins, such as protein kinases, which could be targeted with small molecule inhibitors [184].

After an extensive literature search, we selected 11 hits for phenotypic verification (Table 2).

HIT	Name	Localization
SIK3	Salt-inducible kinase 3	Cytoplasm
NTSR2	Neurotensin receptor 2	Surface
MLN	Motilin	Extracellular
MAST3	Microtubule associated serine/threonine kinase 3	Cytoplasm
IL36G	Interleukin-36 gamma	Extracellular
LIMK2	LIM domain kinase 2	Cytoplasm
CDC42BPA	CDC42 binding protein kinase alpha	Cytoplasm
GPR31	G-protein coupled receptor 31	Surface
FAM195A	Family with sequence similarity 195, member A	Unknown
ASTL	Astacin-like metallo-endopeptidase	Surface & Extracellular
FAT1	Atypical cadherin 1	Surface & Extracellular

Table 2. List of selected hits for further validation analysis and their cell localization.

3.3.1 Hits´ expression in tumor cell lines

As first validation step, we checked the expression of selected candidate molecules in PANC-1 cells and additional tumor cell lines, namely MCF7 (breast carcinoma), M579 (melanoma), HEK293 (human embryonic kidney) and Caco-2 (colorectal adenocarcinoma). Hits expression was measured at mRNA level using conventional PCR (Figure 12) We detected abundant expression of 6 hits, namely SIK3, MAST3, LIMK2, CDC42BPA, FAT1 and FAM195A in all tested cell lines (Figure 12A). ASTL is a metalloprotease whose expression is exclusively observed in the oocyte *zona pellucida* [185]. Interestingly, all tested tumor cells showed weak but consistent ASTL expression.

Expression of NTSR2 was only detected in PANC-1 and MCF7, whereas GPR31 mRNA was found at low levels in PANC-1, M579 and HEK293 cells. Although showing expression in several tumor cell lines, IL36G was not found in PANC-1 cell lines, hinting

that the phenotype observed in the screening, after IL36G-specific siRNA transfection, was caused by siRNA off-target effects. For this reason, IL36G was excluded from further analysis.

MLN is a 22-amino acid long polypeptide hormone, which is secreted by endocrine M cells in the small intestine [186]. PANC-1 cells showed ectopic expression of this hormone, suggesting its potential role as an immune suppressor (Figure 12 B).

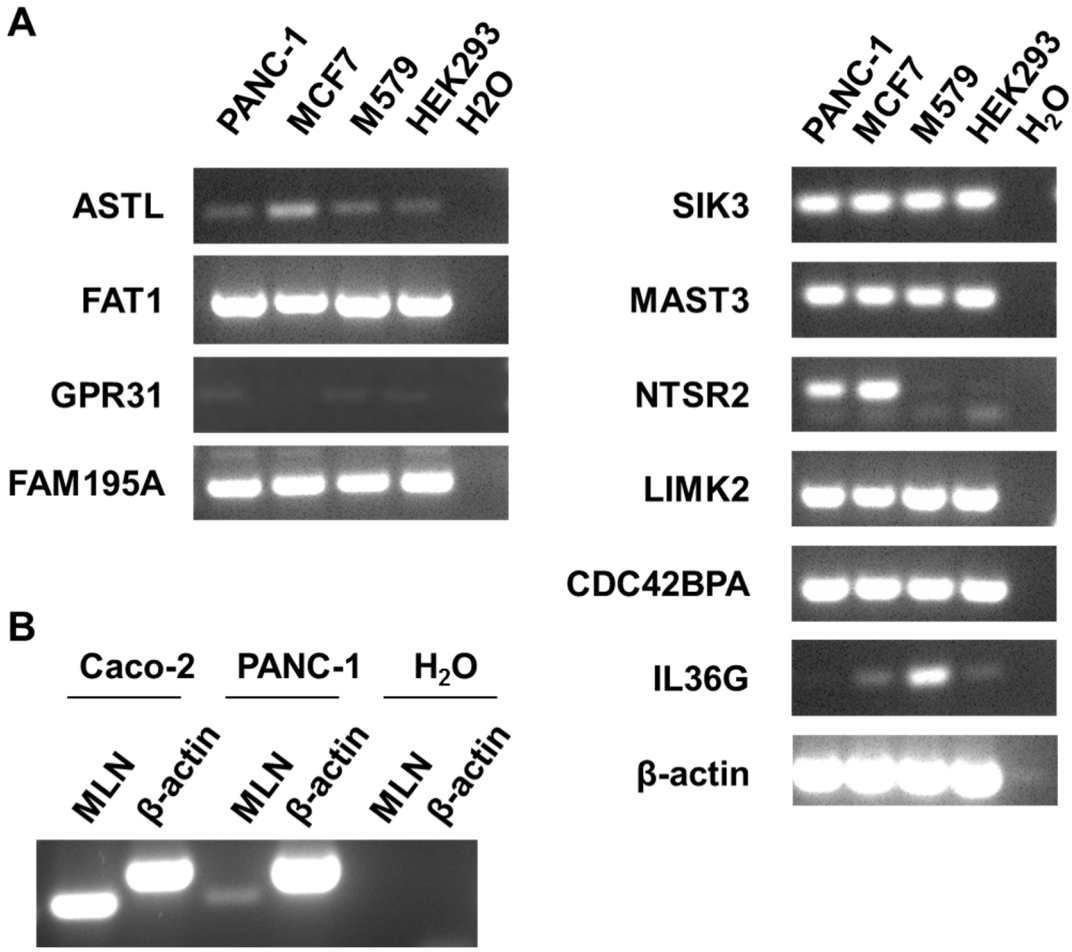

Figure 12. Expression of hits in various tumor cell lines. **(A)**. Conventional PCR was performed in PANC-1, MCF7, M579 (melanoma) and HEK293 for detection of ASTL, FAT1, GPR31, FAM195A, SIK3, MAST3, NTSR2, LIMK2, CDC42BPA and IL36 transcripts. **(B)** Caco-2 and PANC-1 cells were tested for MLN expression. β-actin was used as house-keeping gene. H_2O served as no template control. Exemplary data of two independent assays. Experiments were conducted by Ayse Nur Menevse (Prof. Beckhove´s group) under my supervision.

3.3.2 Verification of siRNA on-target effect for selected hits

One of the major drawbacks of RNAi-based screens is the occurrence of off-target gene silencing [187, 188]. Off-target effects arise from unspecific binding of siRNAs to other RNAs in the cytosol. A possible consequence of this phenomenon is that the observed phenotype in the screen is elicited by siRNA-mediated silencing of an unrelated mRNA or non-coding RNA. To exclude this possibility, we transfected PANC-1-luc cells either with four single siRNAs targeting the same hit or with the siRNA pool used in the screen. We then conducted luciferase-based killing assay using TIL#1 or survivin-specific T cell clones, as indicated in Figure 13. The assay was performed for the 10 selected hits and results were compared to PD-L1 knockdown. On-target effect was only attributed to genes whose knockdown led to increased T cell-mediated killing with at least two single siRNA sequences. We further excluded siRNA sequences showing more than 40% viability effect in the absence of T cells.

We observed that transfection with three out of four SIK3-specific single siRNAs (s1, s2, s3) or siRNA pool, increased cytotoxicity mediated by TIL#1 or survivin-specific TCs. As observed in the screen, the effect was stronger than PD-L1 downregulation (Figure 13A). Two out of four MAST3-targeting siRNAs (s3, s4) improved T cell-mediated killing after addition of TIL#1 while the phenotype was confirmed with four out of four siRNA sequences when using survivin-specific TCs (Figure 13B). ASTL knockdown showed the same phenotype as in the screening using s1 and s3 siRNA sequences, while s2 and s4 sequences were excluded because of their high viability impact (Figure 13C). Transfection with three MLN-specific siRNAs (s1, s2, s3) enhanced T cell-mediated killing, while s4 and pool strongly affected tumor cell viability (Figure 13D).

The remaining hits, namely FAT1, NTSR2, LIMK2, CDC42BPA, GPR31 and FAM195A, were excluded from further analysis either because only one out of four siRNA showed increased T cell-mediated killing or because more than one siRNA showed the phenotype but viability effect was stronger than 40% (Figure 13E - L).

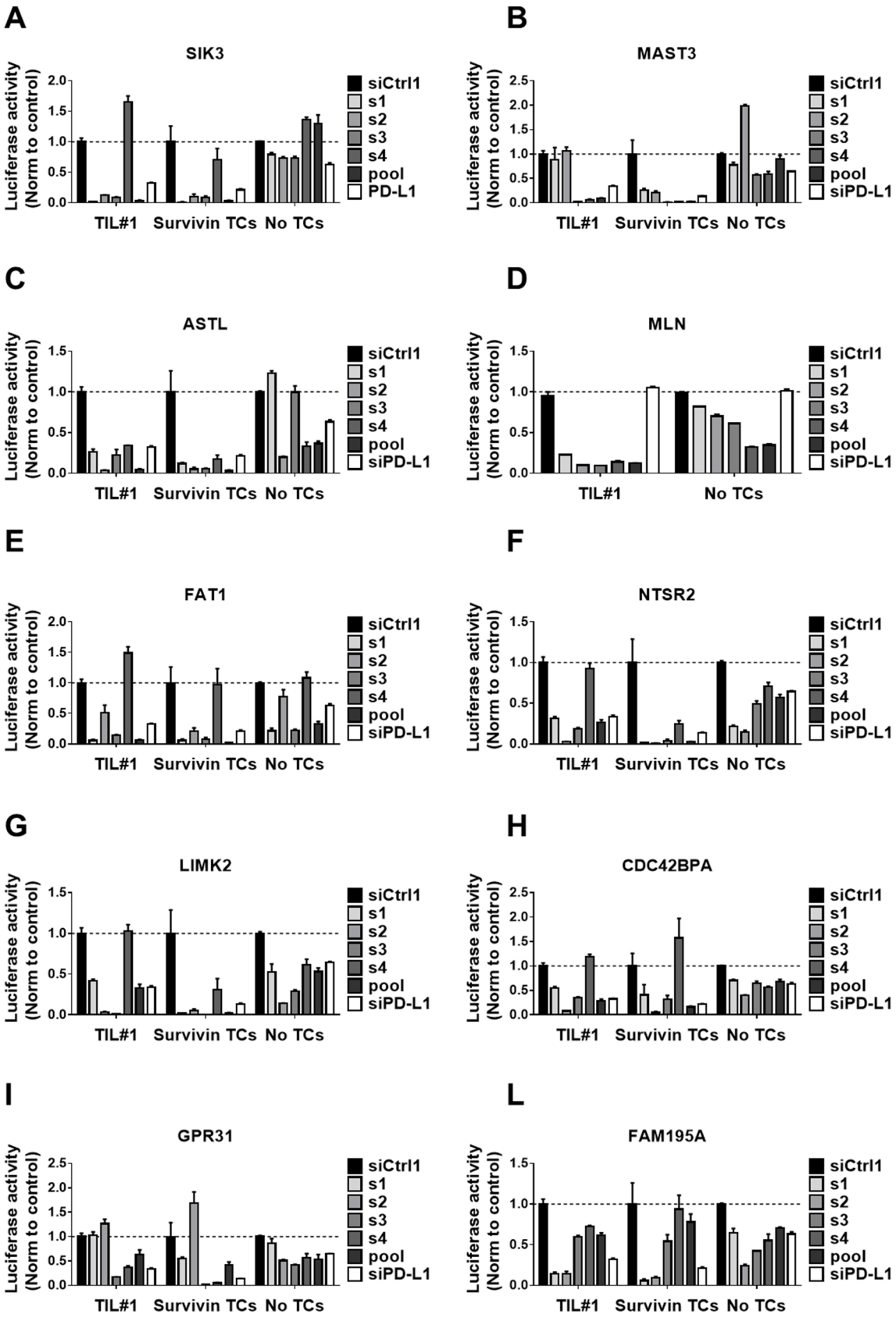
A
SIK3
Luciferase activity (Norm to control)
siCtrl1
s1
s2
s3
s4
pool
PD-L1
TIL#1
Survivin TCs
No TCs
B
MAST3
siPD-L1
C
ASTL
D
MLN
E
FAT1
F
NTSR2
G
LIMK2
H
CDC42BPA
I
GPR31
L
FAM195A

Figure 13. Validation of siRNA on-target effect. PANC-1-luc cells were transfected either using single (s1-s4) or pooled non-overlapping siRNAs targeting **(A)** SIK3, **(B)** MAST3, **(C)** ASTL, **(D)** MLN, (**E)** FAT1, **(F)** NTSR2, **(G)** LIMK2, **(H)** CDC42BPA, **(I)** GPR31 and **(L)** FAM195A. Control siRNA (siCtrl1) was used as negative control whereas siPD-L1 served as positive control. Transfected cells were co-cultured either with TIL#1 at 50:1 E:T ratio or, with survivin-specific TCs at 5:1 E:T ratio for the cytotoxicity setting. For the viability setting, only culture medium was added, instead of T cells. T cell-mediated cytotoxicity was measured using luciferase-based cytotoxicity assay. Values were normalized to siCtrl in each setting. Graphs show median +/- SEM. Representative data of at least two independent experiments. Experiments were conducted by Ayse Nur Menevse (Prof. Beckhove´s group) under my supervision.

Based on these data, SIK3, MAST3, ASTL and MLN were selected for further validation.

We sought to evaluate siRNA knockdown efficiency after transfection of tumor cells with single or pooled siRNAs. We performed qPCR to measure mRNA abundance and, for SIK3 and MAST3, we evaluated knockdown at protein level using western blot (Figure 14). Transfection with SIK3-specific siRNAs resulted in significant SIK3 mRNA reduction, ranging from 60% to 80%, depending on the used siRNA sequence (Figure 14A, left panel). Despite the variability in knockdown efficiency at mRNA level, SIK3 protein level was remarkably reduced after transfection with each tested siRNA (Figure 14A, right panel). MAST3-specific siRNAs showed knockdown efficiency ranging from 55% to 85% at mRNA level (Figure 14B, left panel), while MAST3 protein was undetectable after siRNA transfection (Figure 14B, right panel).

ASTL depletion with several siRNAs showed similar results to SIK3 and MAST3 (Figure 14C), while detection of MLN depletion after siRNA transfection, was complicated by its low mRNA abundance in wild type or siCtrl1-transfected PANC-1 cells. For instance, we were unable to detect MLN mRNA level after transfection with s1 siRNA, because its abundance was below the detection limit of the assay. However, we observed reduction of MLN transcripts ranging from 55% to 90% with other siRNA sequences (Figure 14D).

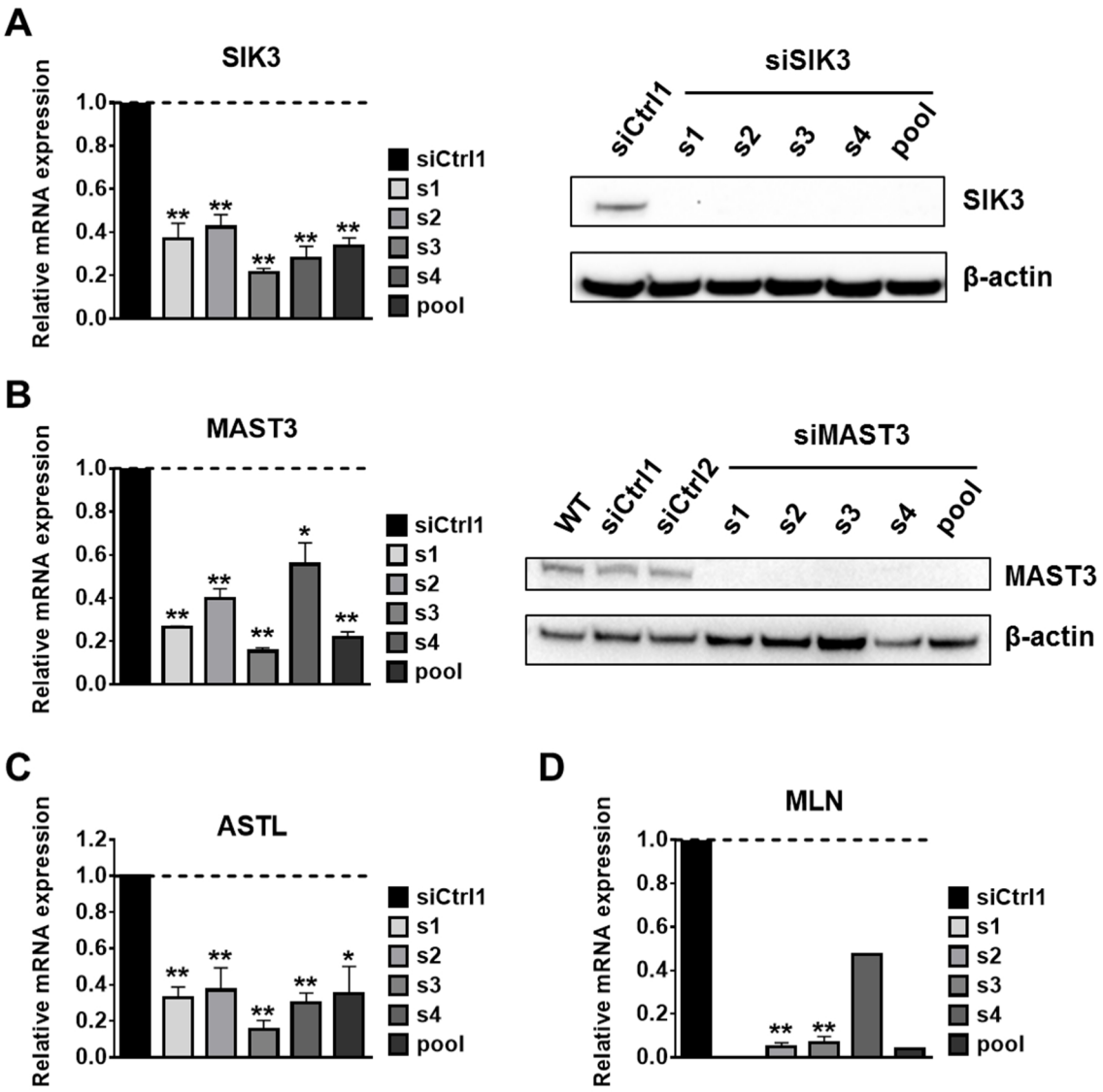

Figure 14. Evaluation of knockdown efficiency of several hit-specific siRNAs. Analysis of knockdown efficiency of siRNAs targeting **(A, left panel)** SIK3, **(B, left panel)** MAST3, **(C)** ASTL, **(D)** MLN. PANC-1 cells were transfected with single (s1-s4) or pooled siRNA, and 72h later mRNA expression levels were determined by qPCR. Results are presented in terms of fold change after normalizing to β-actin mRNA. **(A and B, right panel)** Western blot analysis for detection of SIK3 and MAST3 protein levels after 72h transfection of PANC-1 cells with single (s1-s4) or pooled siRNAs. Wild type (WT) or scramble sequences (siCtrl1, siCtrl2) were used as negative controls. (A, left panel) Cumulative data of three independent experiments. (A, right panel, B, C and D) Representative data of at least two independent experiments. Columns show mean +/- SEM. P-values were calculated using two-tailed student´s t-test. * $p < 0.05$, ** $p < 0.01$. Experiments were conducted in collaboration with Ayse Nur Menevse (Prof. Beckhove´s group) and Dr.Katharina Jeltsch (Prof. Beckhove´s group).

To increase the confidence of selected candidate genes as reliable hits, we conducted chromium release assay as independent method to measure T-cell mediated killing. For this assay, PANC-1 cells were transfected with several hit-specific siRNAs and co-cultured with TIL#2 for 6h. In all cases, siRNA transfection with 3 hit-specific sequences or with pooled siRNA enhanced target cells lysis by T cells over scramble transfected tumor cells (siCtrl1) (Figure 15A-D). CEACAM6 depletion was used as positive control.

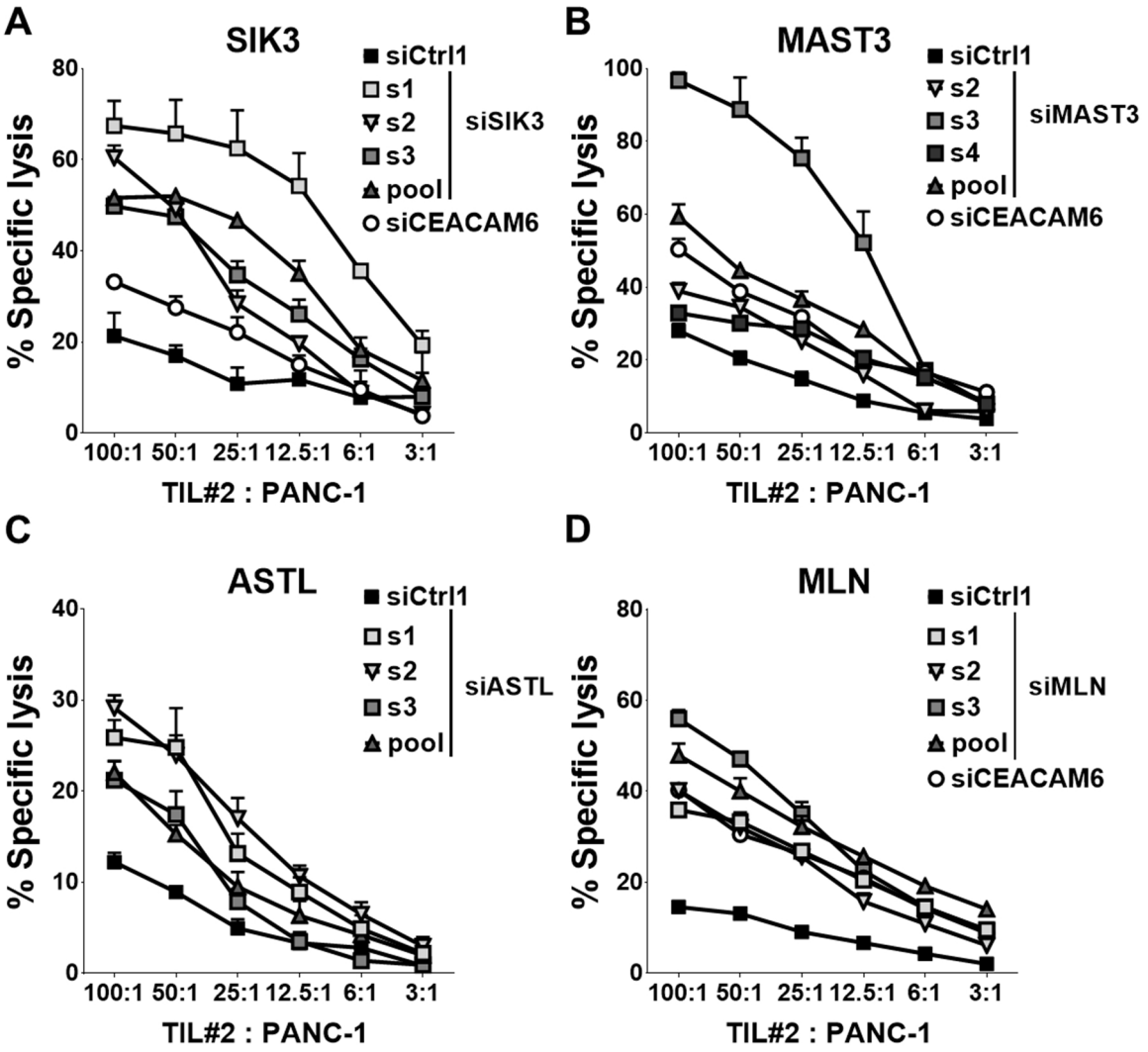

Figure 15. Assessment of T cell-mediated killing upon knockdown of selected HITs by chromium release assay. PANC-1 cells were transfected either using single non-overlapping siRNAs or pooled siRNAs targeting **(A)** SIK3, **(B)** MAST3, **(C)** ASTL and **(D)** MLN. Scramble siRNA was used as negative control whereas CEACAM6 knockdown was used as positive control. Tumor cells cell were co-cultured withTIL#2 for 6h. Data indicate mean +/- SEM. Representative data of at least two independent experiments.

In summary, we successfully validated the role of SIK3, MAST3, ASTL and MLN as novel regulators of T cell-mediated cytotoxicity. For each target, at least 2 non-overlapping siRNAs showed efficient gene silencing, which resulted in increased T cell mediated killing both in luciferase-based and in chromium release assays.

3.4 SIK3 is a novel immune modulator in solid tumors

Based on the strength of the phenotype observed in the screens (section 3.2), as well as in the validation assays (section 3.3), SIK3 was selected for detailed analysis of its function as novel immunosuppressive protein and its translational relevance. SIK3 was the 14th strongest hit both in melanoma and PDAC screens, whereas it was the sixth candidate in the secondary screen. SIK3 is a serine/threonine kinase involved in cell cycle progression and tumorigenesis [189, 190]. Analysis of patient´s tumor microarray data from the Oncomine^{TM} database, revealed SIK3 overexpression in several tumors such as breast and colorectal cancer, compared to healthy tissues. Furthermore, immunohistochemical (IHC) studies indicated that SIK3 is highly expressed in ovarian cancer [189]: Interestingly, its role in mechanisms of cancer immune evasion remains elusive.

3.4.1 SIK3 depletion does not affect tumor cell viability *per se*.

In the last sections, it was shown that SIK3 depletion with three single siRNAs, as well as with pooled siRNA, strongly increased lysis of PANC-1 tumor cells after co-culture with several T cell sources (Figure 13A and 15A).

However, in the absence of T cells, the effect of SIK3 knockdown on tumor cells depended on the utilized siRNA sequence, with s1, s2 and s3 showing only slight reduction of cell viability, while the pool siRNA moderately increased cell survival (Figure 13A). To accurately evaluate the intrinsic viability impact of SIK3 on PANC-1 cells, the water-soluble tetrazolium salts-1 (WST-1) viability assay was performed. As expected, transfection with several SIK3-specific siRNAs did not significantly alter viability of PANC-1 cells (Figure 16).

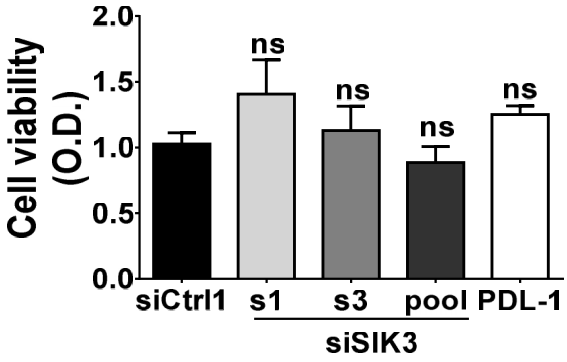

Figure 16. Effect of SIK3-specific siRNA sequences on tumor cell viability. WST-1 assay. PANC-1 cells were transfected with indicated siRNAs for 72h. Data were normalized to siCtrl1. Cumulative data of three independent experiments. Columns show mean +/- SEM. P-values were calculated using two-tailed student´s t-test. ns = not significant.

3.4.2 Increased T cell-mediated killing upon SIK3 knockdown in several tumor entities

After having excluded that SIK3 depletion intrinsically affects tumor cell viability, we sought to investigate the role of this kinase as modulator of T cell killing in additional co-culture models. We knocked down SIK3 in breast (MCF-7) and colorectal (SW480) cancer cell lines and challenged them either with survivin-specifc TCs or with TIL#1, respectively. In both cases, depletion of SIK3 increased tumor cell death as measured by real-time live-cell microscopy (Figure 17A and 17B).

In a primary melanoma co-culture model, we observed that SIK3 knockdown potentiated TIL-mediated cytotoxicity both using TIL209 (Figure 17C) and TIL412 (Figure 17D). These data suggest that SIK3 plays a role as an immune modulator in several tumor entities.

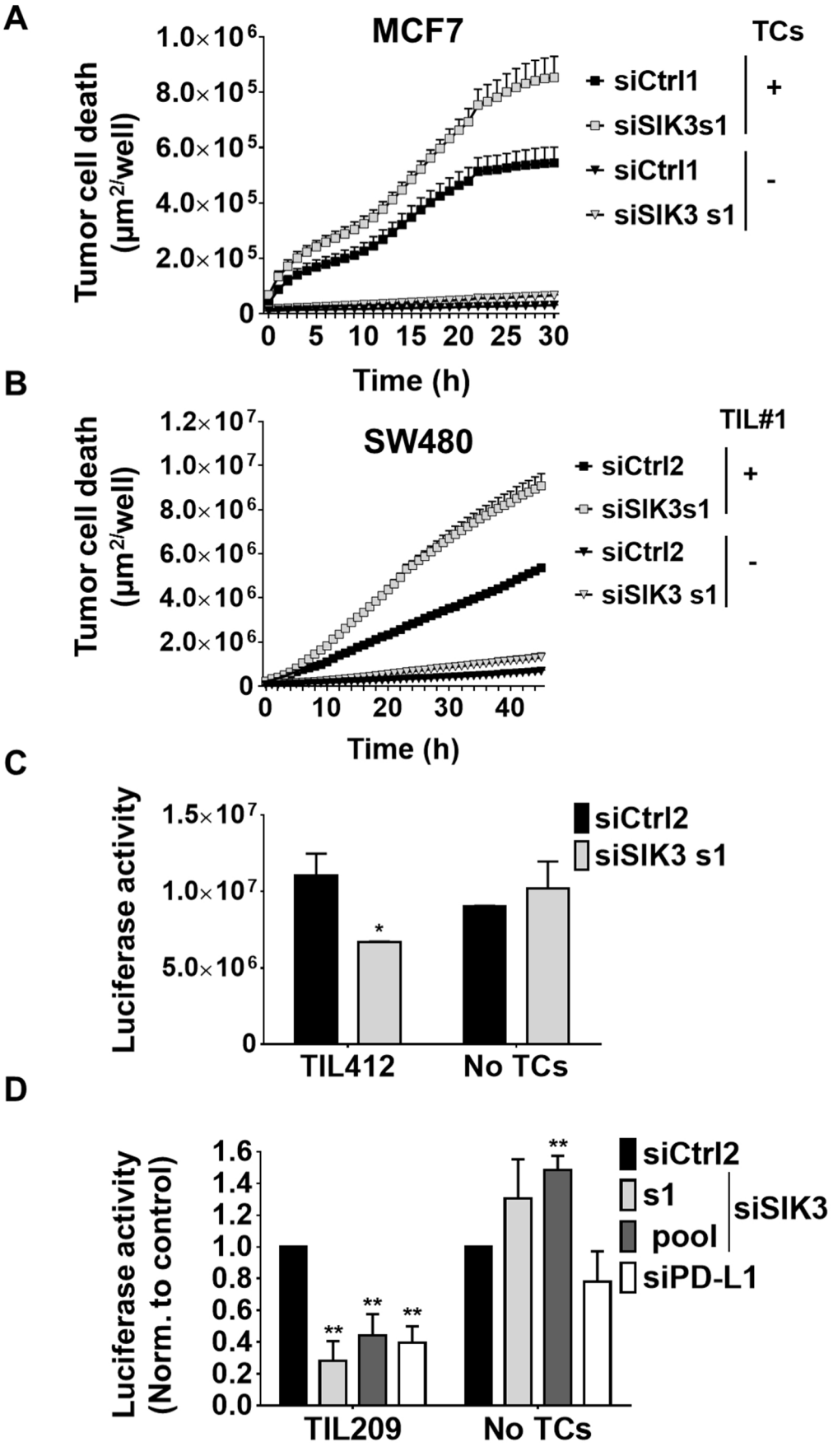
A
MCF7
TCs
Tumor cell death (µm²/well)
1.0×10⁶
8.0×10⁵
6.0×10⁵
4.0×10⁵
2.0×10⁵
0
0 5 10 15 20 25 30
Time (h)
siCtrl1
siSIK3s1
siCtrl1
siSIK3 s1
+
-
B
SW480
TIL#1
Tumor cell death (µm²/well)
1.2×10⁷
1.0×10⁷
8.0×10⁶
6.0×10⁶
4.0×10⁶
2.0×10⁶
0
0 10 20 30 40
Time (h)
siCtrl2
siSIK3s1
siCtrl2
siSIK3 s1
+
-
C
Luciferase activity
1.5×10⁷
1.0×10⁷
5.0×10⁶
0
*
TIL412
No TCs
siCtrl2
siSIK3 s1
D
Luciferase activity (Norm. to control)
1.6
1.4
1.2
1.0
0.8
0.6
0.4
0.2
0.0
**
**
**
**
TIL209
No TCs
siCtrl2
s1
pool
siPD-L1
siSIK3

Figure 17. SIK3 depletion increases T cell-mediated killing in several tumor entities. (A and B) Real-time live cell microscopy for the evaluation of tumor cell death using YOYO-1 dye. 72h from siRNA transfection, MCF-7 **(A)** and SW480 **(B)** were co-cultured either with survivin T cell clones (E:T = 1:1) or with TIL#1 (E:T = 12,5:1), respectively. Graph shows the area of YOYO-1+ cells/well (μm^2/well). **(C and D)** M579-luciferase expressing melanoma cells were transfected with indicated siRNAs and co-cultured either with **(C)** TIL412 (E:T = 5:1) or **(D)** TIL209 (E:T = 5:1). Luciferase-based killing assay was performed 20h after co-culture. Representative data of at least two independent experiments. Columns show mean +/- SEM. P-values were calculated using two-tailed student´s t-test. * $p < 0.05$, ** $p < 0.01$.

3.4.3 SIK3 overexpression reduces T cell-mediated killing

Next, we aimed to investigate whether overexpression of SIK3 correlated with poor immune response. Hence, we transfected patient-derived M579 melanoma cells with SIK3 overexpression plasmid. SIK3 overexpression resulted in about 80 times mRNA increase in melanoma cells (Figure 18A). We then challenged tumor cells with TIL209 culture and performed luciferase-based killing assay. Coherently with our previous observations, SIK3 overexpression did not affect tumor cell viability but rendered tumor cells less susceptible to T cell-mediated killing (Figure 18B).

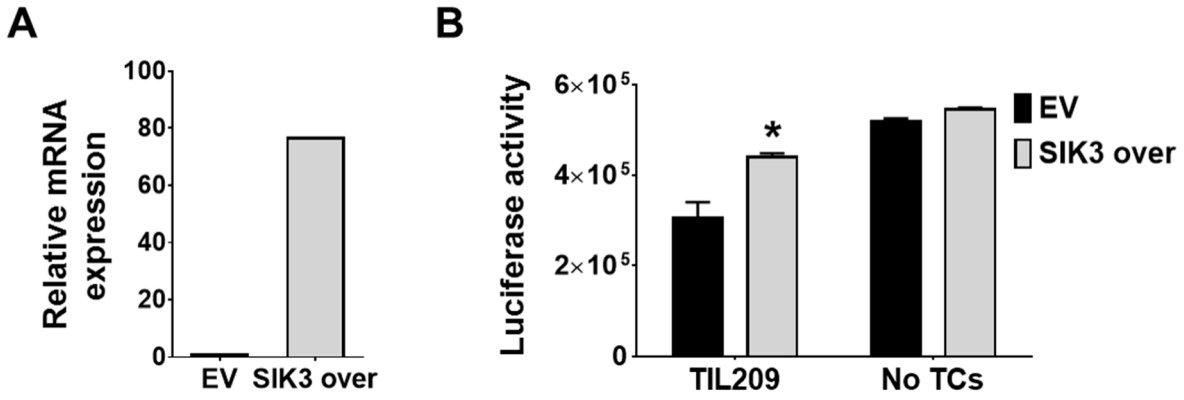

Figure 18. Overexpression of SIK3 increases resistance to T cell attack. (A) qPCR analysis of SIK3 mRNA expression in M579 cells after transfection with either overexpression plasmid (SIK3 over) or control vector (EV) for 48h. Results are presented in terms of fold change after normalizing to β-actin mRNA. Representative data of at least two independent experiments. (B) M579 cells were transfected as in (A) and challenged with TIL209 (E:T = 1:1) or control medium for 48h. Then, luciferase-based killing assay was performed. Columns show mean +/- SEM. P-values were calculated using two-tailed student´s t-test. * $p < 0.05$, ** $p < 0.01$.

3.4.4 Inhibition of SIK3 with a small molecule compound recapitulates the effect of SIK3 gene silencing

In order to prove the role of SIK3 as potential therapeutic target in cancer, we evaluated the effect of SIK3 inhibition with the small molecule compound HG-9-91-01. PANC-1-luc cells were co-cultured with TIL#1 in the presence of increasing concentrations of the SIK3 inhibitor. We detected a dose-dependent improved TIL-mediated killing after treatment with HG-9-91-01 (Figure 19A). As this compound targets SIK1 and SIK2 isoforms as well [191], we evaluated the individual impact of SIK isoforms in modulating T cell-mediated cytotoxicity. Knockdown of SIK1 and SIK2 did not improve T cell-mediated killing in luciferase-based kill assay (Figure 19B). These data imply a specific role of SIK3 in tumor escape mechanisms.

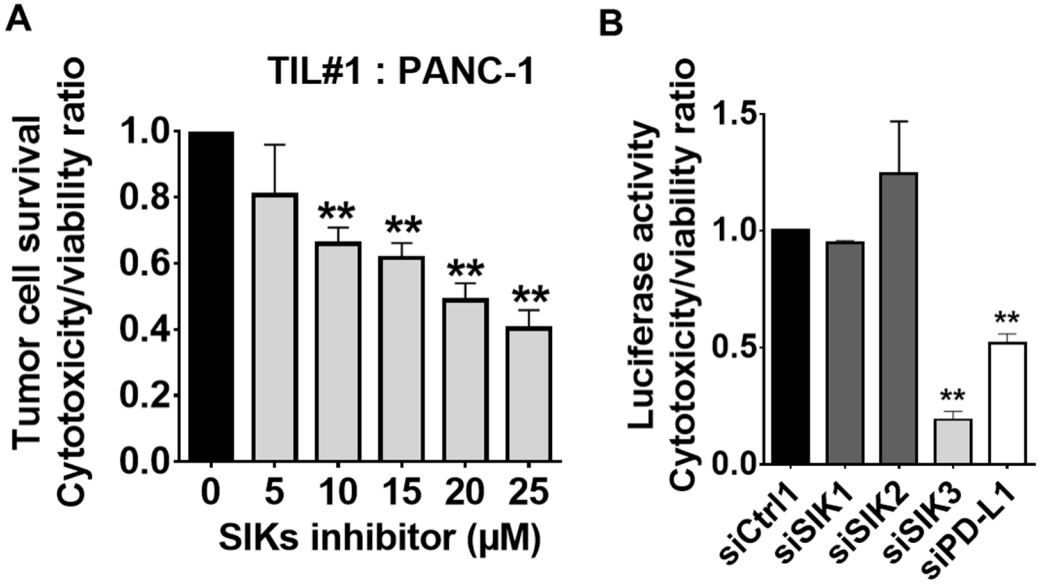

Figure 19. SIK3 inhibition enhances T cell attack. (A) PANC-1-luc cells were co-cultured with TIL#1 (E:T = 50:1) in the presence of indicated concentrations of the SIK inhibitor HG-9-91-01 for 20h. T cell mediated cytotoxicity was measured by luciferase-based killing assay and data were normalized using cytotoxicity/viability ratio (see section 6.2.8.4). **(B)** PANC-1-luc cells were transfected with pool siRNA targeting SIK isoforms, scramble siRNA (siCtrl) or PD-L1-specific siRNA pool for 72h. TIL#1 were co-culture with transfected tumor cells at E:T = 25:1 and T-cell mediated cytotoxicity was measured as in **(A)**. **(A)** Cumulative data of three independent experiments, **(B)** representative data of two independent experiments. Columns show mean +/- SEM. P-values were calculated using two-tailed student´s t-test. * $p < 0.05$, ** $p < 0.01$.

3.4.5 SIK3 depletion in tumor cells does not alter T cell activation

Next, we wanted to identify the mode by which SIK3 mediates resistance to immune cell attack. Cancer cells can exploit several mechanisms to evade immune-mediated destruction [192, 193]. Such mechanisms either dampen immune cell functionality or confer intrinsic tumor resistance to effector molecules secreted by immune cells (section 1.3). We first investigated whether SIK3 impairment in tumor cells resulted in enhanced T cell activity and cytotoxic potential. We measured interferon-γ production by T cells, as this cytokine is a marker of T cell activation and differentiation towards Th1 phenotype [70]. However, knockdown of SIK3 in tumor cells resulted in either slight reduction or non-significant alteration of IFN-γ secretion by antigen-specific T cells (Figure 20A). We then assessed the role of SIK3 in the regulation of canonical cytotoxic effector proteins secreted by T cells [194]. Of note, we did not observe increased release of either perforin or granzyme B from T cells after co-culture with SIK3-depleted tumor cells (Figure 20B - D). This data suggested that SIK3 impairment in tumor cells does not regulate T cell activation and functionality.

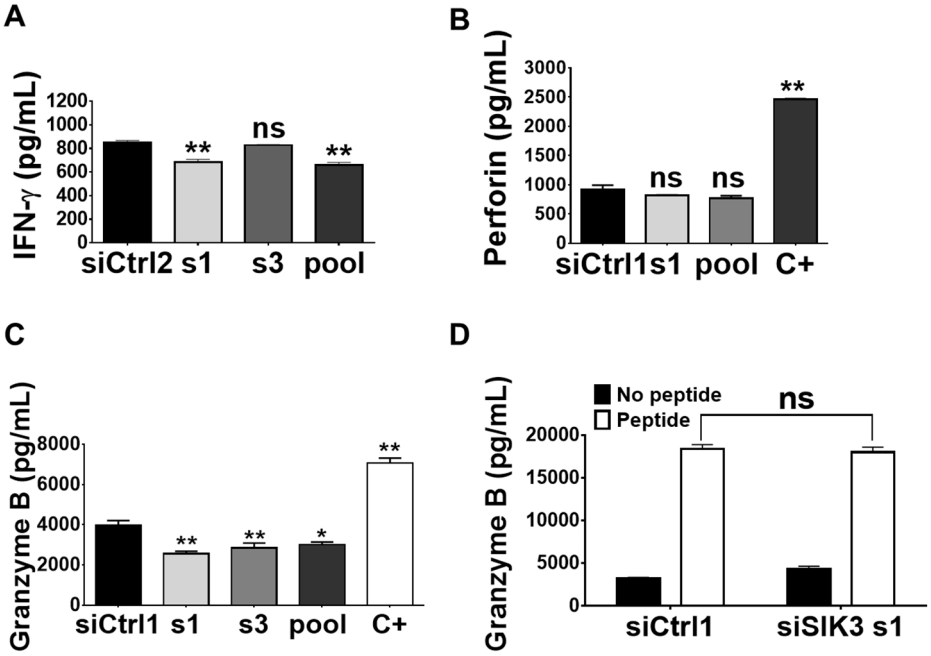

Figure 20. SIK3 depletion in tumor cells does not increase T cell activation. (A) IFN-γ ELISA. PANC-1 cells were transfected with the indicated SIK3-specific siRNAs (s1, s3, pool) or scramble siRNA (siCtrl2) for 72h. Afterwards survivin-specific TCs were added (E:T = 5:1) and INF- γ secretion was measured 20h from co-culture. **(B)** Perforin ELISA. M579 cells were transfected as in (A) and co-cultured with TIL209 (E:T = 5:1). Perforin secretion was detected

20h after co-culture. Phorbol 12-myristate 13-acetate (PMA)/ Ionomycin stimulation served as positive control (C+). **(C-D)** Granzyme B ELISA. **(C)** PANC-1 cells were transfected as in **(A)** and TIL#1 was added at E:T = 50:1. Granzyme B secretion was measured 20h from co-culture. **(D)** PANC-1 cells were transfected as in **(A)** and then flu-antigen specific T (FluT) cells were added in the presence or the absence of flu-peptide (E:T = 5:1). Granzyme B secretion was measured as in **(C)**: Representative data of two independent experiments. Columns show mean +/- SEM. P-values were calculated using two-tailed student´s t-test. * $p < 0.05$, ** $p < 0.01$. **(D)** Was performed by Ayse Nur Menevse (Prof. Beckhove´s group).

3.4.6 SIK3 mediates intrinsic tumor resistance to T cell attack

Given the results in the last paragraph, we hypothesized that SIK3 is involved in intrinsic mechanisms of tumor resistance towards T cell effector molecules. To prove this, we treated SIK3-depleted PANC-1 cells with the supernatant of activated TILs. T cell activation was induced either after co-culture with tumor cells (Figure 21B) or with anti-CD3/CD28 beads (Figure 21C). Paradoxically, addition of supernatant from CD3/CD28 bead-activated T cells resulted in increased proliferation of SIK3 proficient tumor cells (siCtrl1-transfected tumor cells). However, SIK3 depletion induced dramatic cell death after tumor cell stimulation with the same supernatant (Figure 21C). This effect was reproducible when siRNA-transfected tumor cells were treated with the supernatant from T cells that were pre-activated with tumor cells (Figure 21B). In this case, the effect after SIK3 depletion was weaker than in the experiment using polyclonally activated T cells, because of the different degree of T cell activation in the two settings.

Coherently with our hypothesis, supernatant of unstimulated T cells did not alter tumor cell survival after SIK3 siRNA transfection (Figure 21A). Using an independent viability assay, we recapitulated the decreased tumor cell viability after SIK3 depletion and stimulation with supernatant of polyclonally activated T cells (Figure 21D). PD-L1 knockdown did not sensitize tumor cells towards T cell effector molecules, confirming its involvement in mechanisms of T cell activation rather than intrinsic tumor cell resistance towards T cell attack [169, 195, 196].

These data suggest that SIK3 is a pivotal intrinsic mediator of tumor cell resistance towards cytotoxic molecules released by activated T cells.

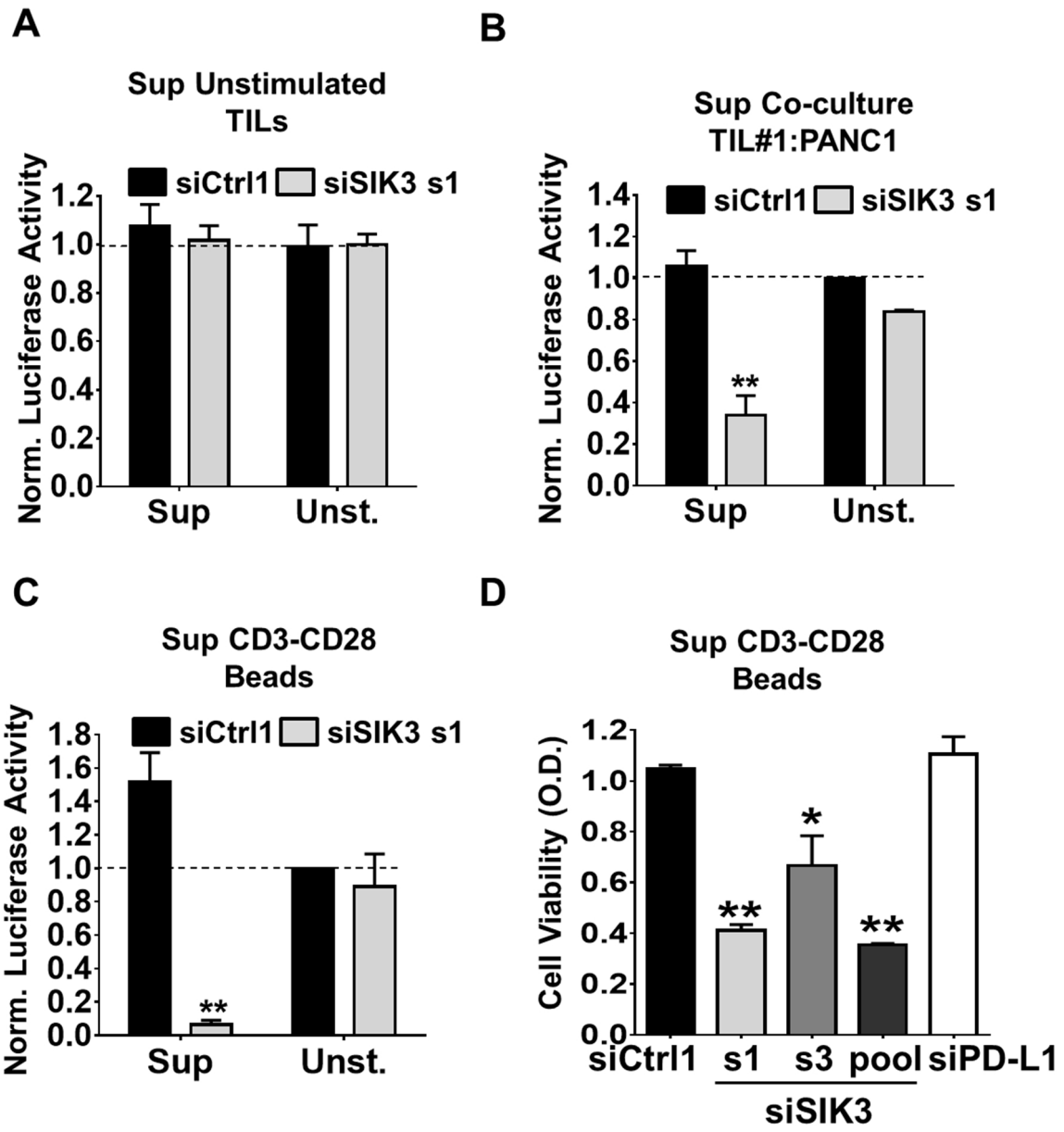

Figure 21. SIK3 intrinsically mediates tumor resistance to T cell effector molecules. (A-C) PANC-1-luc cells were transfected either with siSIK3 s1 (light grey bar) or with the indicated siRNA sequences. After 72h, tumor cells were treated with the supernatant (Sup) of **(A)**unstimulated, **(B)** tumor-activated, or **(C)** CD3/CD28 bead-activated TIL#1. For each setting, transfected tumor cells were treated with culture medium as negative control (Unst.). 20h after stimulation, the effect of the supernatant on tumor cell cytotoxicity was measured using luciferase-based killing assay. Data are represented as fold change luciferase activity compared to unstimulated siCtrl1. **(D)** WST-1 assay. PANC-1 cells were transfected with indicated siRNAs for 72h. Afterwards, supernatant of CD3/CD28 TILs was added as in **(C)**. Data were normalized to siCtrl1. **(A, B)** Representative data of at least two independent experiments. **(C-D)** Cumulative data of three independent experiments. Columns show mean +/- SEM. P-values were calculated using two-tailed student´s t-test. * $p < 0.05$, ** $p < 0.01$.

3.4.7 Identification of T cell effector molecules upstream SIK3

Upon activation, CD8+ T cells secrete different effector molecules that are endowed with cytotoxic ability [197-200]. Each factor induces different pathways in tumor cells, which ultimately culminate in caspase activation and apoptosis induction [201-203]. We aimed to identify which effector molecule mediates the increased cytotoxicity in SIK3 knockdown cells.

Therefore, we blocked TNF- α, TRAIL and FASL in the supernatant of CD3/CD28 bead-activated T cells and subsequently subjected siRNA-transfected tumor cells to this supernatant. We observed that the neutralization of FASL or TRAIL did not prevent tumor cell death in SIK3 deficient cells. On the contrary, TNF-α blockade, partially abrogated the cytotoxic potential of the activated supernatant on SIK3 depleted cells (Figure 22).

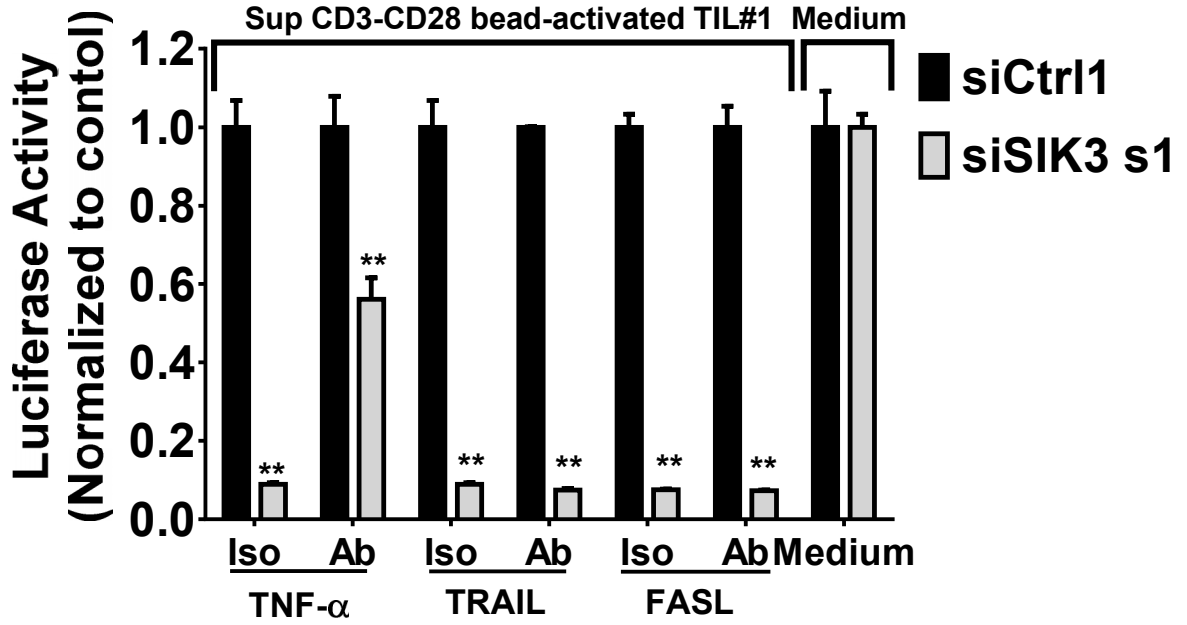

Figure 22. Identification of T cell effector molecules upstream of SIK3. PANC-1-luc cells were transfected with indicated siRNAs for 72h and subjected to the supernatant of CD3/CD28 bead-activated TIL#1. Stimulation was conducted for 20h in the presence of anti-TNF-α, anti-TRAIL or anti-FASL (Ab) antibodies or isotype controls (Iso). Luciferase-based cytotoxicity assay was conducted to determine cytotoxicity of tumor cells upon the indicated treatment. Data are represented as fold change to siCtrl1 (black bars). Representative data of 2 independent experiments. Columns show mean +/- SEM. P-values were calculated using two-tailed student´s t-test. * $p < 0.05$, ** $p < 0.01$.

3.4.8 SIK3 dictates the fate of TNF-α treated tumor cells

Given the previous results, we sought to further characterize the role of TNF-α in the regulation of SIK3-mediated tumor cell responses to T cell attack. TNF-α is a cytokine secreted by CD8+ T cells upon activation [199, 204]. Several studies describe TNF-α as an important cytokine in T cell-mediated cancer rejection [199, 204, 205]. Furthermore, it was demonstrated by our group that TNF-α expression delineates a population of CTLs present within tumors from colorectal cancer patients [206]. Yet, in some tumors, TNF-α can act as pro-tumorigenic factor [207-209]. First, we sought to investigate whether TNF-α was secreted in our co-culture models. TILs stimulation either with tumor cells or with CD3/CD28 beads resulted in significant TNF-α production (Figure 23A). However, TNF-α concentration was sensibly higher after polyclonal stimulation. To determine the abundance of TNF-α secreting CTLs, we performed TNF-α secretion assay. We found that only a sub-population of CD8+ T cells secreted TNF-α after stimulation with tumor cells. On the contrary, the majority of polyclonally stimulated T cells produced TNF-α (Figure 23B).

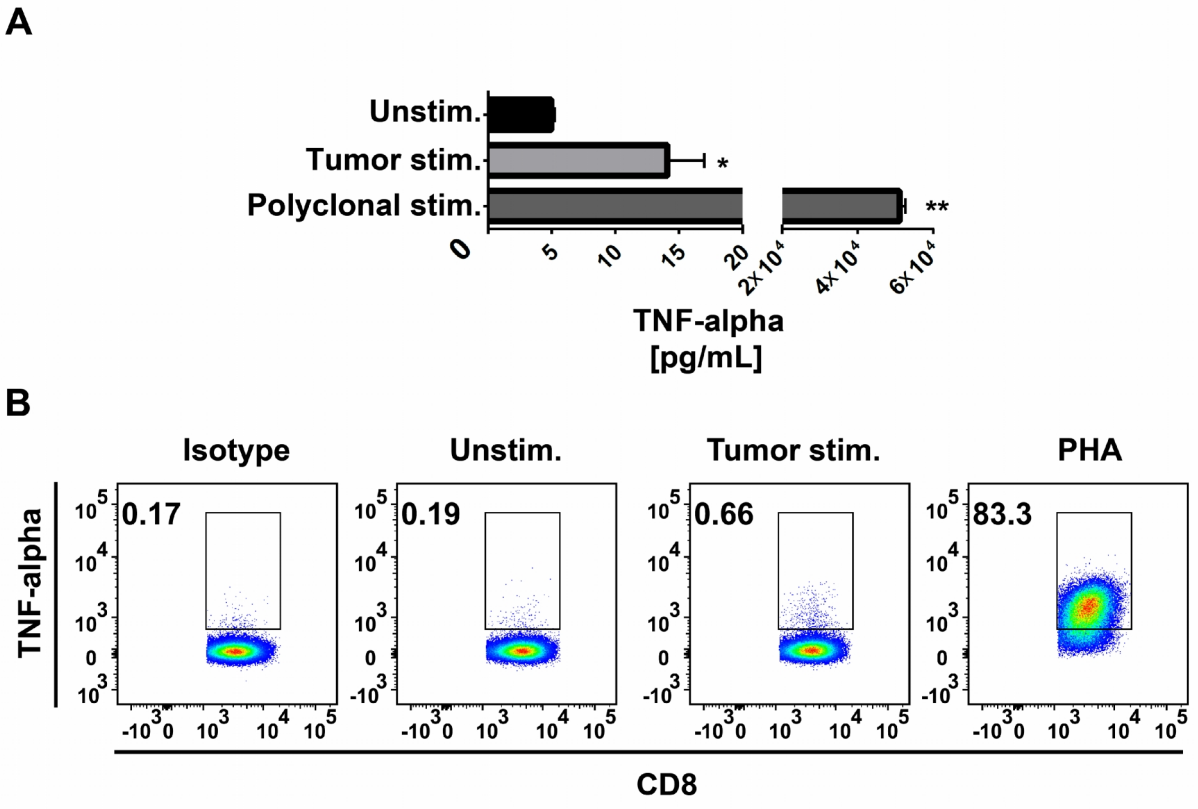

Figure 23. TNF-α secretion upon TIL activation. **(A)** Luminex assay for detection of secreted TNF-α from TIL#1. TIL#1 were co-cultured either with PANC-1 cells (Tumor stimulation) or with CD3/CD28 beads (Polyclonal stimulation). 24h after stimulation, supernatant was collected for TNF-α measurement. Supernatant of unstimulated TIL#1 was used as negative control. **(B)** Catch assay for the detection of TNF-α-secreting $CD8^+$ T cells from TIL#1. T cells were stimulated either with PANC-1 cells (tumor stimulation) or with phytohemagglutinin (PHA) for 12h. Unstimulated TILs were used as negative control. Gates show the percentage of TNF-α secreting cells. Representative data of two independent experiments. Columns show mean +/- SEM. P-values were calculated using two-tailed student´s t-test. * $p < 0.05$, ** $p < 0.01$.

Next, we treated transfected tumor cells with different concentrations of TNF-α neutralizing antibody, after treatment with the supernatant of CD3/CD28 bead-activated TILs. We observed that increasing concentrations of the neutralizing antibody led to a dose-dependent rescue from tumor cell death in SIK3 depleted cells (Figure 24A). Notably, 900 ng/mL of anti-TNF-α antibody was sufficient to induce complete rescue from supernatant-induced cytotoxicity. Neutralization of TNF-α in siCtr1-transfected cells did not alter cell viability in comparison to isotype control (Figure 24B).

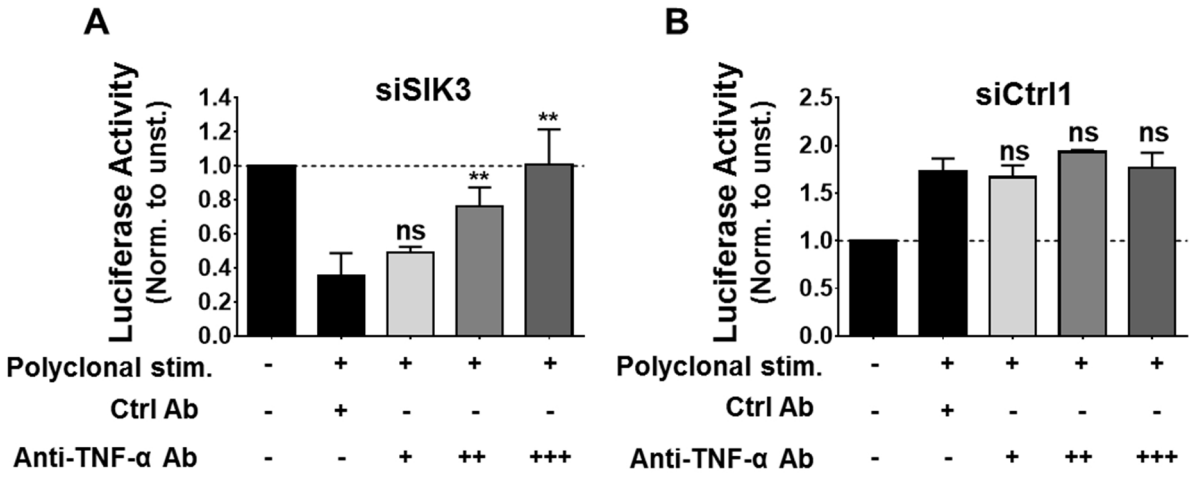

Figure 24. Effect of TNF-α neutralization on tumor cell death. Supernatant from CD3/CD28 bead-stimulated T cells was pre-incubated with 100 (+), 300 (++) or 900 (+++) ng/mL of anti-TNF-α neutralizing antibody for 30 min. Isotype control (Ctrl Ab) was used at concentration of 900 ng/mL. Afterwards, siSIK3 **(A)**, or siCtrl1 **(B)** transfected PANC-1-luc cells were subjected to the pre-treated supernatant or control medium for 24h and cytotoxicity was measured using luciferase-based killing assay. Data are presented as fold change to unstimulated control. Cumulative data of 3 independent experiments. Columns show mean +/- SEM. P-values were calculated using two-tailed student´s t-test. * $p < 0.05$, ** $p < 0.01$.

To confirm these data, we tested whether the addition of recombinant human TNF-α (rHuTNF-α) was sufficient to recapitulate the effects observed with supernatants of activated T cells. Therefore, we stimulated transfected tumor cells with increasing concentrations of this cytokine. We observed that rHuTNF-α reduced the viability of SIK3 deficient tumor cells in a dose-dependent manner, while scramble transfected tumor cells (siCtrl1) showed enhanced viability after rHuTNF-α stimulation (Figure 25A). Real-time live-cell microscopy was used to determine the kinetic of TNF-α mediated cytotoxicity. We observed massive cell death of SIK3 depleted PANC-1 cells within the first 6 hours of TNF-α treatment, while siCtrl1-transfected tumor cells were resistant to TNF-α stimulation (Figure 25B). In MCF-7 cells, we observed a basal sensitivity to rHuTNF-α in siCtrl1-transfected tumor cells (Figure 25C). However, SIK3 knockdown markedly enhanced tumor cell susceptibility to rHuTNF-α treatment.

Next, we tested whether SIK3 blockade with the pan-SIKs inhibitor HG-9-91-01 recapitulated the effects observed with SIK3 gene silencing. PANC-1-luc cells were stimulated with rHuTNF-α in the presence of increasing concentrations of the SIK3 inhibitor. We detected a dose-dependent tumor cell cytotoxicity after treatment with HG-9-91-01 in combination with rHuTNF-α addition.

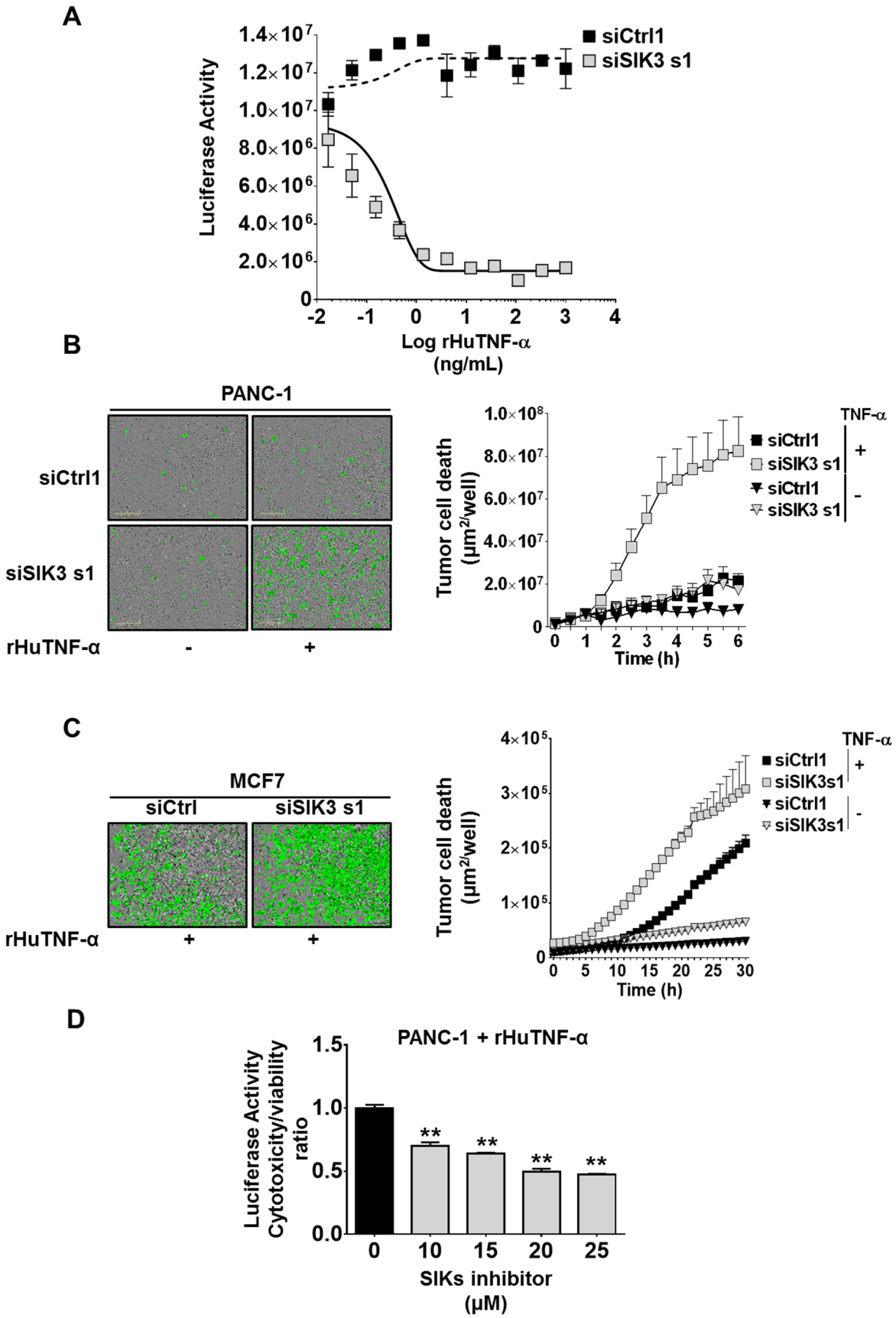
A
Luciferase Activity
1.4×10^7
1.2×10^7
1.0×10^7
8.0×10^6
6.0×10^6
4.0×10^6
2.0×10^6
0
siCtrl1
siSIK3 s1
-2 -1 0 1 2 3 4
Log rHuTNF-α (ng/mL)
B
PANC-1
siCtrl1
siSIK3 s1
rHuTNF-α
-
+
Tumor cell death (μm²/well)
1.0×10^8
8.0×10^7
6.0×10^7
4.0×10^7
2.0×10^7
0
0 1 2 3 4 5 6
Time (h)
TNF-α
siCtrl1
siSIK3 s1
siCtrl1
siSIK3 s1
+
-
C
MCF7
siCtrl
siSIK3 s1
rHuTNF-α
+
+
Tumor cell death (μm²/well)
4×10^5
3×10^5
2×10^5
1×10^5
0
0 5 10 15 20 25 30
Time (h)
TNF-α
siCtrl1
siSIK3s1
siCtrl1
siSIK3s1
+
-
D
PANC-1 + rHuTNF-α
Luciferase Activity Cytotoxicity/viability ratio
1.5
1.0
0.5
0.0
**
**
**
**
0 10 15 20 25
SIKs inhibitor (μM)

Figure 25. Effect of TNF-α treatment on SIK3 depleted tumor cells. **(A)** Dose-response effect of rHuTNF-α treatment on the viability of siRNA transfected PANC-1-luc cells. Tumor cells were transfected with siCtrl1 or siSIK3 sRNAs for 72h and subsequently stimulated with indicated concentrations of rHuTNF-α for 24h. Afterwards, cytotoxicity was measured by luciferase-based cytotoxicity assay. **(B)** Effect of 100 ng/mL TNF-α treatment on the viability of transfected PANC-1 cells. siRNA transfection was conducted as in **(A)**. Cell death was evaluated using real-time live cell microscopy, measuring the nuclear incorporation of YOYO-1 dye. Left panel, representative images after 6h stimulation. Right panel, cumulative data of nine different per time point pictures from the same experiment. Graph shows the area of YOYO-1+ cells/well (μm^2/well). **(C)** Effect of 100 ng/mL TNF-α treatment on the viability of MCF-7 cells. The experiment was conducted as in **(B)** and YOYO-1 incorporation was measured for 30h **(D)** PANC1-luc cells were stimulated with 100 ng/mL TNF-α or culture medium in the presence of indicated concentrations of the SIK inhibitor HG-9-91-01 for 24h. Tumor cell viability was measured by luciferase-based cytotoxicity assay. Data were normalized using cytotoxicity/viability ratio (see section 6.2.8.4). **(A, B, C)** Representative data of at least two independent experiments. **(D)** Cumulative data of three independent experiments. Columns show mean +/- SEM. P-values were calculated using two-tailed student´s t-test. * $p < 0.05$, ** $p < 0.01$. **(D)** was conducted by Damian Mikietyn (University of Regensburg) under my supervision.

3.4.9 TNF-α induces cytotoxicity in SIK3 depleted tumor cells via TNFR-I

TNF-α mediates its biological effects by binding to two distinct receptors: TNFR-I and TNFR-II [27, 210]. To understand which receptor was responsible of tumor cell cytotoxicity after SIK3 knockdown, we performed flow cytometry analysis to detect the expression of these receptors on the surface of tumor cells. We identified TNFR-I but not TNFR-II on PANC-1 cells (Figure 26A). Therefore, we focused our next experiments on the study of TNFR-I. We blocked TNFR-I in transfected tumor cells before treatment with TNF-α. We observed that TNFR-I inhibition abrogated TNF-α induced cytotoxicity after SIK3 knockdown (Figure 26B, right panel), while TNFR-I blockade in siCtrl-transfected PANC-1 cells did not significantly alter tumor cell viability compared to isotype control (Figure 26B, left panel).

In summary, these data suggest that SIK3 determines the fate of tumor cells after TNF-α treatment by modulating the TNFR-I signaling pathway.

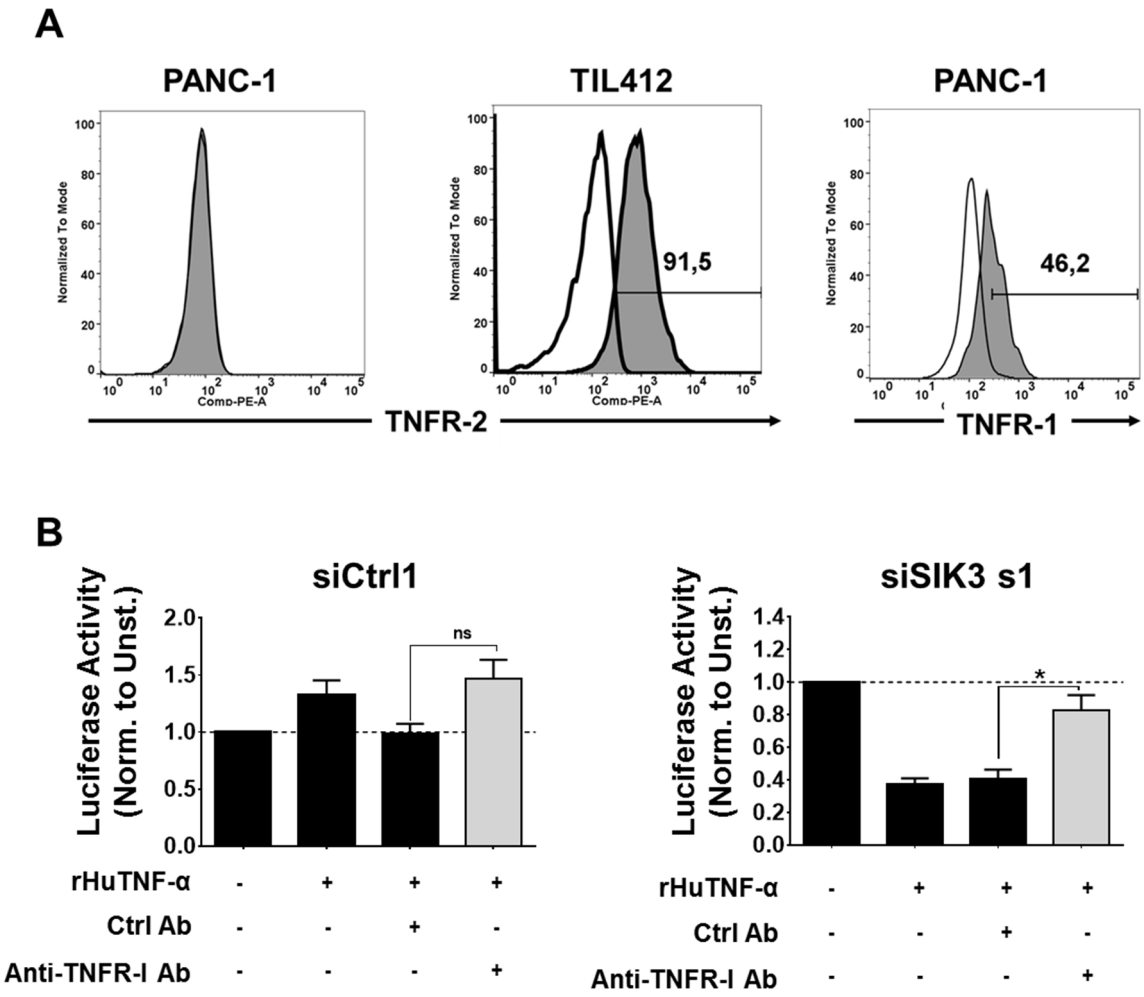

Figure 26. TNFR-I mediates TNF-α responses after SIK3 knockdown. **(A)** Analysis of TNFR-I (Right panel) and TNFR-II (Left panel) expression on PANC-1 cells. TIL412 were used as positive control for TNFR-II expression. Histograms show live single cells after staining with primary anti-TNFR-I or anti-TNFR-II antibodies and and PE-labeled secondary antibody. White histogram: isotype control, grey histogram: anti-TNFR-I or anti-TNFR-II as indicated in the picture. **(B)** Effect of TNFR-I blockade on TNF-α stimulated tumor cells. PANC-1-luc cells were transfected with siCtrl1 (left panel) or siSIK3 (right panel) siRNA for 72h. Afterwards tumor cells were incubated for 30 min with anti-TNFR-I or isotype control (Ctrl Ab) and rHuTNF-α (50 ng/mL), or control medium were subsequently added to the culture. After 24h, TNF-α mediated cytotoxicity was measured by luciferase-based cytotoxicity assay. Data are presented as fold change to unstimulated control. **(A)** Representative data of two independent experiments**. (B)** Cumulative data of three independent experiments. Columns show mean +/- SEM. P-values were calculated using two-tailed student´s t-test. * $p < 0.05$, ** $p < 0.01$.

3.4.10 Activation of the SIK3 master-kinase LKB-1 upon TNF-α stimulation

Given the previous observations on the involvement of SIK3 in the TNF-α-TNFR-I axis, a potential role of TNF-α in activating SIK3 was hypothesized. SIK3 is canonically

activated by phosphorylation of its T-loop tyrosine residue by the master-kinase LKB-1 [211, 212]. Because of lack of pSIK3-specific antibodies, direct activation of SIK3 could not be detected. However, treatment of PANC-1 cells with TNF-α induced a rapid increased phosphorylation of the upstream SIK3 kinase, LKB-1. Of note, total levels of LKB-1 were not affected upon TNF-α treatment (Figure 27).

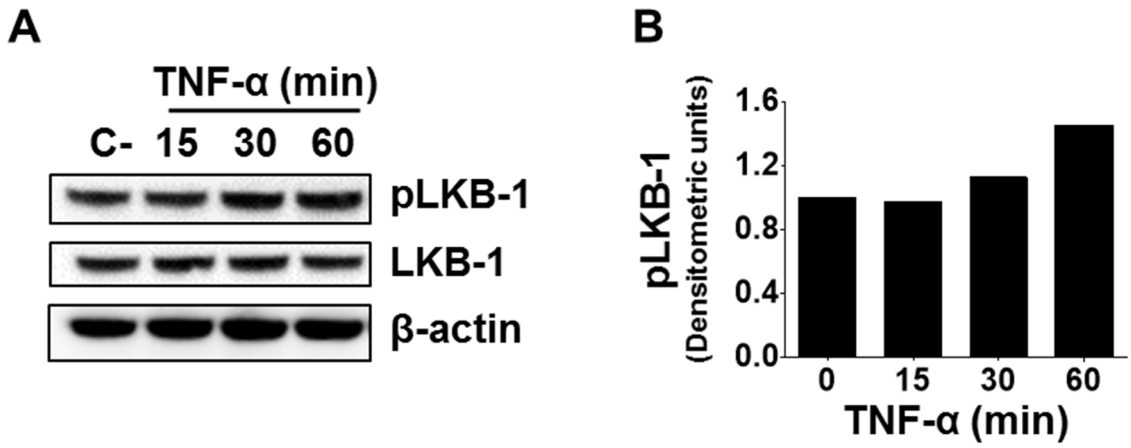

Figure 27. **(A)** Western blot analysis for the detection of pLKB-1 and total LKB-1 in PANC-1 cells after stimulation with rHuTNF-α (100 ng/mL) for the indicated time points (min). Culture medium was used as unstimulated control. β-actin served as loading control **(B)** Densitometric analysis of **(A)**. The ratio between p-LKB1 abundance and total LKB1 was calculated. Data were further normalized to β-actin. Representative data of two independent experiments. Experiments were performed by Dr. Katharina Jeltsch (Prof. Beckhove´s group).

3.4.11 SIK3 inhibits TNF-α-induced apoptosis in tumor cells

TNFR-I activation results in multiple signaling events leading on one side to apoptosis induction via caspase cleavage and, on the other side, to the activation of pro-survival factors such as NF-κB [213, 214]. The balance of these signaling cascade events dictates the fate of tumor cells after TNF-α stimulation [214, 215]. We sought to better understand the involvement of SIK3 in the TNFR-I signaling cascade. Therefore, we performed luminex assay to detect apoptosis activation markers in total lysates of PANC-1 cells. We observed increased cleavage of both caspase 8 and 9 after SIK3 depletion in tumor cells following rHuTNF-α treatment (Figure 28A and B). Furthermore, SIK3 depleted cells showed increased levels of phosphorylated c-Jun N-terminal

protein kinase (pJNK) as well (Figure 28C). JNK phosphorylation occurs upon TNF-α stimulation and mediates apoptosis in the absence of NF-κB activation [216-218].

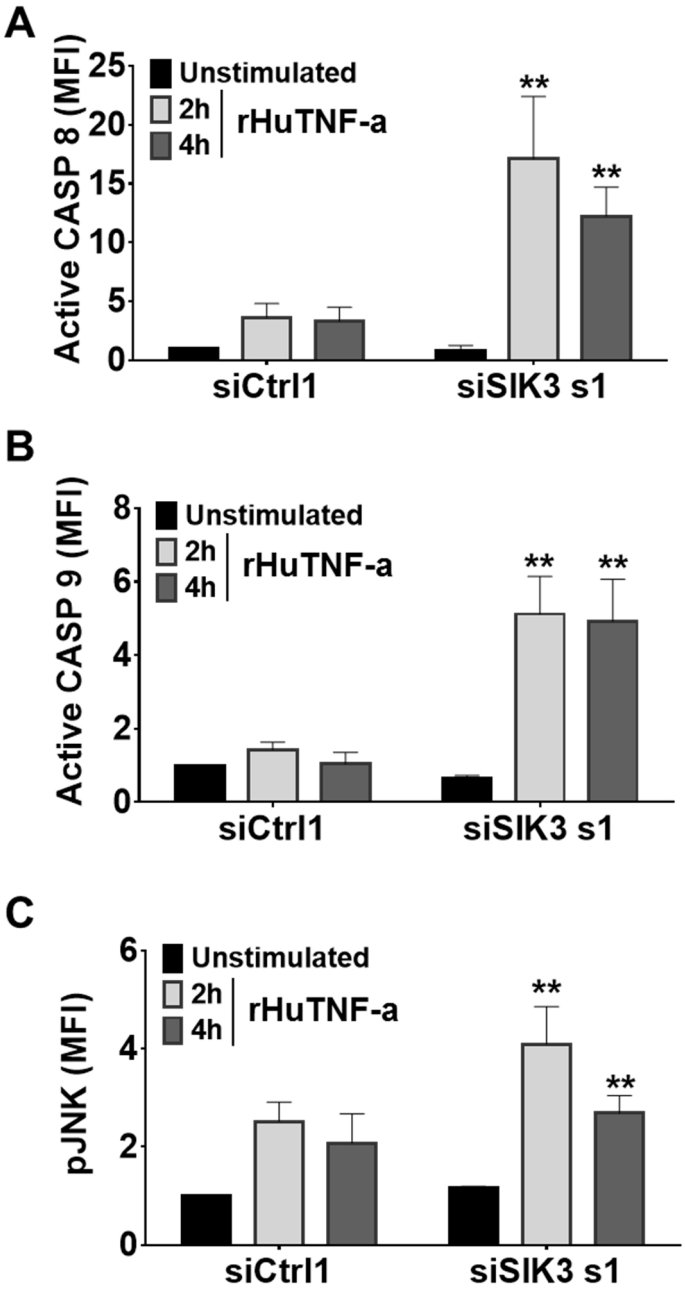

Figure 28. SIK3 inhibits TNF-α-induced apoptosis in tumor cells. siRNA transfected PANC-1-luc cells were treated with 100 ng/mL of rHuTNF-α. After the indicated time points, tumor cells were harvested and total protein fraction was isolated. Luminex assay was performed for active caspase 8 **(A)**, active caspase 9 **(B)** and pJNK **(C)**. Graphs show median fluorescent intensity (MFI) of analyte-specific beads after normalization to GAPDH. Cumulative data of three independent experiments. Columns show mean +/- SEM. P-values were calculated using two-tailed student´s t-test. * $p < 0.05$, ** $p < 0.01$.

3.4.12 SIK3 sustains NF-κB activation upon TNF-α treatment

Several studies show that TNF-α does not induce apoptosis unless NF-κB is inhibited [108-110]. Therefore, we hypothesized that SIK3 regulates apoptosis in TNF-α stimulated tumor cells thorough modulation of NF-κB. To prove this hypothesis, we evaluated nuclear NF-κB translocation in transfected tumor cell upon treatment with TNF-α or control medium. PANC-1 cells showed a constitutive activation of NF-κB (p65 subunit) without TNF-α stimulation, as compared to unstimulated Hela control (Figure 29A, black bars). SIK3 depletion was not sufficient to impair constitutive NF-κB nuclear translocation in the absence of TNF-α. However, upon TNF-α stimulation, SIK3 depleted PANC-1 cells showed a remarkable impairment of p65 subunit nuclear translocation (Figure 29A). Coherently, SIK3 overexpression resulted in increased p65 subunit nuclear translocation in unstimulated PANC-1 cells (Figure 29B).

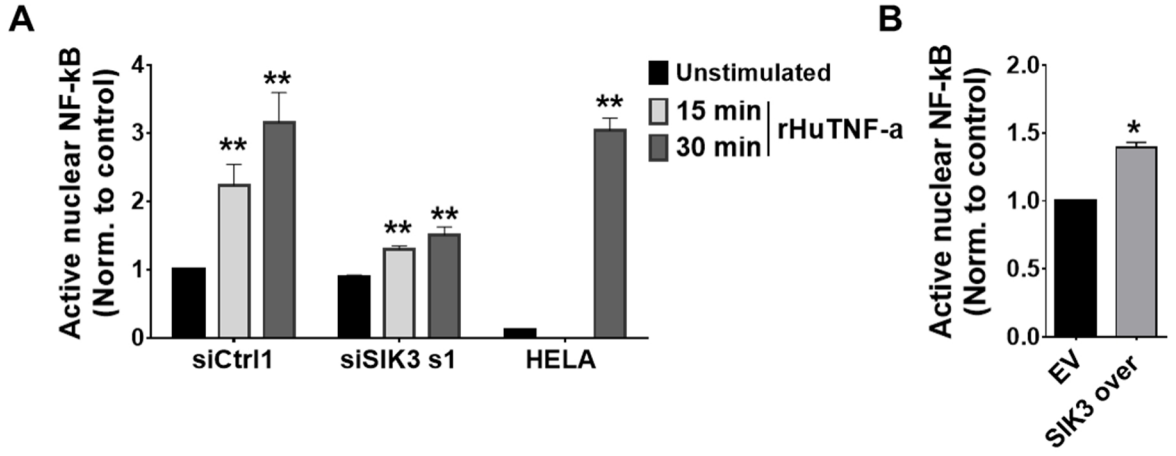

Figure 29. SIK3 modulates NF-κB nuclear translocation upon TNF-α treatment. **(A)** PANC-1 cells were transfected with indicated siRNAs for 72h and stimulated with 100 ng/mL rHuTNF-α or culture medium for the indicated time points. Afterwards, nuclear lysates were extracted and ELISA was performed for detection of p65 subunit of NF-κB. Graph shows absorbance at λ450nm after normalization to unstimulated siCtrl1. **(B)** PANC-1 cells were transiently transfected either with SIK3 overexpression vector (SIK3 over) or with control empty vector (EV) for 48h. Afterwards, p65 NF-κB ELISA was conducted as in **(A)**. HELA cells served as negative (unstimulated) and positive (30 min rHuTNF-α) controls. **(A)** Cumulative data of three independent experiments. **(B)** Representative data of at least two independent experiments. Columns show mean +/- SEM. P-values were calculated using two-tailed student´s t-test. * $p < 0.05$, ** $p < 0.01$.

To confirm these data, RNA –seq analysis was conducted in PANC-1 cells after siSIK3 or siCtrl transfection and rHuTNF-α or cell culture medium treatment. In the absence of rHuTNF-α, the only depletion of SIK3 substantially altered gene signature of tumor cells (Figure 30A and B). Particularly, two-dimensional hierarchical clustering analysis showed that 2185 genes were either up- or down-regulated after SIK3 knockdown (Figure 30C). Gene ontology analysis revealed that SIK3 depletion resulted in significant downregulation of genes involved several homeostatic cellular processes such as mitotic cell cycle and organelle fission (Figure 30C, right panel).

Gene clustering analysis was further conducted to compare genes whose expression was affected by rHuTNF-α treatment in siSIK3-transfected versus siCtrl1-transfected tumor cells. rHuTNF-α stimulation affected the expression of 386 genes in total. In particular, 205 of these genes were strongly upregulated in siCtrl1 cells after rHuTNF-α stimulation. Of note, SIK3 depletion led to a remarkable impairment of the induction of these genes (Figure 30D). The interrogation of databases for eukaryotic transcriptional regulation (such as TRANSFAC® and JASPAR®), revealed that most of these genes are under the regulation of the p65 (RELA) and the p50 (NFKB1) subunits of the NF-κB complex (Figure 30D, right panel). Gene ontology analysis showed that these genes are involved is processes of cell proliferation and differentiation (Figure 30D, right panel). Among them, several anti-apoptotic and mitogenic factors were identified, such as: the transcriptional activator Myb (MYB), which was shown to suppress apoptosis in breast cancer [219], the serpin family E member 2 (SERPINE2), which is required for proliferative expansion of medulloblastoma [220], and intracellular adhesion molecule 1 (ICAM-1), which is an anti-apoptotic factor in tumor cells under stress conditions [221].

Taken together these data confirm the role of SIK3 in sustaining NF-κB nuclear translocation and transactivation upon TNF-α stimulation.

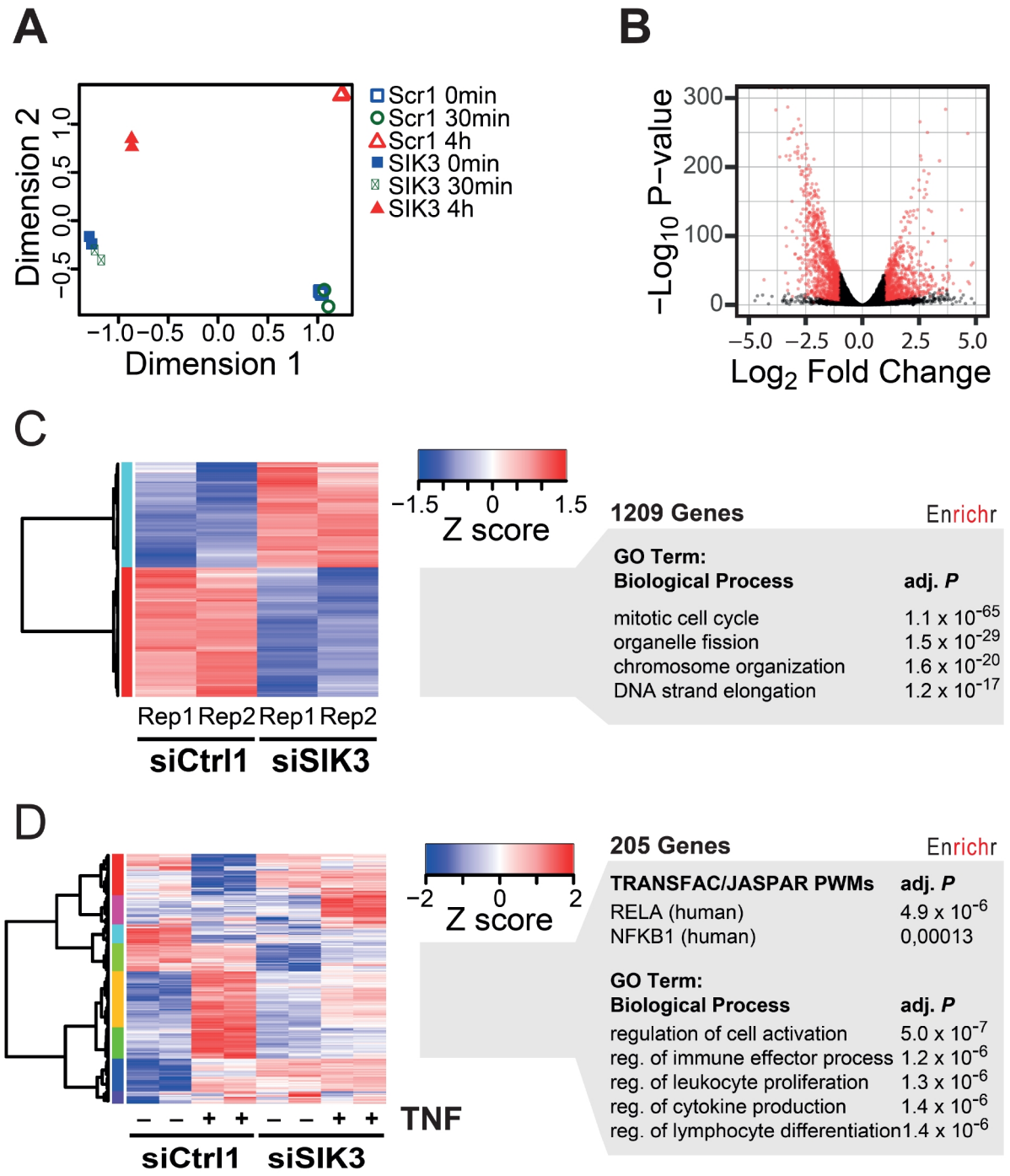

Figure 30. Effect of SIK3 knockdown on basal gene expression in PANC-1 cells and after TNF-α stimulation. PANC-1 cells were treated with siCtrl1 or siSIK3 for 72h. Afterwards TNF-α stimulation was applied for 30min and 4h and gene espression levels were measured using RNAseq. **(A)** The multidimensional scaling (MDS) plot for replicate RNAseq data sets shows that siRNA and TNF treatment separate samples by at least 1 dimension. **(B)** Volcano Plot highlighting differentially expressed genes after SIK3 knockdown alone (fold change ≥ 2, normalized counts per million > 2, FDR ≤ .05). Red dots = genes with significant differential expression **(C)** Two-dimensional hierarchical clustering of 2185 differentially expressed genes

(Z-score transformed, normalized counts per million; Manhattan distance, Ward method). The right panel shows representative gene enrichment analysis results for genes downregulated after SIK3 knockdown. **(D)** Two-dimensional hierarchical clustering (as in C) of 386 genes that were significantly regulated by TNF-α after 4h and significantly affected by SIK3 knockdown. The right panel shows representative gene enrichment analysis results for genes having reduced or missing induction by TNF-α after SIK3 knock down (fold change ≥ 2, normalized counts per million > 2, FDR ≤ .05). Experiments and data analysis were conducted in collaboration with Prof. Michael Rehli and Dr. Claudia Gebhard (University of Regensburg)

3.4.13 SIK3 modulates NF-κB activation via HDAC4

Next, we aimed to understand the mechanism by which SIK3 modulates NF-κB activation. One described target of SIK3 is histone deacetylase 4 (HDAC4) [212, 222, 223] SIK3 cytoplasm [212]. It was shown that in macrophages, nuclear HDAC4 physically interacts with NF-κB p65 subunit, leading to its deacetylation and decreased transactivation [224]. Hence, we hypothesized that the increased cytotoxicity in SIK3 knockdown tumor cells, after rHuTNF-α stimulation, was caused by elevated levels of nuclear HDAC4. To prove this hypothesis, we silenced HDAC4 in SIK3 depleted tumor cells and evaluated tumor cell cytotoxicity after rHuTNF-α treatment. Double knockdown PANC-1 cells showed decreased cytotoxicity compared to tumor cells transfected with SIK3-specific siRNA alone (Figure 31A). HDAC4 depletion alone did not significantly alter tumor cell viability compared to siCtrl transfection. In the absence of rHuTNF-α, co-transfection of siSIK3 and siHDAC4, did not show major impact on tumor cell viability (Figure 31B).

These findings suggest that in tumor cells, SIK3 sustains NF-κB activation upon TNF-α stimulation by preventing HDAC4 nuclear translocation.

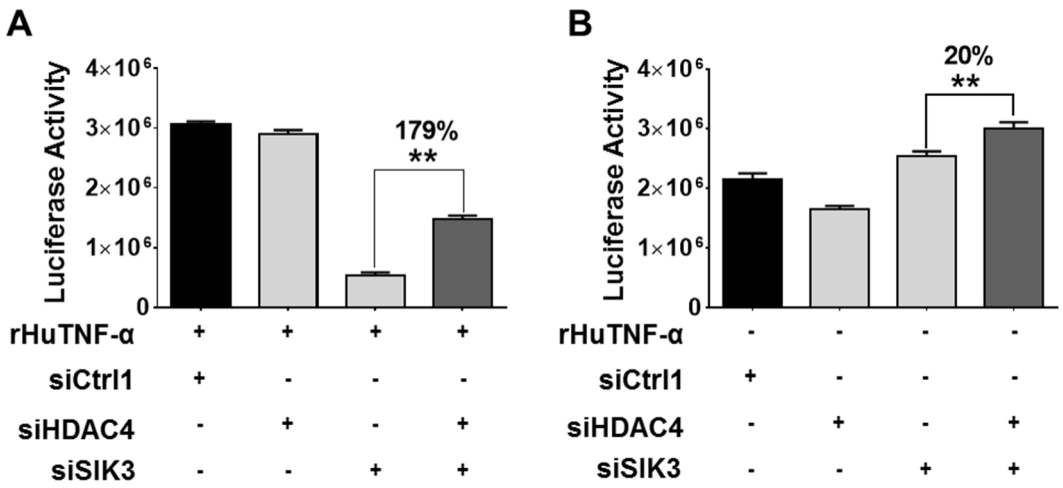

Figure 31. SIK3 modulates NF-κB activation via HDAC4. Luciferase-based cytotoxicity assay. PANC-1-luc cells were transfected with indicated siRNAs for 72h and stimulated with 100 ng/mL of rHuTNF-α **(A)**, or culture medium **(B)** for 24h. Graph shows the remaining luciferase activity of tumor cells. Representative data of two independent experiments. Columns show mean +/- SEM. P-values were calculated using two-tailed student´s t-test. * $p < 0.05$, ** $p < 0.01$.

3.4.14 SIK3 mediates tumor resistance to adoptive T cell transfer (ACT) *in vivo*

To evaluate the *in vivo* relevance of SIK3 in mediating cancer protection to immune attack, we stably knocked down SIK3 in the primary melanoma M579 cell line using SIK3-specific shRNA (shSIK3) or the control non-targeting shRNA sequence (shCtrl). First, we co-cultured shSIK3 or shCtrl transduced tumor cells with HLA-A2.1$^+$-matched TIL209, and assessed T cell-mediated killing using *in vitro* real-time live-cell microscopy. TIL209 showed increased killing efficacy towards shSIK3 depleted tumor cells compared to shCtrl (Figure 32A). Hence, we subcutaneously injected shCtrl and shSIK3 cells in the left and the right flank of non-obese diabetic (NOD)-severe combined immune deficient (SCID) gamma (NSG) immune deficient mice, respectively. ACT of TIL209 or PBS control injection was applied i.v. once per week (Figure 32B). Coherently with our *in vitro* data, we did not observe difference in the tumor growth kinetic between shCtrl and shSIK3 in PBS-treated mice, whereas TIL209 treatment caused retardation of tumor growth in SIK3-impaired tumor cells compared to shCtrl-transduced cells (Figure 32C).

Taken together, these results designate SIK3 as a novel potential immunotherapeutic target, whose blockade sensitizes tumor cells towards immune cell attack.

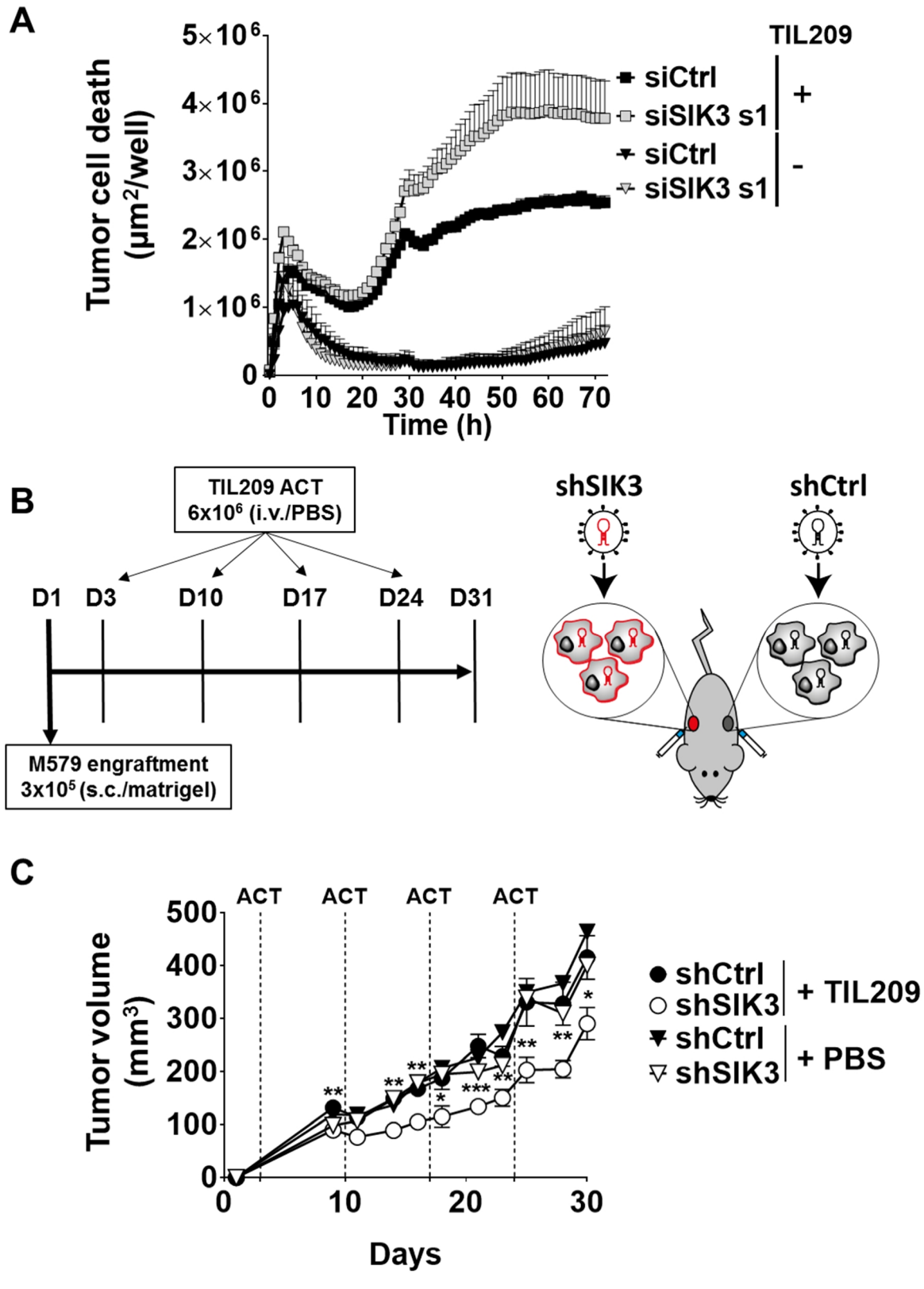

Figure 32. Stable SIK3 knockdown sensitizes tumor cells to ACT *in vivo*. **(A)** Real-time live cell microscopy for *in vitro* detection of TIL209-mediated lysis of lentivirial-transduced M579 cells. Tumor cells were transduced with shCtrl or shSIK3 lentiviral constructs and

subjected to antibiotic selection. Afterwards tumor cells were co-cultured with TIL209 (5:1) or culture medium for 70h. The graph indicates the area of YOYO-1^+ cells/well (μm^2/well). **(B)** Schematic representation of the *in vivo* mouse experiment. Subcutaneous (s.c.) implantation of shCtrl or shSIK3- transduced M579 cells was applied to the left and the right flank of NSG mice, respectively. Mice received intravenous (i.v.) injection of TIL209 (n=9) or PBS alone (n=7) at day 3, 10, 17 and 24. (C) Tumor growth curves showing mean +/- SEM of tumor volume (mm^3) of shCtrl or shSIK3-engrafted M579 tumors in mice treated with either TIL209 or PBS. Representative data of two independent experiments. Statistical difference was calculated using unpaired one-side Mann-Whitney U-test. **(C)** was conducted in collaboration with Dr. Melanie Werner-Klein (University of Regensburg).

4. Discussion

Despite the clinical success of immune checkpoint blockade in many cancer entities [125, 155, 156, 173, 174, 225], a large proportion of cancer patients does not respond to anti-CTLA4 or anti-PD-1/PD-L1 antibodies [143, 146, 226], emphasizing the need to identify more key players that could radically improve immunotherapy.

In this study, we developed a patient-derived PDAC model for the identification of novel immune modulators in a high-throughput fashion. Our screening revealed 108 potential genes that mediate immune suppression in tumor cells. Among them, SIK3 was selected for further validation. We demonstrated for the first time that SIK3 controls the switch between tumor survival and cell death upon T cell attack in several solid tumors. SIK3 alters tumor susceptibility towards T cell mediated cytotoxicity, rather than increasing T cell activation status. We found that T cells express TNF-α upon co-culture with tumor cells, and that this cytokine elicits tumor cell growth in SIK3-expressing cells. On the contrary, SIK3 depletion sensitized tumor cells towards TNF-α treatment by regulating NF-κB activation via HDAC4. We demonstrated the potential translational impact of our results with a SIK3 small molecule inhibitor that recapitulated the effects of gene silencing. Additionally, stable knockdown of SIK3 in tumor cells resulted in retardation of tumor growth after adoptive cell transfer of TILs in an *in vivo* model.

4.1 RNAi screen for tumor-associated immune checkpoints

4.1.1 Design and rationale

In the current study, a method developed in this laboratory by Dr. Nisit Khandelwal was adopted [152]. However, the following modifications were applied, with the aim of improving qualitative and quantitative aspects of the screen.

- *The tumor entity*. Pancreatic cancer was used as tumor model instead of breast cancer. The reason of performing the RNAi screen in another tumor entity was based on the consideration that cancer is a highly heterogenic disease [227].

Such heterogeneity results in diversity of immune escape mechanisms across tumor entities. As a result, different tumors show variable response to immunotherapy (section 1.4.1). Therefore, we envisioned that the performance of the RNAi screen in another tumor entity would unravel a novel immune modulatory landscape, compared to the one characterized in breast cancer. Pancreatic cancer is one of the most resistant cancer types to current immunotherapeutic regimens [138, 143, 228]. As an example, a phase 2 clinical trials showed that treatment with ipilimumab is ineffective as monotherapy in PDAC [143]. For this reason, we decided to conduct the RNAi screening in this tumor type.

- *The T cell source.* We chose TILs, instead of polyclonally stimulated PBMCs or antigen-specific lymphocytes, as T cell source. TILs are lymphocytes that reside in the tumor or around tumor margins [229]. In accordance with published data, we observed that TILs isolated from PDAC patient´s biopsies showed a marked exhaustion phenotype [64, 159, 160, 162]. Exhausted cells are generally less reactive, resembling the situation in cancer patients. Additionally, their low reactivity against target cells represents an optimal characteristic for the screening, as we wanted to identify genes whose depletion increase T cell functionality. Adoptive cell transfer of TILs (ACT) is a promising branch of immunotherapy [230, 231], therefore we envisioned that the use of these cells in the screening would increase the translational impact of the assay.
- *The siRNA library*. We expanded the pilot siRNA library to a wider library containing 2514 genes. In the breast cancer screen, a library of 500 G-protein coupled receptors (GPCRs)-targeting siRNAs was used. GPCRs are interesting targets for cancer immunotherapy for several reasons: i) they are expressed on the plasma membrane of cells and therefore they are suitable targets for the generation of large molecule compounds. ii) Because of their cellular localization, these proteins might directly mediate immune suppression by binding to a potential molecular partner expressed on the surface of immune cells. iii) The biological and immunological role of several proteins belonging to this class is still unknown. iv) They include orphan receptors, which are of high biological relevance, as their ligands remain undiscovered.

However, GPCRs represent only a small proportion of the “surfaceome” (i.e. the collection of cell surface proteins in human cells). Therefore, we aimed to increase the coverage of surface-related proteins in the library. Unfortunately, this intent was limited by the lack of commercially available surfaceome libraries, and the high cost of customized libraries. To circumvent this limitation, Tillmann Michels (Prof. Beckhove´s group) performed a bionformatic analysis with the aim of identifying parts of commercially available libraries having the highest representation of genes expressed on the plasma membrane [232]. In addition, we included a kinome library (protein kinases library), comprising both cytoplasmic and surface-bound proteins. This class of proteins mediates a plethora of processes that are important for cell survival and homeostasis. For some of them, such as JAK2, immune regulatory functions have already been demonstrated [233, 234]. Furthermore, such proteins are suitable targets for small molecule inhibitors and it has been reported that treatment of tumor cells with tyrosine-kinase inhibitors, synergizes the effects of cancer immunotherapy [235]. After these improvements, we generated a library comprising 1117 surface-associated genes (53%) and 1397 intracellular (47%) proteins for a total of 2514 genes (Figure VIA). The library covers about 30% of the whole “surfaceome” (Figure VIB). Hence, we referred to it as the “surfaceome-enriched library”.

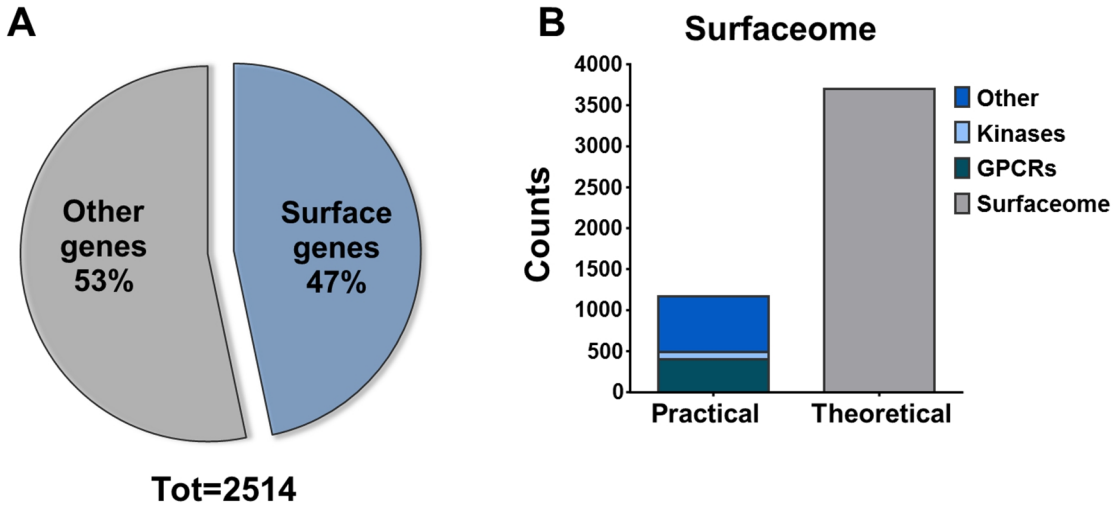

Figure VI. Graphical representation of the surfaceome-enriched library. (A) The pie chart divides the genes into surface-associated entities (47%) and “other” genes (having nuclear or

cytoplasmic localization) (53%). **(B)** Graphical representation of practical versus theoretical coverage of surface-associated genes. The list of surfaceome genes was retrieved from published data [232].

4.1.2 Performance and data interpretation

Bi-dimensional RNAi screens can be technically challenging. Therefore, a variety of parameters must be included in order to accurately verify the quality and the reliability of the assay. As first quality assessment, we evaluated the correlation among repeated measurements. As mentioned above, each setting was conducted in technical duplicates. The high correlation observed in each setting was the first indicator of the high quality of the method. Another important aspect to consider is the performance of assay controls. Both PD-L1 and CEACAM6 were successfully identified as negative immune modulators in the RNAi screen. As discussed in the introduction, PD-L1 involvement in mechanisms of immune regulation has been established in several tumor entities including pancreatic cancer [47, 236]. The role of CEACAM6 as immune checkpoint molecule was previously demonstrated in multiple myeloma in Prof. Beckhove´s group [66], and preliminary data show that inhibition of CEACAM6, both with gene silencing and blocking antibodies, enhances T cell-mediated cytotoxicity in breast cancer (Khandelwal et al., unpublished data). Interestingly CEACAM6 is overexpressed in a plethora of malignancies and it promotes tumor progression and invasiveness in pancreatic cancer [65, 237-239]. In this study, we show for the first time that this antigen acts as immune modulator in pancreatic cancer as well.

Besides providing essential information on the HT-screen quality, assay controls are fundamental for the definition of appropriate cut-off parameters for hit´s identification. In an optimal scenario, positive controls should encompass a range of strengths to develop an assay that can identify both weak and strong hits [163]. In this assay, we observed that PD-L1 showed a weak phenotype, as knockdown of more than 150 genes elicited stronger T cell-mediated cytotoxicity. For this reason, PD-L1 differential score was used as a threshold for hits´ identification. Assessment of threshold parameters for hits´ identification can vary substantially across HT-screens. For instance, in an analogous screen in multiple myeloma (conducted by Valentina Volpin – Prof. Beckhove´s group), PD-L1 was not involved in mechanisms of tumor immune resistance, whereas CCR9 was used as reference gene for gating strategy.

The primary RNAi screen in pancreatic cancer revealed 155 potential immune modulators. Of note, the hit-list contained several genes with known cancer immune regulatory function such as IL17RA [175], IL1RAP [176-178], and JAK2 [179]. IL17RA constitutes one subunit of the receptor for IL-17A. Notably, IL17RA was identified in a panel of breast cancer cell lines and its ligand promoted proliferation and chemoresistance of tumor cells via activation of extracellular signal-regulated kinases 1 and 2 (ERK1/2) [175]. IL1RAP is a necessary part of the IL-1 receptor complex, as it initiates signaling events that result in the activation of interleukin 1-responsive genes. IL1RAP is upregulated in chronic myeloid leukemia (CLM) stem cells and its blockade with a monoclonal antibody shows therapeutic efficacy in a CLM mouse model [240]. Furthermore, IL1α promotes tumorigenesis, tumor invasiveness and metastasis in several tumors such as breast cancer [176, 241]. One of the hits that showed the strongest phenotype in the RNAi screen was JAK2. JAK2 is a well-characterized immune modulatory molecule that mediates tumor cell resistance towards NK-cell attack. NK cells secrete IFN-γ after encountering tumor cells. This cytokine stimulates JAK1/2 activation in tumor cells, which in turn results in PD-L1 upregulation on the tumor cell surface. Hence, JAK2 depletion using shRNA-lentiviral constructs or small molecule inhibitors enhanced NK-cell mediated lysis by preventing PD-L1 upregulation in tumor cells [179, 234].

Together with novel immune-inhibitors, the established HT-screen has the potential to identify novel activators of the immune system. As described in 1.4, agonistic monoclonal antibodies targeting co-stimulatory molecules are currently the object of early stage clinical studies [242]. Because of lack of positive co-stimulatory controls, we could not accurately define the appropriate cut-off for the identification of novel immune-stimulatory molecules. However, among the top 100 immune-activator candidates, we identified several proteins belonging to the class of cytokines, chemokines and the TNF-receptor superfamily, such as CCR2, CCL3, CXCL9 and TNFSF11 [243-246]. Further investigation will be necessary to validate the potential role these receptor and ligand in cancer immunity. Discovery of novel co-stimulatory molecules is not only relevant for the identification of novel therapeutic targets in cancer, but it is important for the treatment of autoimmune diseases as well [247]. In this laboratory, Ayse Nur Menevse is currently conducting a research project with the

aim of investigating whether some of the immune-stimulatory molecules identified in the PDAC RNAi screening, would play a role in multiple sclerosis (MS) as well. MS is one of the most common and disabling autoimmune disorders, which is characterized by infiltration of auto-reactive $CD8^+$ T cells into the brain. Therefore, blockade of key co-stimulatory molecules would result in decreased T cell activation and better patient´s outcome.

Despite the robustness and reliability of the primary screen, secondary screens are indispensable for the identification of genes that are particularly relevant [163]. As secondary screen, the luciferase-based killing assay was conducted using a library comprising only the 155 hits from the primary screen. To obtain more information on the relevance of the individual hits, the assay was performed both with TILs and with T cell clones. The advantage of using two T cell sources is the possibility of excluding eventual hits whose validity is constrained to a particular T cell type. About 30% of the hits were not confirmed as negative modulators of immunity in the secondary screen. Therefore, the list was reduced to 108 hits. Interestingly, the performance of individual hits varied in the primary and secondary screens, with some hits showing stronger phenotype in the secondary screen compared to the primary, and *vice versa*. This variability is a common denominator in high-throughput screens and it stresses the need of an extensive validation strategy that allows to identify “real hits” [163].

4.1.3 Comparative analysis of immune RNAi screens

Over the last six years, several screens were conducted in Prof. Bechove´s laboratory by different doctoral students. After the pilot screen in breast cancer [152], Tillmann Michels performed a HT-screen using patient-derived melanoma cells and HLA-$A2^+$-matched TILs. Valentina Volpin conducted the HT-screens with multiple myeloma (MM) cancer cells and marrow infiltrating lymphocytes (MILs), showing the applicability of this approach for hematological tumors (Figure VIIA). As mentioned in paragraph 4.1.1, the reason of performing screens in multiple cancer types is based on the hypothesis that the biological heterogeneity across tumor entities results in the expression of a different repertoire of immune modulators. Indeed, the comparative analysis of the primary hit-lists between the PDAC, the melanoma and the MM screens revealed a small overlap among the different tumor entities (Figure VIIB). The differential

landscape of immune modulators across several screens might explain the heterogeneity of clinical responses to immunotherapy in different tumor patients. The breast cancer screen [152] was not include in the analysis because of the different size of the library compared to the other screens.

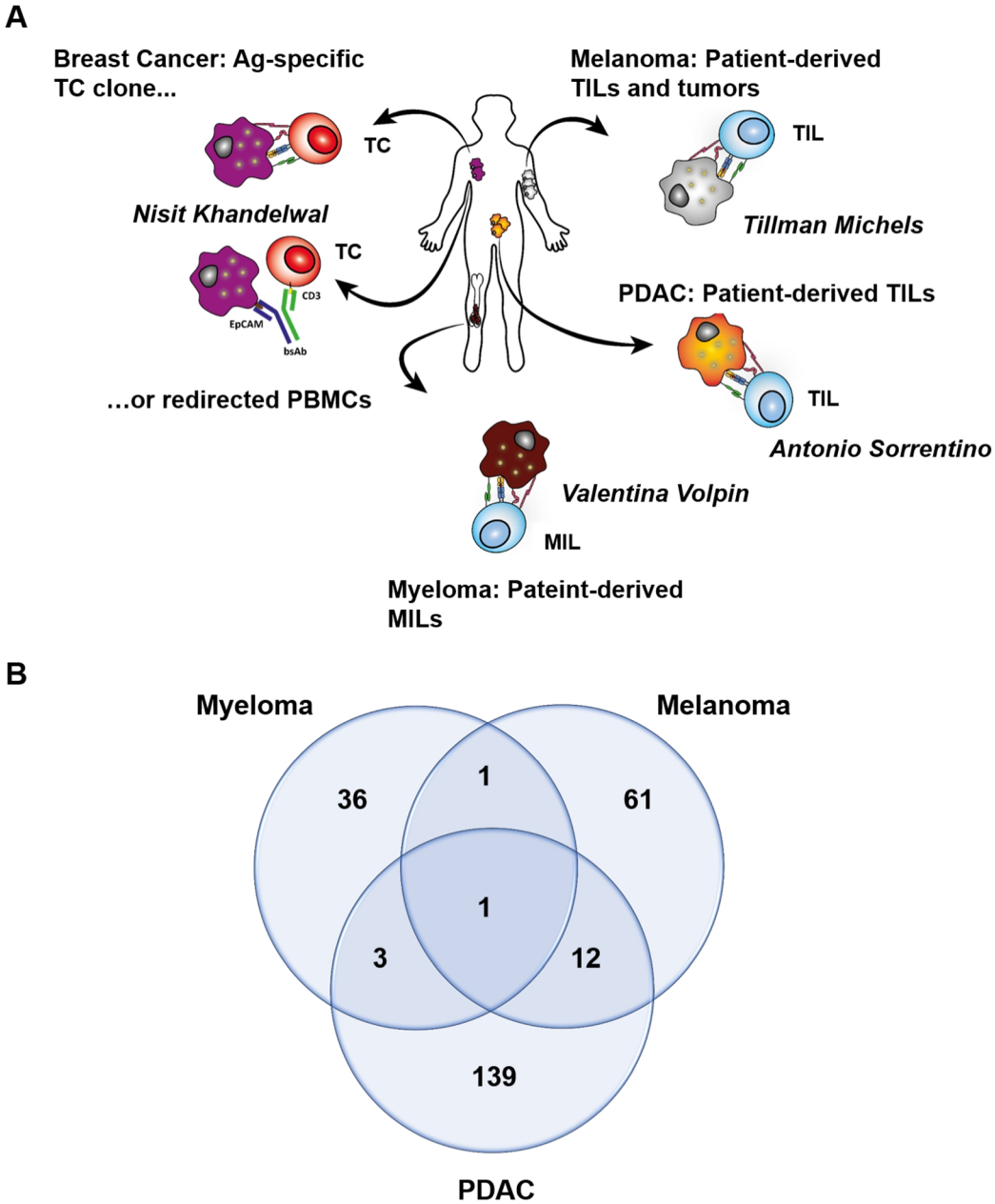

Figure VII. Comparative analysis of immune RNAi screens. (A) Schematic representation of the performed immune RNAi screenings, including the tumor entity and the sources of tumor and T cells. **(B)** Venn diagram showing the overlap of the primary hit-lists across the melanoma, the multiple myeloma and the PDAC screens. The analysis was performed by Tillmann Michels (Prof. Bechove´s group).

4.2 Rationale of Hit selection

To identify reliable immune modulatory molecules from the hit-list of the PDAC screenings, a rigorous approach of target validation was applied. About 10% of the hits were chosen for next steps. As one of the main goals of this project was to discover novel targets for clinical applications, candidate genes had to fulfil the following criteria:

- *The novelty.* The discovery of proteins with undescribed function in immune escape mechanisms is relevant on a scientific perspective.
- *Favorable expression profile*. The major advantage of targeted therapy over chemotherapy is the increased selectivity towards tumors [248]. It can be assumed that the broader the expression the higher the risk for adverse events, when the drug has to be administered systemically [248]. Therefore, hits showing overexpression in cancer tissues versus normal tissues were preferred. Many candidate genes could not be considered for further validation because of their essential role in cell homeostasis. For instance, phosphomevalonate kinase (PMVK) was among the top 10 hits. However its pleiotropic expression and its fundamental function in mevalonate pathway and cholesterol biosynthesis, made this candidate unsuitable for targeted therapy [249, 250]. Although not broadly expressed, other candidate genes were excluded because of their essential roles in vital organs. As an example, myotonic dystrophy protein kinase (DMPK) was the strongest hit in the secondary screen. Yet, its dysregulation results in atrioventricular conduction abnormalities in a mouse myotonic dystrophy model [251, 252]. Among the selected hits, MLN and ASTL were of particular relevance as the expression of these molecules is restricted to specialized compartments of the body. ASTL is a metalloprotease which is only expressed in the *zona pellucida* of oocytes [185]. MLN is a 22-amino acid polypeptide hormone, which is secreted only by endocrine M cells in the small intestine [186]. Therefore, it is conceivable that therapeutic tools targeting these genes would show low toxicity profile. The observation that several cancer cell lines ectopically express these genes, makes MLN and ASTL attractive targets for cancer immunotherapy.

- *The druggability*. Strategies to evaluate protein druggability include methods exploring sequence-related properties as well as methods exploring the 3D-structures of proteins [248]. Information on the protein crystal structure and protein domains enables the prediction of potential binding sites for small molecule inhibitors or biological drugs, depending on their cell localization [253]. Despite recent progresses, some class of proteins, such as phosphatases and transcription factors, remain undruggable [254]. Following these considerations, six hits were selected either due to their expression on the plasma membrane (NTSR2, GPR31, ASTL, FAT1), or due to their secretion in the extracellular space (MLN ad IL36G). In fact, for these candidates the production of biological compounds, like monoclonal antibodies, is conceivable. Four selected hits (SIK3, MAST3, LIMK2 and CDC42BPA) belonged to the class of protein kinases. Protein kinases are well studied druggable targets, as secondary structures and catalytic domains are known for a plethora of proteins belonging to this class [184].

A fundamental step for target selection and validation is the verification of siRNA on-target effect. Off-target effects are a major concern of RNAi-based screening and may prominently contribute to the false discovery of candidate genes [255, 256]. Off-target effects refer to all possible phenotypic results arising from unspecific interactions between the silencing molecules (siRNA or shRNA) and mRNAs. Three main reasons can cause off-target effects [257]: i) the generation of an siRNA sequence which is identical or nearly identical to a sequence present in an unrelated mRNA [257]. ii) The siRNA can act as a microRNA, as its partial complementarity with an un-related mRNA is sufficient to elicit gene silencing. Specifically, the 5´ region of the siRNA from 2nd to 7th/8th nucleotide (known as “seed sequence”) can bind to the 3’ UTR of several of unrelated mRNAs, leading to their degradation. iii) siRNAs may activate type I interferon response in mammalian cells, as intrinsic defense mechanism to exogenous oligonucleotides [257]. iv) As siRNAs are delivered as double strand oligonucleotides, off-target effects can arise from the binding of the complementary strand to the transcription machinery.

In this screening, several measures were adopted to increase siRNA efficacy and reduce unspecific binding of the siRNAs to unwanted mRNA sequences. All sequences in the siRNA library were designed by the manufacturer (Dharmacon – GE Healthcare), using an algorithm that accounts for several important features for siRNA stability and potency, such as low G/C content or lack of inverted nucleotide repeats [258]. To reduce off-target effects, each gene of the library was silenced using a pool of 4 non-overlapping siRNAs targeting the same mRNA ("pooled approach"), instead of single siRNAs. As the occurrence of off-target effects is concentration dependent, the pooled approach allows to reduce the concentration of each individual siRNAs, without affecting the knockdown efficiency towards the desired target mRNA [259]. However, off-target effects cannot be completely excluded using this approach and further validation is necessary. To discriminate between real hits and false positive entities, the luciferase-based killing assay was repeated by using individual siRNAs present in the pool (deconvolution). The probability that different non-overlapping siRNAs share the same off-target effect is very low, therefore the observation of the same RNAi-induced phenotype using at least 2 distinct siRNAs supports and validates the on-target effect and thereby the gene-specific phenotype [255]. siRNA deconvolution, in the luciferase-based killing assay, revealed that four out of 11 hits (SIK3, MAST3, ASTL and MLN) fulfilled the validation criteria, and data were further confirmed by qPCR knockdown analysis and chromium release assay. Among the validated hits, SIK3 was selected for further validation because of the strength of the phenotype and its biological relevance.

4.3 SIK3 as potential therapeutic target for cancer immunotherapy

4.3.1 Structure, distribution and function of SIK kinases

SIK3 is a 1236-amino acid serine/threonine kinase belonging to the salt-inducible kinase (SIKs) subfamily [260]. The first identified isoform of these proteins, SIK1, was found in adrenal glands of high salt diet-fed rats [261]. Subsequent studies demonstrated the existence of two additional isoforms, SIK2 in adipose tissues [262] and SIK3, which was identified by sequence homology [263]. The three isoforms have the following structure: an N-terminal catalytic domain, a sucrose-nonfermenting-1

protein kinase homology (SNH) domain and a phosphorylation domain, which are highly conserved, an ubiquitin-associated domain, and a long C-terminal sequence, which differs among the three isoforms [263, 264].

SIKs belong to the AMPK (AMP-activated protein kinases)—related kinases, which include 13 proteins in total [211]. AMPK is an important regulator of cell metabolism as it is activated in response to low ATP levels within the cell [265]. Upon activation, AMPK allows several metabolic changes such as decreased cell growth and metabolism [265]. The kinase domains of AMPK-related kinases are highly related to the catalytic α1/α2 subunits of AMPK, but their physiological functions varies from regulation of cell polarity to modulation of cell differentiation [264]. All proteins of this subfamily are activated by the liver kinase B1 (LKB-1) master kinase [211].

A comprehensive analysis of SIKs distribution in healthy human tissue is still missing. However, SIK1 was found in many types of tissues including: adipose tissue, brain, adrenal glands, pituitary, ovary, lung and heart of normal rats [261, 266-268]. SIK2 was detected in murine brown and adipose tissue, although its expression in other tissues cannot be excluded [263]. SIK3 distribution was studied to a lesser extent. This protein was identified in murine hair follicles and in mouse hepatocytes. To obtain more information on SIK3 expression, the GTEx database was interrogated [181]. This analysis suggested ubiquitous expression of SIK3 mRNA in human tissues (data not shown), which needs to be further confirmed with more accurate experimental procedures.

Despite their sequence similarity, SIK isoforms can exert distinct functions across different tissues. The physiological role of SIK3 was broadly studied using a $Sik3^{-/-}$ mouse model. Sik3 KO mice showed a malnourished phenotype, characterized by ipodystrophy, hypolipidemia, hypoglycemia, and hyper-insulin sensitivity [269]. Therefore, SIK3 is an important regulator of glucose and lipid metabolism in the liver [269]. Another study suggests that Sik3 is required for correct auditory function in mice [270].

4.3.2 Role of SIK kinases in cancer

The role of SIK kinases in cancer is controversial, as different isoforms showed opposite effects. Literature data, suggest that SIK1 might act as tumor suppressor, whereas SIK2 and SIK3 might promote cancer progression and proliferation. Loss of SIK1 correlates with increased metastatic spread breast cancer [271]. Furthermore, SIK1 depletion results in increased migration of gastric adenocarcinoma cells [272].

The role of SIK2 and SIK3 in cell proliferation and cancer progression has been addressed in several studies. Overexpression of SIK2 correlates with poor prognosis in ovarian cancer, while its depletion sensitizes tumor cells to paclitaxel [273] .SIK3 is required for proper mitotic exit and its knockdown sensitizes tumor cells to antimitotic drugs [190]. In ovarian cancer, SIK3 promotes cancer cell proliferation by downregulating p21 via c-Src activation [189]. The Drosophila orthologue of the *SIK3* gene regulates apical-basal polarity in retinal cells [274], suggesting its potential role in epithelial to mesenchymal transition (EMT) during cancer progression [275]. Furthermore, Drosophila Sik2 and Sik3 are negative regulators of the Hippo pathway, an important controller of tissue overgrowth whose impairment is associated with cancer [276-278].

To corroborate these data, a database comparison of healthy versus cancer biopsies was performed, using the Oncomine™ database [182]. *SIK3* mRNA was significantly overexpressed in multiple myeloma, colorectal cancer and breast cancer. The expression and functional data, underlined the relevance of SIK3 as promising candidate for further validation analysis.

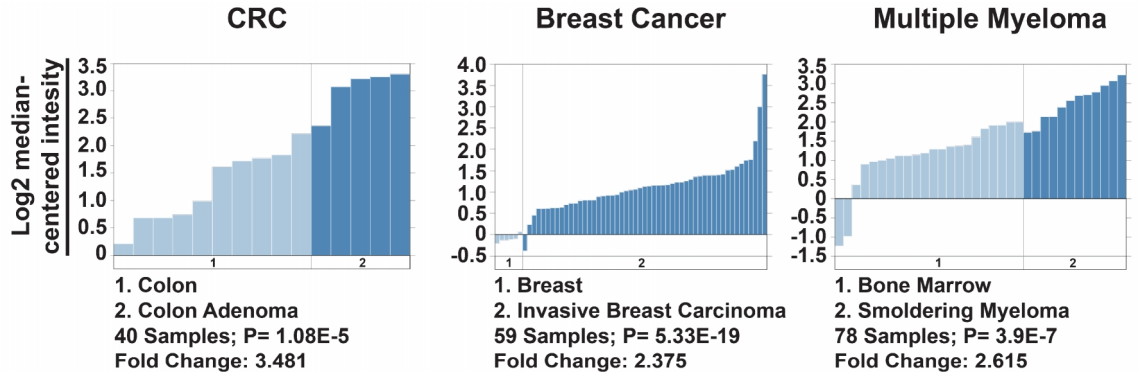

Figure VIII. Comparison of *SIK3* mRNA expression in healthy versus cancer tissues. Data were obtained using the Oncomine™ cancer microarray database. P= p-value.

4.3.3 SIK3 mediates intrinsic tumor resistance to T cell attack

SIK3 was among the top 15 hits in the melanoma and the PDAC screening and among the top 10 candidates in the secondary screen. Validation assays showed remarkable increased T cell-mediated lysis upon SIK3 knockdown with three non-overlapping siRNA sequences. Interestingly, without the addition of T cells, SIK3 depletion did not affect tumor cell viability. These data seem to question the described role of SIK3 in tumor progression and metastasis (section 4.3.2). However, it is possible that some cancer cells (such as PANC-1) respond to SIK3 depletion by activating compensating signaling loops, which sustain tumor cell viability [279]. Other cell lines, such as Hela, are indeed sensitive to SIK3 knockdown and undergo massive cell death in the absence of other stimuli (data not shown).

Experimental measurement of T cell-mediated lysis showed that SIK3 proficient tumor cells are resistant to the attack of T cells. As broadly explained in the introduction, tumor cells can resist to immune cell attack using several tricks that can either dampen immune cell activation or intrinsically increase tumor resistance to immunity (section 1.3). Our data show that T cells did not increase their activation after impairment of SIK3 in tumor cells, while the only addition of the supernatant of activated T cells resulted in dramatic tumor cell death. These data suggest that SIK3 acts as key mediator of intrinsic tumor resistance towards immunity.

Interestingly, SIK3 proficient tumor cells increased their proliferation rate after stimulation with the supernatant of activated T cells. This observation was further confirmed in co-culture models of several T cells and tumor cells (data not shown). The mechanism underlying this paradoxical effect remains elusive, although tumor proliferation may be the result of multiple signals mediated either by soluble or surface associated ligands from T cells. Coherently with this hypothesis, it was shown that MDA-MB231 breast cancer cells proliferate after co-culture with activated T cells because of the induction of CD40 signaling in tumor cells by CD40L from T cells [280].

4.3.4 SIK3 is a molecular switch for TNF-α-induced responses in tumor cells

In this study, TNF-α was identified as a key cytokine that mediates tumor cell death in SIK3-depleted cells. A small sub-population of $CD8^+$ T cells from TIL#1 secreted TNF-α

after stimulation with tumor cells. A recent study from Prof. Beckhove's group, demonstrated that TNF-α expression in CRC infiltrating lymphocytes is restricted to tumor-specific TCs [206]. Similar to CRC, it is conceivable that the TNF-α-secreting PDAC T cells express a TCR, which specifically recognize tumor-associated antigens on PANC-1 cells. However further studies must be conducted to obtain more accurate information on antigen specificity of this bulk population of T cells.

Blockade of TNF-α in the supernatant of activated TILs abrogated cytotoxicity in SIK3 deficient cells, whereas the only addition of TNF-α was sufficient to induce killing of tumor cells after SIK3 depletion. Of note, TNF-α treatment enhanced proliferation of SIK3 proficient tumor cells. These findings underline the role of SIK3 as molecular switch for tumor responses to TNF-α.

TNF-α is a pleiotropic cytokine exerting several homeostatic and pathogenic bioactivities. TNF-α is necessary for optimal host defense mechanisms against pathogens, proper lymphoid-organ architecture and tissue regeneration [281]. During inflammation, this cytokine coordinates recruitment of immune cells into tissues, thus promoting their destruction. Furthermore, TNF-α is responsible of hypernociception and neuronal sensitization of inflamed tissues [281]. It has been shown that uncontrolled TNF-α production is linked to the progression of inflammatory diseases such as rheumatoid arthritis (RA), inflammatory bowel disease (IBD) and psoriasis [281]. TNF-α is implicated in the pathogenesis of cardiovascular diseases, as it can induce apoptosis of cardiomyocytes and promote atherosclerosis by affecting lipid metabolism and inducing vascular inflammation [281].

Despite its well-characterized function during inflammation, the impact of TNF-α in cancer is controversial. TNF-α was primarily identified as tumor-protective cytokine, as several tumor cell lines (such as MCF-7) underwent cell death upon TNF-α treatment [282]. These observations were confirmed *in vivo*, as intratumoral addition of TNF-α resulted in tumor hemorrhagic necrosis in syngeneic and xenograft mouse models [283]. Beside its direct effect on tumor cells, it was shown that high doses of TNF-α cause destruction of newly formed blood vessels, thus compromising blood supply in the tumor [283-285].

However, accumulating evidence suggests that TNF-α might also exert the opposite effect in cancer, i.e. induction of carcinogenesis and promotion of tumor progression [286]. For instance, genetic ablation of TNF-α in mice resulted in dramatic reduction of skin tumors after treatment with oxadaic acid and 12-O-tetradecanoylphorbol 13-acetate (TPA) [287, 288]. Similar results were obtained in transgenic mice lacking TNFR-I or TNFR-II [289]. Furthermore, in a mouse model of inflammation-induced colon carcinogenesis, impairment of TNFR-I signaling significantly reduced the incidence of colonic tumors as compared to WT control mice [290].

It is currently conceived that chronic inflammation plays a pivotal role in tumorigenesis and cancer progression [291]. Being one of the major drivers and sustainers of inflammation, TNF-α is produced by several cell types in the tumor microenvironment, such as myeloid cells and TILs [206, 283]. Its action on tumor cells induces further genetic damage of malignant cells and promotes EMT [292-294]. Upon TNF-α stimulation, tumor cells are prompted to produce additional TNF-α as well as other cytokines and chemokines, which in turn stimulate remodeling of the extracellular matrix and promote angiogenesis [295, 296].

Because of its pivotal role in cancer, several attempts were made to target TNF-α axis for cancer treatment. Systemic administration of TNF-α is not applicable in cancer patients as it causes severe toxicity, such as cytokine storm [207, 208]. For this reason, this cytokine is only administered through locoregional drug delivery systems, such as isolated limb perfusion or isolated hepatic perfusion. Several studies show clinical benefit in patients with soft tissue limb sarcomas and with non-resectable liver malignancies [297, 298]. However, clinical benefit is only achieved by combining the cytokine with conventional anticancer agents. Therapeutic approaches antagonizing TNF-α are currently used for the treatment of inflammatory and autoimmune diseases . However, several Phase II clinical trials have been conducted using this class of drugs in cancer. Administration of Etanercept, a TNF-α antagonist, showed prolonged disease stabilization in patients with advance ovarian cancer [299]. In another study, Infliximab, a human TNF-α neutralizing IgG, sowed efficacy in some patients with advanced renal cell cancer refractory to standard treatments [300]. These

contradictory findings suggest that further investigation must be conducted to elucidate which kind of tumor patients would befit from TNF-α agonist or antagonist therapy.

Taken together, these studies underline the translational impact of this work, as elevated levels of intratumoral TNF-α in conjunction with SIK3 inhibition, may lead to effective tumor regression. Furthermore, the relatively low levels of systemic TNF-α compared to tumor tissues, would ensure confined cytotoxicity in the tumor microenvironment in response to SIK3 blockade, without having major systemic adverse effects.

4.3.5 Molecular aspects of SIK3 involvement in the TNF-α axis

TNF-α can canonically bind to two receptors, TNFR-I and TNFR-II. TNFR-I is pleiotropically expressed, while TNFR-II expression is restricted to specific neuronal subtypes, endothelial cells and some immune cells [301]. Coherently with literature data, FACS analysis revealed that PANC-1 cells express TNFR-I but not TNFR-II. Additionally, blockade of TNFR-I, rescued SIK3-depleted tumor cells from TNF-α induced cell death. Therefore, further experiments were focused on the TNFR-I pathway.

In this work, the involvement of SIK3 in TNFR-I downstream signaling was hypothesized. SIK3 phosphorylation upon TNF-α stimulation could not be directly proven, because of lack of pSIK3-specific antibodies. However, this work shows for the first time that the upstream master kinase of SIK3, LKB1 [211, 212, 302, 303] is activated upon TNF-α stimulation. Coherently with this observation, Lombardi et al., detected higher pLKB1 in macrophages after activation of TLR4 and IL1R [304], two receptors sharing multiple intracellular pathways with the TNFR-I downstream signaling cascade [305, 306].

TNFR-I activation exerts versatile bioactivities comprising inflammation, proliferation and apoptosis. TNF-α binding to TNFR-I results in the recruitment of the adaptor molecule TRADD (TNFR-I-associated death domain protein) and the formation of diverse signaling complexes: i) the complex I, which results in pro-inflammatory and proliferative effects via activation of NF-κB and mitogen-activated protein kinases (MAPKs) pathways [307-309]; ii) the complexes IIa and IIb which can induce caspase-

dependent cell death (apoptosis); iii) the complex IIc which can results in the activation of programmed caspase-independent cell death (necroptosis) [281, 310]. The responsible factors that determine which complex is engaged upon TNFR-I activation, are not well understood. A simplified model suggests that TNFR-I binds as first instance to the complex I, and after 15-20 min, de-ubiquitination of some proteins from the complex I, such as receptor interacting serine/threonine kinase 1 (RIPK1) and TNF receptor associated factor 2 (TRAF2) lead to the formation of the complex II (a, b or c) [281, 310]. Ultimately, the fate of a TNF-α stimulated cell depends on the balance between pro-survival and pro-apoptotic factors [310].

Increased levels of cleaved caspase 8 [311] and caspase 9 [311] and pJNK [216-218] were observed in SIK3 impaired tumor cells following TNF-α treatment, suggesting that SIK3 prevents ,directly or indirectly, apoptosis induction in tumor cells upon TNF-α stimulation.

Based on the evidence of NF-κB being the major transcription factor that determines the fate of TNF-α-stimulated cells [110], and the observation that its activation prevents apoptosis induction via trans-activation of pro-survival and anti-apoptotic genes [103], a putative role of SIK3 in modulating NF-κB activation was hypothesized. The current study shows that the NF-κB pathway is constitutively active in PANC-1 cells and that SIK3 promotes NF-κB nuclear translocation after TNF-α stimulation, resulting in increased tumor cell proliferation. These data were corroborated by the RNA-seq results showing a striking impairment of NF-κB target genes in TNF-α stimulated tumor cells that were depleted of SIK3. Coherently with these data, Luan et al., showed that in murine bone marrow macrophages (BMMs), knockdown of SIK proteins resulted in reduced NF-κB binding to promoters of pro-inflammatory cytokine genes, in response to lipopolysaccharide (LPS) stimulation [224].

The same authors showed that depletion of SIK proteins decreased HDAC4 phosphorylation [224]. HDAC4 is a direct target of SIK kinases in several cell types such as mouse macrophages, mouse hepatocytes and human adipocytes [224, 302, 312]. Its phosphorylation leads to its shuttling form the nucleus to the cytoplasm, where it binds to 14-3-3 and remains inactive [313, 314]. In BMMs, HDAC4 physically interacts with p65 subunits of NF-κB and its knockdown results in increased NF-κB

acetylation [224]. It was demonstrated that acetylated p65 is retained longer in the nucleus, because of its lower affinity to IκBα, compared to its de-acetylated counterpart [315-317]. Given these studies, it is reasonable to hypothesize that SIK3 modulation of NF-κB occurs via HDAC4. The observation that knockdown of HDAC4 rescued SIK3-depleted cells from TNF-α mediated killing, confirmed the validity of this hypothesis.

In contrast to these observations, two studies suggest that, in macrophages SIK3 can actually act as negative regulator of NF-κB activation [318, 319]. In particular, SIK3 overexpression resulted in impaired NF-κB activation and proinflammatory cytokine secretion in LPS-stimulated macrophages [318], while SIK3 KO mediated the opposite effect [318, 319]. However, Darling et al. [320], could not reproduce these results using SIK3 kinase-dead macrophages, hinting that the loss of the entire SIK3 protein may influence NF-κB activation in ways that are independent of its catalytic activity.

Other reported targets of SIK kinases are CREB-regulated transcription coactivators (CTRCs) [314, 321, 322]. It was shown that SIK3 phosphorylates CTRC2 [323], resulting in its deactivation and nuclear export [323]. CTRCs sustain CREB-dependent gene expression [324-326] and the latter competes with NF-κB activity [327-329]. In this study, the impact of CTRCs in NF-κB modulation was not addressed in the used tumor models. The current work suggests that SIK3-induced HDAC4 phosphorylation is the major mechanism promoting NF-κB nuclear retention; although the possibility that that SIK3-mediated CTRCs phosphorylation contributes to sustain NF-κB transactivation, cannot be excluded.

A schematic representation of the suggested molecular mechanisms that governs SIK3-dependent tumor cell response to TNF-α is depicted in Figure IX.

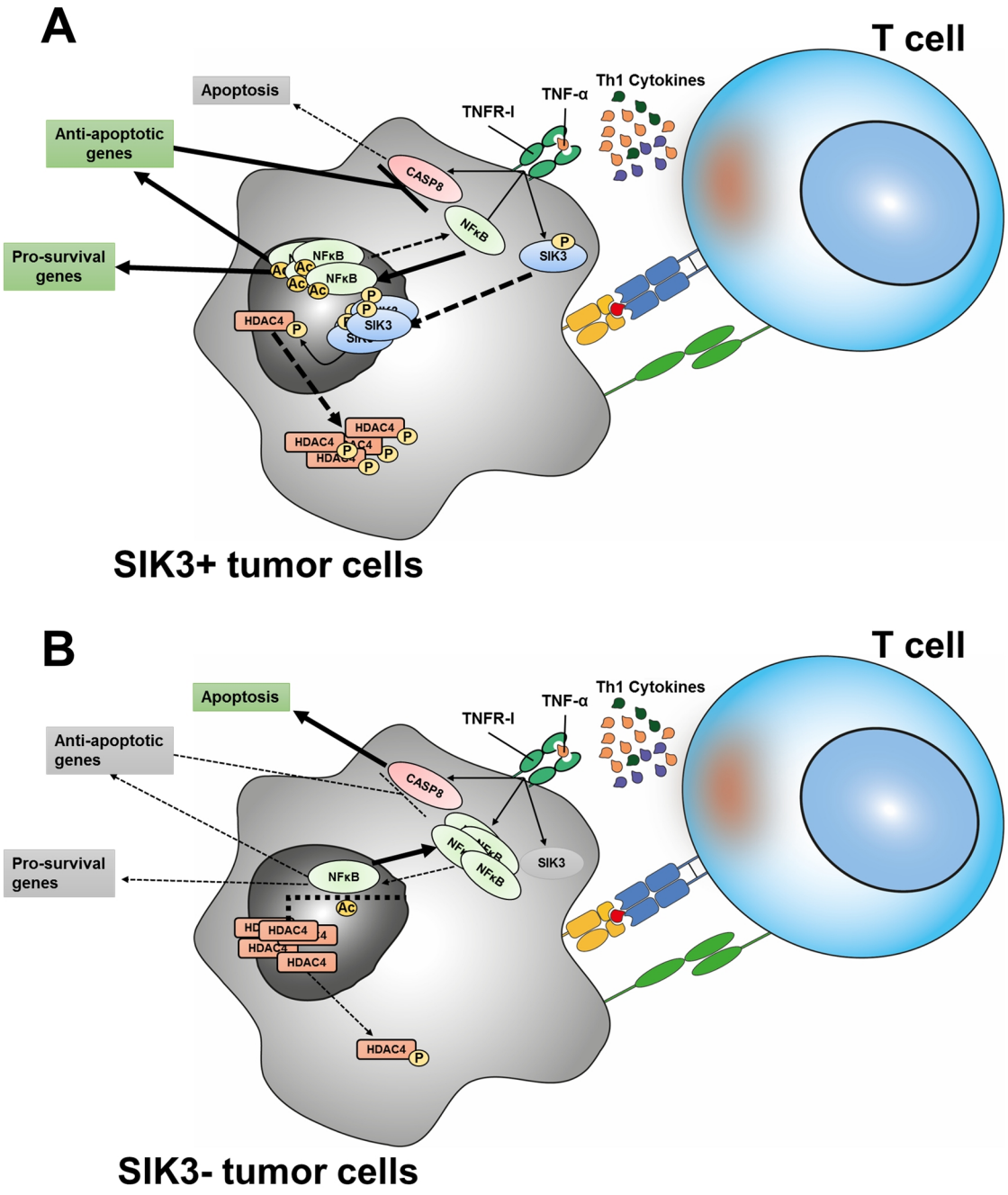

Figure IX. Proposed molecular mechanisms of SIK3 involvement in TNF-α biological response. T cell recognition of tumor cells results in Th1 cytokine secretion including TNF-α. Alternatively, TNF-α can be released by other cells in the tumor microenvironment. **(A) SIK3 proficient cells.** Binding of TNF-α to TNFR-I on tumor cells results in multiple downstream signaling cascade that involves caspase 8 cleavage, NF-κB nuclear translocation and SIK3 phosphorylation. NF-κB nuclear retention is sustained by its acetylation, and HDAC4 deacetylase acts as negative regulator of NF-κB. SIK3 phosphorylates HDAC4, thereby initiating its shuttling from the nucleus to the cytoplasm. The lack of nuclear HDAC4 sustains NF-κB nuclear retention. Nuclear NF-κB leads to the transactivation of pro-survival and anti-

apoptotic genes, which in turn impede caspase 8 activation. **(B) SIK3 deficient cells**. In the absence of SIK3, HDAC4 is predominantly retained in the nucleus, thus leading to NF-κB de-acetilation. Non-acetylated NF-κB preferentially shuttles from the nucleus to the cytoplasm. As a result, the impairment of NF-κB-induced anti-apoptotic genes, results in caspase 8 cleavage and apoptosis induction.

4.3.6 Translational implications of SIK3 inhibition for cancer immunotherapy

The major aim of this work was to identify novel immune modulatory molecules that could be used as potential targets for the development of novel therapeutic tools. Some aspects hinting to the translational relevance of SIK3 blockade in cancer therapy have been already addressed in this chapter (sections 4.3.2, 4.3.3, 4.3.4). In addition, further experiments were conducted to prove the clinical applicability of SIK3 inhibition. A summary of the rationale of SIK3 inhibition in cancer therapy is schematized in Table 3.

Inhibition of SIK protein kinases with a small molecule compound resulted in a dose-dependent enhancement of TIL-mediated killing in tumor cells. Similar results were obtained when tumor cells were stimulated with TNF-α instead of TILs. Due to the lack of a SIK3-specific compound, a pan-SIKs inhibitor was used for these assays. Of note, single knockdown of SIK1 and SIK2 did not enhance TIL-mediated killing, hinting to an isoform-specific role of SIK3 in mediating resistance towards immune attack. This finding was not surprising as SIK isoforms share highly similarity in several domains and yet they exert opposite functions in tumors (section 4.3.2).

Gene expression databases suggest that SIK3 is expressed in T cells as well (data not shown). Hence, it is possible that inhibition of this protein kinase may on one side, render tumor cells more susceptible to the attack of T cells, and on the other side, impair T cell functionality. As an example, JAK2 blockade sensitized tumor cells to the attack of NK cells [234]. However, two recent studies show that ruxolitinib, a clinically approved JAK1/2 inhibitor, impairs NK and T cell function in myeloproliferative neoplasms [330-332]. In the experimental model used in this work, the pan-SIK inhibitor was not removed before the addition of T cells to tumor cells. Hence, the observation that increased TIL-mediated cytotoxicity occurs in the presence of the pan-SIKs inhibitor, suggests that SIKs inhibition does not affect T cell cytotoxic ability. Nevertheless, further experiments must be conducted to elucidate the exact role of SIK3 blockade in T cells.

Several recent studies showed that antiangiogenic tyrosine kinase inhibitors (TKIs) target multiple components of the tumor microenvironment and synergize with cancer immunotherapy. For instance, cabozantinib, an inhibitor of the rearranged during transfection (RET) receptor tyrosine kinase [235], can sensitize Lewis lung carcinoma cells and MC38 murine colon carcinoma cells to the attack of CEA-specific T cell clones [235, 333]. Furthermore, combination of cabozantininb with the cancer vaccine MVA/rF-CEA/TRICOM, results in increased intratumoral infiltration of $CD8^+$ T cells and decrease of T_{regs} and MDSCs, thus promoting anti-tumoral immune environment [333].

Likewise, it is conceivable that inhibition of SIK3 kinase activity might affect the tumor immune environment as well, and that combination of a SIK3 inhibitor with immunotherapeutic strategies, such as cancer vaccine or immune checkpoint blockade, would on the one side boost immune cell activation and, on the other side, sensitize tumor cells towards immunity.

A *proof-of-principle* experiment to test the therapeutic applicability of SIK3 blockade in cancer immunotherapy was conducted *in vivo*, using NSG mice and ACT. Adoptive transfer of melanoma-derived human TIL209 into tumor-bearing immunodeficient mice resulted in significant retardation of SIK3 deficient tumor cell growth compared to control. Adoptive cell therapy is one of the most effective immunotherapeutic approaches for the treatment of metastatic melanoma, as it induces durable tumor regression in these patients [230]. However, in vitro studies conducted in this laboratory showed weak activity of some TIL cultures from melanoma patients after co-culture with their respective autologous tumor pair (data not shown), suggesting that not all tumor patients might benefit from this therapy. Given the pivotal role of SIK3 in mediating resistance to the immune system, it is reasonable that combination of SIK3 inhibition with ACT may represent a novel path in cancer immunotherapy.

Rationale of SIK3 blockade for cancer therapy	Section
As monotherapy	
Affects intrinsic tumor cell survival	4.3.2
Sensitizes tumor cells to the attack of residing TILs	4.3.3
Sensitizes tumor cells to intratumoral TNF-α	4.3.4
As combined therapy	
With cancer vaccines	4.3.6
With immune checkpoints blockade	4.3.6
With ACT	4.3.6

Table 3. Summary of therapeutic approaches using SIK3 inhibition in cancer.

4.3.7 Concerns about SIK3 inhibition

One of the major concerns about SIK3 targeted therapy is the presence of *SIK3* mRNAs in a variety of healthy tissues, as shown in databases for gene expression profiles (data not shown). These microarray-based results would need an experimental confirmation; however, they hint to possible adverse effects of systemic SIK3 blockade. Furthermore, $Sik3^{-/-}$ mice show malnourished phenotype, and the majority of these animals dies within the first day after birth [269]. However, Sundberg et al., generated a novel pan-SIK kinases inhibitor and tested its toxicity *in vivo* [334]. Mice that received daily injection of pan-SIK inhibitor for one week did not show changes in weight or adipocyte-derived metabolites, suggesting that acute inhibition of SIK kinases does not recapitulate the adverse effects observed after genetic deletion of *Sik3* [334].

SIK inhibitors have been widely tested in the context of macrophage biology. Several reports show that pan-SIK kinase inhibition switches activated macrophages from pro-inflammatory M1 to the tolerogenic M2 phenotype [224, 304, 322, 334, 335]. For this reason, SIK inhibition has been proposed for the treatment of chronic relapsing

inflammatory disorders such as IBD [191]. The presence of M2 macrophages correlates with poor prognosis in cancer patients [336, 337]. Hence, the usage of pan-SIK inhibitors in cancer could be hypothetically compromised by the establishment of an immunosuppressive tumor microenvironment. However, it was shown that SIK3 kinase activity in bone marrow-derived dendritic cells (BMDCs) is about 10 times weaker than SIK2, and that blockade of SIK3 kinase activity is not sufficient to induce IL-10 production in LPS-stimulated macrophages [320]. Coherently with these observations, Sundberg et al., showed that IL-10 production in zymosan-activated DCs correlates with the potency of small molecule compounds in inhibiting specifically SIK2 kinase [191]. Taken together, these studies suggest that immunosuppression can be mostly attributed to blockade of SIK2, rather than SIK3. Hence, the generation of a SIK3-specifc inhibitor would elicit tumor sensitization to immune attack, without inducing a tolerogenic microenvironment.

5. Conclusion

Therapeutic strategies that reinforce the immune system against cancer are opposed by the numerous immune modulatory mechanisms exploited by the tumor and its microenvironment. This work aimed to achieve a comprehensive overview of tumor immunological features by unravelling the whole arsenal of immune modulators expressed by tumor cells. Performance of RNAi based screens in several tumor models underlined the considerable heterogeneity of immunological features in different cancer types. In this context, this work contributes to a better understanding of cancer immunology, suggesting that the variability of patients' responses to immunotherapy can be ascribed to a differential immune signature across different tumors. This interpretation underlines the idea that personalized medicine holds the future for cancer therapy.

The list of potential immune modulators obtained by this, and related RNAi screens, revealed a multitude of molecular factors with diverse functions in cell biology. This observation leads to the consideration that the current vision of cancer immune escape is reductive and that most key immune escape mechanisms remain obscure.

In this direction, the discovery of SIK3 as a key modulator of tumor intrinsic resistance towards immune cell attack opens new horizons for the development of novel classes of drugs that could efficiently render tumor cells more susceptible to the immune system.

6. Materials and Methods

6.1 Materials

6.1.1 Laboratory equipment

Instrument	Company
7300 Real-Time PCR System	Applied Biosystems
Bolt® Mini Gel Tank	Life Technologies
Casy cell counter	Innovatis
FACS Canto II Flow cytometer	BD
FACSARIA II cell sorter	BD
Gamma Cell 1000	Best Theratonics
Gamma Counter (Cobra Packard)	PerkinElmer
GeneMate Electrophoresis Systems	Starlab
HiSeq 3000	Illumina
Incucyte ZOOM	Essen bioscience
Infinite M200 plate reader	Tecan
MAGPIX system	Merk Millipore
Mini Trans-Blot Cell	Biorad
Mithras LB 940 microplate reader	Berthold
Molecular Imager (ChemiDoc XRS+)	Bio-Rad
NanoDrop 2000c UV-Vis Spectrophotometer	Peqlab
Phero-stab 500 Electrophoresis power supply	Biotec-Fischer
PowerPac 3000 Power supply	Biorad
Spark microplate reader	TECAN
Thermal Cycler	Thermo scientific
Thermomixer comfort / compact	Eppendorf
UV gel documentation system	Konrad Benda
Vernier caliper (Digital)	Carl Roth

6.1.2 Chemicals and reagents

Material	Company
1 kb DNA Ladder (GeneRuler)	Thermo Scientific
2x MyTaq HS Red Mix	Bioline
Agarose	Life Technologies
Altogen PANC-1 transfection reagent (Altogen 1)	Altogen Biosystem
Altogen PANC-1 transfection reagent plus liposome condenser (Altogen 2)	Altogen Biosystem
Amersham ECL Prime Western Blotting Detection Reagent	GE Healthcare
Ampicillin	Sigma-Aldrich
Aqua ad iniectabilia	B. Braun
Assay Diluent	BD
Benzonase	Merck
Beta-mercaptoethanol	Gibco
Biocoll separating solution	Millipore
Bovine serum albumin (BSA)	Sigma-Aldrich
Customized ASTL primers for qPCR Fwd: GCGCCCCTGGCCTCCAGCTGCGCA Rvs: CACGACACCACTACCACCCATGGG	Sigma-Aldrich
Customized CEACAM6 primer for PCR and qPCR Fwd: CAAAAGGAACGATGCAGGAT Rvs: TGGCAGGAGAGGTTCAGATT	Sigma-Aldrich
Customized β-actin primer for PCR and qPCR Fwd: AGAAAATCTGGCACCACACC Rvs: GGGGTGTTGAAGGTCTCAAA	Sigma-Aldrich
Dimethyl sulfoxide (DMSO)	Sigma-Aldrich
Dynabeads Human T-Activator CD3/CD28	Thermo Scientific
EDTA 1% (w/v) without Mg2+	Biochrom
Ethanol absolute	Sigma-Aldrich
GelRed Nucleic Acid Gel Stain	Biotium

Geneticin sulfate (G418)	Gibco
G-Rex100 Gas permeable cell culture device	Wilson Wolf Manufacturing
HiPerfect transfection reagent	Qiagen
Hs CDC42BPA 1 SG, Hs MLN 1 SG QuantiTect Primer Assay (for PCR and qPCR)	Qiagen
IL-2 (human, recombinant)	Novartis
Ionomycin calcium salt	Sigma-Aldrich
Isopropanol	Fluka
Jet-PEI	Polyplus-transfection
Kiovig	Baxter
Kiowig	Baxter
Lipofectamine LTX with Plus™ reagent	Thermo Scientific
Lipofectamine RNAiMAX	Life Technologies
Loading dye solution (6x)	Fermentas
Mammalian Protein Extraction Reagent (MPER)	Thermo Scientific
Matrigel growth factor reduced (Cat. N. 356230)	Corning
MES SDS running buffer (20x)	Life Technologies
Methanol	Sigma
$Na_2\,^{51}CrO_4$ (5 mCi, 185 MBq)) (^{51}Chromium)	Perkin Elmer
Negative control siRNA 1 and 2	Ambion
Nuclease free water	Ambion
NuPAGE 4-12% Bis-Tris Gels	Thermo Scientific
NuPAGE LDS Sample Buffer	Thermo Scientific
Pacific orange dye	Thermo Scientific
PageRuler Prestained Protein Ladder	Thermo Scientific
pCDNA3.1 empty vector (EV)	GenScript
pEGFP-Luc plasmid	Provided by Dr. Rudolf Haase. LMU Munich

Phorbol 12-myristate 13-acetate (PMA)	Sigma-Aldrich
Phosphatase inhibitor III	Sigma-aldrich
Phytohaemagglutinin (PHA)	Sigma-Aldrich
Polyvinylidene diflouride (PVDF) membrane	Millipore
Ponceau S solution	Sigma-Aldrich
Protease Inhibitor Cocktail Set III, EDTA-Free	Calbiochem
Puromycin (10 mg/mL)	GIBCO
RT² qPCR Primer Assay for Human ASTL (for PCR)	Qiagen
RT² qPCR Primer Assay for Human SIK3, MAST3, NTSR2, IL36G, LIMK2, FAM195A, GPR31 and FAT1, CD274 (PD-L1) (for PCR and qPCR)	Qiagen
SDS polyacrylamide gels (4-12% Bis/Tris)	Life Technologies
SIK3 overexpression plasmid (pCDNA3.1 backbone)	GenScript
Skimmed milk powder	Carl Roth
TransIT	Mirus
Triton X-100	Fluka
Trypan blue solution (0.4 %)	Fluka
Trypsin-EDTA (1x)	Sigma-Aldrich
Tween 20	Sigma-Aldrich
Whatman 3 mm gel blot paper	Sigma-Aldrich

6.1.3 Assay kits

Material	**Company**
BioPlex ProHuman Chemokine TNF-α Set	Bio-Rad
Human Granzyme B ELISA development kit	Mabtech
Human IFN-γ ELISA Set	BD OptEIA
Human Perforin ELISA PRO kit	Mabtech
MILLIPLEX MAP Early Phase Apoptosis 7-plex-kit	Merck Millipore
NF-κB p50/p65 EZ-TFA Transcription Factor Assay kit	Millipore

Pierce BCA Protein Assay Kit	Thermo Scientific
QuantiFast SYBR Green PCR Kit	Qiagen
QuantiTect Reverse Transcription Kit	Qiagen
RNeasy Mini Kit	Qiagen
ScriptSeqTM Complete Kit	Illumina
TNF-α secretion assay (catch assay)	Miltenyi biotech
WST-1 Cell Proliferation Assay	Roche

6.1.4 siRNAs, siRNA libraries and lentiviral particles (shRNAs)

Material	Company
siGENOME set of four upgrade siRNAs against: SIK3, MAST3, MLN, ASTL, IL36G, NTSR2, LIMK2, CDC42BPA, GPR31, FAM195A and FAT1	Dharmacon, GE healthcare
siGENOME smart pools against: PD-L1, CEACAM6, Fluc, RCAS-1, GAL-3, UBC, CHK1, COPB2, PLK1	Dharmacon, GE healthcare
AllStars Hs Cell Death Control siRNA	Qiagen
ON-TARGET plus pool of four siRNAs for HDAC4	Dharmacon, GE
Silencer Negative control No.1 (shCtrl1)	Thermo Scientific
Silencer Negative control No.2 (shCtrl2)	Thermo Scientific
Sub-library of the siGENOME library for the primary screen	Dharmacon, GE healthcare
Customized siRNA library for the secondary screen	Dharmacon, GE healthcare
Mission Non-Mammalian shRNA Control (shCtrl) Lentiviral Transduction Particles (Clone SHC016H)	Sigma-Aldrich
Mission Non-Mammalian shRNA SIK3 (shSIK3) Lentiviral Transduction Particles (Clone TRCN0000037452)	Sigma-Aldrich

6.1.5 Consumables

Material	Company
384-well plates white opaque	Greiner
96-well plates white opaque	Perkin Elmer
Conical centrifuge tubes (15 and 50 mL)	TPP
Cryogenic vials (2 mL)	Corning
Disposable needles (0,4 x 20 mm)	Henke Sass Wolf
Disposable syringes (1 mL)	Henke Sass Wolf
Disposable syringes (50 mL)	BD
Flat-bottom plates (6 and 96 well)	TPP
Freezing container (Mr. Frosty)	Nalgene, Thermo Scientific
Luma plates	PerkinElmer
Pipette filter tips (10 µl - 1000 µl)	Starlab
Polystyrene round bottom tubes with caps	Falcon
Round-bottom plate (96 well)	TPP
Safe-lock tubes (0.5, 1.5, 2.0 mL)	Eppendorf
Syringe filter units (0.22 µm-pores)	Millipore
Tissue culture flask/filter cap (25, 75, 150 cm2)	TPP

6.1.6 Buffers

Buffer	Ingredients	Volume
Phosphate saline buffer (PBS)	PBS 10x (Sigma-Aldrich) ddH2O	100 mL 900 mL
Tris Buffer Saline (TBS)	TBS 10x (Sigma-Aldrich) ddH2O	100 mL 900 mL
Immunoblot washing solution (TBS-T)	TBS (10x) ddH2O Tween-20	100 mL 900 mL 0.5 mL

Immunoblot blocking solution for phosphorylated proteins	Immunoblot washing solution BSA	50 mL 5 g
Immunoblot transfer buffer (10x)	Tris base Glycine ddH2O	30.3 g 144 g 1 L
Immunoblot blocking solution for phosphorylated proteins	Immunoblot washing solution Milk	50 mL 2,5 g
SDS-PAGE running buffer	MES SDS running buffer (20x) ddH2O	50 mL 950 mL
Tris-acetate-EDTA (TAE) buffer (50x)	Tris Glacial acetic acid 0.5 M EDTA ddH2O pH	242 g (2 M) 57.1 mL 100 mL 1 L 8.5
BL Buffer	ddH2O HEPES (50 mM) EDTA (0,5 mM) Phenylacetic acid (0,33 mM) Oxalic acid (0,07 mM) pH	84,8 mL 5 mL 0,1 mL 0,033 mL 0.07 mL 7,6
B2 Buffer	ddH2O DDT (415 mM) ATP (33 mM) AMP (0,996)	85 mL 6,4 g 1,82 g 0,035 g
Lysis buffer for the luciferase-based cytotoxicity assay	BL buffer 10% Triton-X-100	48,5 mL 1,5 mL
Luciferase assay buffer	BL buffer B2 buffer D-Luciferase (10mg/mL) 1M $MgSO_4$	44,35 mL 5 mL 0,65 mL 751 µL
FACS buffer	FCS PBS	2 % 500 mL

6.1.7 Cell media and supplements

Material	Company
Ab serum (heat-inactivated), human	Valley Biomedical
AIM-V with L-glutamine, streptomycin sulfate, gentamycin sulfate	Gibco
PROLEUKIN (rHuIL2)	Novartis Pharma
Beta-mercaptoethanol	Gibco
DMEM; high glucose (4.5 g/l), L-glutamine, sodium pyruvate, NaHCO3	Sigma-Aldrich
Dulbecco-PBS without Ca2+, MgCl2 (1x)	Sigma-Aldrich
Fetal calf serum (FCS) (heat-inactivated)	Biochrom
Ham's F12 Nutrient Mixture	Gibco
HEPES buffer (1 M)	PAA
Human rIL-2	Novartis
Penicillin/Streptomycin (P/S; 100X)	PAA
RPMI 1640 with L-glutamine	Gibco
RPMI 1640 with L-glutamine and NaHCO3	Sigma-Aldrich
Opti-MEM	Thermo Scientific

Medium	Component	Amount
Freezing Medium for Tumor Cells	FCS	90 %
	DMSO	10 %
TIL freezing medium A	FCS	60 %
	RPMI	40 %
TIL freezing medium B	FCS	80 %
	DMSO	20 %
Complete lymphocyte medium (CLM)	RPMI	500 mL
	AB serum	50 mL
	P/S	5 mL
	HEPES	5 mL

	Beta-mercaptoethanol	50 µL
TIL expansion medium with feeder cells	CLM	50 %
	AIM-V	50 %
	Feeder cells	100x TILs
	OKT3	30 ng/mL
	rHuIL-2	3,000 U/mL
TIL expansion medium without feeder cells	CLM	50 %
	AIM-V	50 %
	rHuIL-2	3,000 U/mL
Complete melanoma medium (CMM)	DMEM	300 mL
	RPMI	100 mL
	Ham's F12 Nutrient Mixture	100 mL
		50 mL
	FCS	5 mL
	P/S	5 mL
	HEPES	
Complete DMEM	DMEM	500 mL
	FCS	50 mL
	P/S	5 mL

6.1.8 Cell lines

Cell Line	Origin	Culture Medium
Caco-2	Colorectal cancer	Complete DMEM
HEK293T	Human embryonic kidney	Complete DMEM
M579	Melanoma patient-derived primary cell culture	Complete melanoma medium
M579 shCtrl	Melanoma patient-derived primary cell culture	Complete melanoma medium, 0,4 µg/mL Puromicin

M579 shSIK3	Melanoma patient-derived primary cell culture	Complete melanoma medium, 0,4 µg/mL Puromicin
MCF7	Breast adenocacinoma	Complete DMEM
PANC-1	Pancreatic ductal adenocarcinoma	Complete DMEM
PANC-1-Luc	Pancreatic ductal adenocarcinoma	Complete DMEM, 1 mg/mL G418
Survivin antigen-specific T cells	Peripheral blood of breast cancer patient	RPMI, 10% Human AB serum, 1% P/S
SW480	Colorectal cancer	Complete DMEM
TIL#1 and TIL#2	Pancreatic cancer patient-derived	Complete lymphocyte medium
TIL209 and TIL412	Melanoma cancer patient-derived	Complete lymphocyte medium

6.1.9 Antibodies and recombinant proteins

6.1.9.1 Western blot

Specificity	Species	Isotype	Conjugate	Company	Application
Anti-CEACAM6	rabbit	IgG	-	Abcam (ab98109)	WB; 1:1000
Anti-LKB1	rabbit	IgG	-	Cell signaling	WB; 1:1000
Anti-MAST3	rabbit	IgG	-	Acris	WB; 1:1000
Anti-PD-L1	mouse	IgG	-	R&D systems	WB; 1:500
Anti-pLKB1	rabbit	IgG		Cell signaling	WB; 1:1000
Anti-SIK3	rabbit	IgG	-	Abcam (ab88495)	WB; 1:1000
Anti-β-actin	mouse	IgG1	-	Abcam	WB; 1:5000
Secondary anti-mouse	goat	IgG	HRP	Santa Cruz	WB; 1:5000
Secondary anti-rabbit IgG	goat	IgG	HRP	Santa Cruz	WB; 1:5000

6.1.9.2 FACS antibodies

Specificity	Species	Isotype	Conjugate	Company	Dilution
Anti-HLA-A2		IgG2b	APC	Biolegend	1:20
Isotype		IgG2b	APC	Biolegend	1:20
Anti-CD3	mouse	IgG2a	APC	BD	1:20
Anti-CD4	mouse	IgG1	PerCP-Cy5.5	BD	1:20
Anti-CD8	mouse	IgG2a	FITC	BD	1:20
Anti-CD8	mouse	IgG1	V450	BD	1:20
anti-PD1	mouse	IgG1	PE/Cy7	BioLegend	1:20
Isotype	mouse	IgG1	PE/Cy7	BioLegend	1:20
Anti-LAG3	Goat	IgG2	FITC	R&D sytem	1:20
Isotype	Goat	IgG2	FITC	R&D sytem	1:20
Anti-TIM3	rat	IgG2a	PE	R&D system	1:5
Isotype	rat	IgG2a	PE	R&D system	1:5
Anti-TNFR-I	mouse	IgG2	-	Hycult biotech	40 µg/mL
Isotype	mouse	IgG2a	-	eBioscience	40 µg/mL
Anti-TNFR-II	mouse	IgG2	-	Acris antibodies	1 µg/mL
Isotype	mouse	IgG2	-	eBioscience	1 µg/mL
Phycoerythrin-F(ab')2 Fragment	goat	IgG	PE	Jackson Immuno	1:4000

6.1.9.3 Functional assays

Specificity	Species	Isotype	Cat. N.	Company	Application
Anti-MHC-I Cone W6/32	mouse	IgG2a	-	-	Prof. Gerd Moldenhauer (DKFZ - Heidelberg
Isotype	Mouse	IgG2a	-	-	Prof. Gerd Moldenhauer (DKFZ - Heidelberg
anti-TNFR-I	mouse	IgG2a	M1013A	Hycult biotech	Functional test
Isotype	mouse	IgG2a	E04251	eBioscience	Functional test
anti-TNFα	mouse	IgG1	ab8348	Abcam	Functional test
Anti-TRAIL	mouse	IgG1	Ab10516	Abcam	Functional test
Isotype	mouse	IgG1	ab18437	Abcam	Functional test
Anti-FASL	mouse	IgG1κ	306409	Biolegend	Functional test
Isotype	mouse	IgG1κ	400153	Biolegend	Functional test
rHuTNF-α	-	-	-	-	Prof. Daniela Männel (University of Regensbug)

6.1.10 Software

Software	Developer
Endnote (X7)	Adept Scienctific
Graph Pad Prism (6)	GraphPad Software
Microsoft Office 2013	Microsoft, USA
ImageJ	Wayane Rasband
Adobe Illustrator	Adobe system
cellHTS2	Boutros et al [338]
FlowJo	Tree Star

6.1.11 Mice

Non-obese diabetic (NOD)-severe combined immunodeficient (SCID) Il2rg$^{-/-}$ gamma (NSG) mice were used in this study. Original mouse strain was obtained from the Jackson Laboratory (strain name: NOD.Cg-*Prkdcscidl2rgtm1Wjl*/SzJ) and were bred at the mouse facility of the University Hospital of Regensburg. Animal experiments were approve by the regulatory authorities (Würzburg). Ethical guidelines were followed according to the local regulations.

6.2 Methods

6.2.1 Tumor cell lines

PANC-1 (pancreatic ductal adenocarcinoma), MCF7 (breast carcinoma), HEK293 (human embryonic kidney), SW480, Caco-2 (both breast cancer) cell lines were acquired from the American Type Cell Culture (ATCC). PANC-1-luc cells were generated after transfection with a plasmid encoding for the GFP-luciferase fusion protein (pEGFP-Luc plasmid) and for the G418-resistance gene. The plasmid was kindy provided by Dr. Haase (LMU-Munich). TransIT was used as transfection reagent according to the manufacturer´s instructions. Transfected cells were selected for 14 days with G418-containing medium (1 mg/mL). The optimal concentration of G418 was established by titration of the toxic dosage of G418 in PANC-1 cells. Afterwards PANC-1 were sorted twice for the expression of GFP by flow cytometry and cultured in the presence of 1 mg/mL G418. Cell sorting was conducted in collaboration with the DKFZ sorting core facility, using the FACSARIA II cell sorter (BD). M579 were kindly provided by Prof. Michal Lotem (Hadassah Hebrew University Medical Center, Israel). These cells carried the expression of the HLA-A201 and the luciferase gene. All cell lines were cultured with the described culture media (section 6.1.7) and maintained at 37°C, 5% CO_2, except for M579 cells, which were maintained at 8% CO_2 .

6.2.2 Generation of stable M579 knockdown cells

Lentiviral transduction particles expressing shRNAs targeting either SIK3-targerting shRNA (shSIK3, section 6.1.2) or control shRNA (shCtrl, section 6.1.2) were used for transduction of M579 melanoma cells. Optimal multiplicity of infection (MOI) was

previously determined as 2, by transducing cells with GFP lentiviral particles at different MOIs. $5x10^4$ M579 cells were seeded in a 6 well plate in complete DMEM. On the next day, cell medium was replaced with DMEM supplemented with 10% FCS (without antibiotics) and the desired amount of lentiviral particles was added. After 24 h of incubation, the particle-containing medium was replaced with complete DMEM. After 24 h of recover, cells were put under positive selection with complete DMEM supplemented with 0,4 µg/mL puromycin. Untransduced cells were cultured with selection medium as control. Selection medium was regularly replenished and transduced cells were transferred to 25 cm^2 and then 75 cm^2 culture flasks as they reached confluency. Knockdown efficiency was tested by qPCR.

6.2.3 Reverse Transcription

Total RNA was isolated from the cell pellets using the RNeasy Mini kit (Qiagen). 1 µg of RNA from each sample was reverse transcribed to complementary DNA (cDNA) using the QuantiTect reverse transcription kit (Qiagen) according to the manufacturer's protocol. To check genomic DNA contamination, water was added instead of reverse transcriptase (-RT controls).

6.2.4 PCR and qPCR

Synthesized cDNA was amplified using conventional PCR. PCR samples were set up in a 25 µL volume using 2x MyTaq HS Red Mix (Bioline), 500 nM of gene-specific primer mix (list of primers in section 6.1.2) and 100 ng of template cDNA. Water was added to the reaction mix instead of cDNA for contamination controls. The PCR program was set as the following: 95°C for 3 min, 35 cycles of a 3 repetitive steps of denaturation (95°C for 15 s), annealing (60°C for 20 s) and extension (72°C for 15 s), and a final step at 72°C for 7 min. PCR products were run on a 2% agarose gel and visualized using the UV documentation system (Konrad Benda). For qPCR, 10 ng of template cDNA, 2x QuantiFast SYBR Green PCR mix (Qiagen) and 300 nM of gene-specific primer mix was used per 20 µL reaction and each sample was prepared in triplicates. Reactions were run using the 7300 Real-Time PCR System (Applied Biosystems). Expression of several gens was normalized to the expression of β-actin gene and the analysis was performed using comparative Ct method. For gene-specific primer list see section 6.1.2.

6.2.5 Western blot

Cell lysates

Tumor cells were harvested and pelleted at 0,5 x g for 5 min and washed once with PBS at 4°C. Cells were re-suspended in one pellet volume of MPER (Thermo Scientific) lysis buffer containing protease inhibitor cocktail (Cabliochem, 1:100) and phosphatase inhibitor cocktail (Sigma-Aldrich, 1:100) Cell lysates were incubated on ice for 20 min, and centrifuged at 13,200 rpm for 15 min at 4°C. Supernatants containing the protein lysates were collected into fresh tubes and quantified using BCA kit according to the manufacturer's protocol.

Immunoblotting

50 µg of protein lysates were denatured in NuPAGE LDS Sample Buffer (Thermo Scientific) at 95°C for 10 min and separated on the NuPAGE 4-12% Bis-Tris Gels (Thermo Scientific). Separated protein bands were transferred onto PVDF membrane (Millipore) using 1X wet-transfer buffer at 400 mA for 1 h at 4°C. Blotting was checked with Ponceau S staining (Sigma-Aldrich). Membranes were blocked with 5% milk powder in TBS-T at room temperature for 1,5 h. For the detection of phosphorylated proteins, membranes were blocked with 10% BSA in TBS-T. Membranes were incubated overnight at 4°C with the indicated primary antibody (see the list of antibodies in section 6.1.9) prepared in 1% milk in TBS-T. Antibodies recognizing phosphorylated protein were diluted in 5% BSA in TBS-T. On the following day, membranes were washed 3 times with TBS-T for 10 min each and then incubated 1 h at room temperature with the HRP-conjugated secondary antibody (section 6.1.9) prepared in 1% milk in TBS-T or in 5% BSA in TBS-T for the detection of Phosphorylated proteins (section 6.1.6). After 3 more washing steps, protein bands were detected using the ECL developing solution and the chemiluminescent signal was detected using the ChemiDoc XRS system.

6.2.6 Reverse siRNA transfection

Reverse siRNA transfection was used as the standard transfection method through this thesis. For the optimization of siRNA transfection efficiency, HiPerfect (Qiagen), Altogen 1 (Altogen Biosystems) or Altogen1 mixed to a liposome condenser (Altogen

2) were used to deliver PD-L1 specific siRNA in tumor cells. Transfection was performed according to the manufacturer's instruction.

For all the other described siRNA transfections, RNAiMAX (Thermo Scientific) was used as transfection reagent. Briefly, 200 µL of 250 nM siRNA solution was added to each well of a 6-well plate. 4 µl of RNAiMAX transfection reagent was diluted in 200 µL of RPMI (Sigma-Aldrich) and incubated for 10 min at room temperature. 400 µL of additional RPMI was added and 600 µL of RNAiMAX mix was given to the siRNA coated well and incubated for 30 min at RT. 2 x 10^5 PANC-1 (WT or -luc), 4 x 10^5 M579 cells were resuspended in 1,2 mL of antibiotic-free DMEM culture medium supplemented with 10% FCS, seeded in the siRNA-RNAiMAX containing wells and incubated for 72 h at 37°C, 5% CO_2. For reverse transfection in 96-well plate, 10 µL of siRNAs (250 nM) were mixed with 4,95 µL of RPMI for 10 min. Afterwards 20 µL of RPMI were added and the diluted transfection regent was given to each siRNA-containing well and incubated for 30 min. Afterward, 2 x 10^4 PANC-1 (WT or -luc), or 2 x 10^4 MCF7 cells, or 3 x 10^4 SW480 or 4 x 10^4 M579 cells were resuspendend in 30 µL of antibiotic-free DMEM culture medium supplemented with 10% FCS and incubated for 72 h at 37°C, 5% CO_2. Final siRNA concentration was 25 nM in all cases. The utilized siRNA sequences are listed in section 6.1.4.

6.2.7 Transient SIK3 overexpression

For SIK3 overexpression in melanoma cells, 3 x 10^5 M579 cells were suspended in 1mL of CMM medium and seeded in a 6-well plate overnight at 37°C, 5% CO_2. For each well, 3µg of SIK3-overexpression plasmid (GenScript) or the empty vector (EV) control (pCDNA3.1; GenScript) were diluted in 150 µL of Opti-MEM in the presence of 3 µL of the plus reagent (provided in the transfection kit). 15 µL of Lipofectamine LTX was suspended in 150 µL of Opti-MEM. Afterwards, the DNA-containing solution was added to the liposome-containing suspension. The DNA-liposome mixture was incubated for 30 min at room temperature. During the incubation time, the tumor cell medium was replaced with 1 mL of Opti-MEM. Afterwards, the DNA-liposome mixture was added dropwise to the tumor cells. After 24h of incubation at 37°C, 5% CO_2, the tumor cell medium was replaced with CMM. For the transfection in 96-well, plate the

abovementioned protocol was proportionally scaled down. 48h after transfection, tumor cells were used for further experiments.

For SIK3 overexpression in PDAC cells, 2 x 10^6 PANC-1 WT cells were cells were suspended in 1mL of CMM medium and seeded in a 6-well plate overnight at 37°C, 5% CO_2. For each well, 6 µg of the abovementioned plasmids were diluted in 100 µL of the NaCl solution provided in the kit (150 nM; Jet-PEI; Polyplus-transfection), and 6 µL of Jet-PEI reagent (Polyplus-transfection) was suspended in 100 µL of NaCl solution. Afterwards, the DNA-containing solution was added to the liposome-containing suspension, and incubated for 30 min at room temperature. During the incubation time, the tumor cell medium was replaced with 1 mL of DMEM 10 % FCS (without P/S). Afterwards, the DNA-liposome mixture was added dropwise to the tumor cells. 48h after transfection, tumor cells were used for further experiments.

6.2.8 Immunological techniques

6.2.8.1 Isolation of PBMCs

PBMCs were isolated from buffy coats of healthy donors via biocoll density gradient centrifugation (Biochrome). Briefly, buffy coats were diluted 1:1 in PBS and added to 50mL conical centrifuge tubes, containing 15 mL of biocoll solution. Density gradient centrifugation was performed at 2000 rpm for 20 min at room temperature using low brake. Afterwards PBMCs were collected, washed three times and resuspended at the desired concentration.

6.2.8.2 Generation of flu-antigen specific $CD8^+$ T cells (FluT)

For the generation of Flu-specific $CD8^+$ T (FluT) cells, PBMCs from HLA-A*02^+ healthy donors were isolated. Total $CD8^+$ T cells were sorted from PBMCs by magnetic separation (day 0), and expanded in the presence of A2-matched Flu peptide (GILGFVFTL) for 14 days. For the first 7 days of expansion, irradiated autologous CD8-fraction was used as feeder cells. On day 7, irradiated T2 cells were used as fresh feeder cells. On day 1 and day 8, 100 U/mL IL2 and 5 ng/µL IL15 were added to expansion. The percentage of Flu-antigen specific T cells were determined by pentamer staining on day 7 and 14.

6.2.8.3 Rapid expansion protocol (REP) for TILs

TIL#1 and TIL#2 (from poorly differentiated PDAC patients) were isolated and enriched in $CD8^+$ T cells by Dr. Isabel Poschke (Division of Molecular Oncology of Gastrointestinal Tumors, DKFZ). TIL209 and TIL412 (from melanoma patients) were kindly provided by Prof. Michal Lotem (Hadassah Hebrew University Medical Center, Israel). Rosenberg's REP protocol was used to rapidly expand TIL cultures [50]. Thawed TILs were treated with benzonase (Merck;100 U/mL) to prevent clumping and the cell density was adjusted to 0,6 x 10^6 cells/mL in CLM supplemented with 6000 U/ml rhuIL-2 (Novartis). Cells were incubated for 48 h at 37°C and 5% CO_2. PBMCs were isolated from three healthy donors as described above and irradiated with 60 Gray (Gammacell 1000). Irradiated PBMCs were used as feeder cells to support TIL expansion. TILs were co-incubated with feeder cells at a ratio of 1:100 in 400 mL of TIL expansion medium in a G-Rex100 flask. After 5 days of incubation, 250 mL of supernatant was changed with 150 mL of fresh media and IL-2 was replenished to keep the concentration at 3000 U/mL. On day 7, TILs were divided into two G-Rex100 flasks in a final volume of 250 mL medium each. On day 11, cells were supplemented with fresh media and 3000 U/mL IL2. TILs were harvested on day 14 and frozen in aliquots of 20 x 10^6 cells/mL in TIL freezing media A and B (1:1). Survivin-antigen specific T cell clones were cultured and provided by Sabrina Wagner (Joint Immunotherapeutics Laboratory, DKFZ).

6.2.8.4 Luciferase-based cytotoxicity (killing) assay

PANC-1-Luc and M579 cells were reverse transfected with the desired siRNA in 96-well white Perkin Elmer plates as described in section 6.2.6 and incubated for 72 h at 37°C, 5% CO_2. At the same day of transfection TILs were thawed and cultured at a density of 0,6 x 10^6 cells/ml in CLM supplemented with 6000 U/ml rhuIL-2 for 48 h. IL-2 was depleted 24 h before the co-culture. For the cytotoxicity setting, TILs or survivin-specific T cells, the supernatant of activated TILs or rHuTNF-α were added to transfected tumor cells at desired E:T ratio/concentration, and incubated for 20-24 h at 37°C, 5% CO_2. For the viability setting, only CLM was added to tumor cells instead of T cells. After co-culture, supernatant was removed and remaining tumor cells were lysed using 40 µL/well of cell lysis buffer for 10 min. After lysis, 60 µL/well of luciferase

assay buffer was added and immediately the luciferase intensity was measured by using a microplate reader (TECAN). Luciferase activities (relative light units = RLUs) were either represented as raw luciferase values or as normalized data to scramble or unstimulated controls. When indicated, *cytotoxicity/viability ratio* was used to represent the data. This ratio was calculated by first normalizing raw RLUs to their respective scramble controls (siCtrl) and then by applying the following formula:

C*ytotoxicity/viability ratio* = (*Norm. RLU cytotoxicity setting / Norm. RLU viability setting).*

6.2.8.5 ^{51}Chromium-release assay

PANC-1 cells were reverse transfected in a 6-well with different siRNA sequences as described above. Afterwards, tumor cells were detached with PBS-EDTA and labeled with 100µL $^{51}Cr/10^6$ target cells in CLM for 1 h at 37°C. Afterwards, cells were washed three times with CLM An intermediate incubation with PBS-EDTA (1:20 dilution) at 37°C for 10 minutes, was performed between the first and the second washing step. Tumor cells were counted and 3000 target cells/well were co-cultured with T cells in 96 well u-bottom plates at the indicated effector cells to target cell (E:T) ratios. The plates were incubated for 6 h at 37°C. After co-incubation, plates were centrifuged and 100 µL of supernatants were collected to 96-well Luma plates. Plates were dried overnight and counted in the Gamma counter (Cobra counter Packard, Perkin Elmer). Spontaneous release was measured from the target cells that are incubated with medium alone, whereas maximum release was determined from the target cells incubated with 10% Triton X-100 instead of T cells. The percent specific lysis was calculated by using the formula given below:

% Specific lysis = (experimental release-spontaneous release) / (maximum release-spontaneous release) × 100.

6.2.8.6 ELISA

PANC-1 or M579 cells were transfected with the indicated siRNAs in a 96-well plate. Afterwards, different T cell sources were added at the indicated E:T ratio for 20h and 100 µL of supernatants were harvested for the detection of IFN-γ (Human IFN-γ ELISA Set; BD OptEIA™), perforin (Human Perforin ELISA PRO kit, Mabtech) and granzyme

B (Human Granzyme B ELISA development kit; Mabtech). Experiments were performed according to the maufacturer´s instructions. PMA/Ionomycin stimulation was used as positive control. PMA was used at final concentration of 50ng/mL and Ionomycin at final concentration of 1 µg/mL. Absorbance was measured at λ = 450 nm, taking λ = 570 nm as reference wavelength using the Spark microplate reader (TECAN).

For the Granzyme B ELISA using FluT cells, transfected PANC-1 cells were pulsed with 0.01 g/mL Flu peptide (GILGFVFTL) for 2 hours at 37°C. Before the co-culture, the peptide containing medium was removed and 100 µL of FluT cells were added at E:T ratio = 5:1 in the tumor-containing wells. After 20h of co-culture Granzyme B ELISA was performed as described above.

6.2.8.7 Flow cytometry (FACS)

Flow cytometry was used for the detection of proteins expressed on the plasma membrane of tumor and T cells. Adherent cells were detached form plates using PBS-EDTA and centrifuged at 500 x g for 5 min. Cells were re-suspended in FACS buffer and distributed in FACS tubes (2 x 10^5 cells/tube). Afterwards, cells were incubated with Kiovig (Baxter) for 20 min on ice, to reduce unspecific antibody binding. After blocking, cells were washed once in cold FACS buffer and stained with the Pacific Orange dye (1:1000 in 100 µL FACS buffer) for 15 min in dark on ice. Next, samples were washed two times in FACS buffer and incubated with either fluorophore-conjugated primary antibody or isotype control at the concentrations indicated in section 6.1.9.2 for 20 min on ice in dark. Afterwards, cells were washed twice and acquired with the FACS Canto II cell analyzer machine (BD). For indirect flow cytometry (TNFR-I or TNFR-II stainings), samples were incubated with the primary (unconjugated) antibody as described above and subsequently stained with the phycoerythrin (PE) -conjugated secondary antibody for 20 minutes on ice in the dark. Samples were washed twice and acquired as described above. Data were analyzed using the FlowJo software.

6.2.8.8 TNF-α catch assay

TNF-α catch assay was used to measure TNF-α from TILs receiving different stimulations. Briefly 1 x 10^6 TIL#1 cells were co-cultured with 1 x 10^6 PANC-1 WT cells (E:T = 1:1) in a 12-well plate. Alternatively, TIL#1 were polyclonally stimulated with PHA at a final concentration of 5 µg/mL. Unstimulated T cells served as negative control. After 12h incubation, T cells were collected and stained with the TNF-α secretion assay (catch assay) kit (Miltenyi biotech) according to manufacturer´s instructions. Briefly, TIL#1 were collected and incubated with the cytokine catch reagent for 5 min on ice. Afterwards, warm medium was added and cells were incubated for 1h at 37°C, 5% CO_2.

Next, the catch reagent was washed out and the cytokine detection antibody (PE-conjugated) was added together with anti-CD3, anti-CD4 and anti-CD8 antibodies in the presence of Pacific orange (1:1000). The reagents were incubated for 20 minutes on ice in the dark. Afterwards, TIL#1 were washed twice and FACS measurement was performed as described above.

6.2.8.9 Generation of supernatants of activated TILs

For the generation of the supernatant of polyclonally activated TILs, 1 x 10^6 TILs were suspended in 1 mL of CLM collected in a 15 mL tube and stimulated with 25 µL of Dynabeads Human T-Activator CD3/CD28 (Thermo Scientific). Afterwards, TILs were distributed in a 96-well plate (U-bottom) at 120 µL/well and incubated at 37°C, 5% CO_2. Alternatively. TILs were stimulated with tumor cells. Briefly, 1,2 x 10^5 TIL#1 were cultivated with 2,4 x 10^3 siCtrl transfected PANC-1 cells (section 6.2.6) in a final volume of 120 µL at 37°C, 5% CO_2. After 24h of stimulation (polyclonal or tumor-stimulation), plates were centrifuged at 450 x g for 5 minutes and 100 µL/well of the supernatant was collected for cytokine detection (luminex assay) or for further functional assays (luciferase-based cytotoxicity assay).

6.2.8.10 Functional neutralization and blocking assays

For the functional blockade of MHC-I molecules, PANC-1 WT cells were pre-labeled with ^{51}Cr as described in section 6.2.8.5. Afterwards, 100 µL of tumor cells were seeded in 96-well plates at a density of 3 x 10^4 cells/well. 50 µL of the MHC-I antibody

or isotype control (both generated by Prof. Gerd Moldenhauer – DKFZ – Heideleberg), were added to the tumor-containing wells for 30 min at 37°C, 5% CO_2. Afterwards, 50 µL of TIL#1 (E:T = 50:1) or control antibody were added and incubated for 6h at 37°C, 5% CO_2. T cell-mediated cytotoxicity was measured as indicated in section 6.2.8.5.

For the functional neutralization experiment in section 3.4.7, anti-TNF-α, anti-TRAIL anti-FASL or isotype controls (section 6.1.9.3) were pre-incubated with the supernatant of activated TIL#1 (polyclonal activation) for 1h at 37°C, 5% CO_2. As negative control, antibodies were cultivated in CLM. Afterwards, antibody-containing supernatants were used to stimulate PANC-1-luc cells which were reverse transfected with the indicated siRNAs. The final concentration of the neutralizing antibodies was 500 ng/mL for anti-TNF-α, 1 µg/mL for anti-TRAIL and 10 µg/mL for anti-FASL. Isotype controls were used at the same concentration of their respective target-specific antibodies. After 24h of stimulation, luciferase-based cytotoxicity assay was performed. Anti-TNF-α was used for further experiments at different concentrations (as indicated in the text), by using the same experimental procedure as described above.

For the experiments using the pan-SIK inhibitor HG-9-91-01, 2 x 10^6 PANC-1-luc cells/well were seeded in a 96-well plate white (Perkin Elmer) in 100 µL of DMEM 10 % FCS, 1 % P/S, and incubated overnight at 37°C, 5% CO_2. Afterwards, HG-9-91-01 was added to the tumor-containing wells at the indicated concentrations, simultaneously with TIL#1 (E:T = 50:1) or rHuTNF-α (final concentration:100 ng/mL). DMSO treatment served as negative control. After 24h stimulation, luciferase-based cytotoxicity assay was performed.

For blockade of TNFR-I, 20 µg/mL (final assay concentration) of anti-TNFR-I or isotype control (section 6.1.9.3) was incubated with 50 ng/mL (final assay concentration) of rHuTNF-α for 1h at 37°C, 5% CO_2. Afterwards, antibody-containing rHuTNF-α media or control medium were used to stimulate PANC-1-luc cells, which were previously reverse transfected with the indicated siRNAs. After 24h of stimulation, luciferase-based cytotoxicity assay was performed.

6.2.8.11 Luminex assays

Detection of TNF-α

For accurate detection of TNF-α secretion from polyclonally or tumor-stimulated T cells (stimulation protocol in section 6.2.8.9), lunminex assay was performed using the BioPlex ProHuman Chemokine TNFa Set (Bio-Rad) according to manufacturer´s instructions. Sample were measured using the MAGPIX luminex instrument (Merck Millipore).

Detection of intracellular analytes involved in apoptosis

PANC-1 cells were reverse transfected with desired siRNAs in 6-well plates as described in section 6.2.6). Afterwards, cells where stimulated with rHuTNFα (conc. 100 ng/mL) for 2h or 4 h. Tumor cells were cultivated with CLM, which served as unstimulated control. Afterwards, the MILLIPLEX MAP Early Phase Apoptosis 7-plex-kit (Millipore) was used for the detection several proteins involved in the activation of apoptosis. Briefly, tumor cells were lysed using the lysis buffer provided in the kit and quantified using the BCA assay according to the manufacturer's protocol. Afterwards 20 µg of protein lysates were diluted in 25 µL assay diluent (provided in the kit) and incubated with 25 µL of beads detecting the following analytes: phosphorylated Akt (Ser473), JNK (Thr183/Tyr185), Bad (Ser112), Bcl-2 (Ser70), p53 (Ser46) or cleaved Caspase-8 (Asp384) and Caspase-9 (Asp315). The assay was performed according to the manufacturer´s instructions and samples were measured using the MAGPIX luminex instrument (Merck Millipore).

6.2.9 High-throughput RNAi screening

6.2.9.1 Primary RNAi screening

The primary RNAi screening was conducted using a sub-library of the genome-wide siRNA library siGENOME (Dhamacon, GE healthcare) which comprised 2514 genes. The library was prepared in Prof. Boutros´s group (DKFZ, Heidelberg) as described in [339]. The following 384-well plates of the genome-wide library were included: 1, 2, 3, 13, 14, 15, 17, 65, 67, 68. Each well contained a pool of four non-overlapping siRNAs targeting the same gene (arrayed screening approach). The screening was performed in duplicates. Positive and negative siRNA controls were added in empty wells of each

384-well plate. For each well, reverse siRNA transfection was performed as follows: 0,05 µL of RNAiMAX were mixed with 4,95 µL of RPMI for 10 min. Afterwards 10 µL of RPMI were added and the diluted transfection regent was added to each siRNA-containing well for 30 min. Next, 750 PANC-1-luc cells resuspended in 30 µL of DMEM 10 % FCS were added and incubated at 37°C, 5% CO_2. The final siRNA pool concentration was 25 nM. 72h after siRNA transfection, tumor cells were either co-cultured with TIL#1 resuspended in 20 µL at E:T = 25:1 (cytotoxicity setting or with 20 µL of CLM (viability setting). 20h after co-culture, the supernatant was removed and 20µL of the lysis buffer (section 6.1.6) was added for 10 min at room temperature. Afterwards, 30 µL of the luciferase assay buffer (section 6.1.6) was added and luminescence was measured using the Mithras reader (Berthold) with 0,1 sec counting time. In addition to the luciferase-based primary screening, PANC-1 WT cells were reversed transfected with the siRNA library as described above and an additional viability screening was conducted using the CellTiter-Glo (CTG) assay (Promega). Briefly, supernatant was removed in each well containing siRNA-transfected tumor cells and 20 µL the CTG reagent (pre diluted 1:4 in RPMI) were added. After 15 min incubation in the dark, plates were measured using the Mithras reader as describe above.

Raw RLUs from the primary screening, were processed using the cellHTS2 package in R/Bioconductor [338]. Values from both conditions were quantile normalized against each other using the aroma.ligh package in R. Differential scores (cytotoxicity vs. viability) were calculated using the LOESS local regression fitting. To identify candidate hits, the following thresholds were applied on the –z scores of the samples: for the viability setting, genes showing a $-z > 2{,}0$ or $-z < 1{,}0$ were excluded. For the cytotoxicity setting, PD-L1 was used as threshold score. Additionally genes having a score > 2,55 or < - 1,55 in the CTG-based viability screening were filtered out from the candidate list. Data analysis was performed by Tillman Michels (DKFZ, Heidelberg).

Secondary screening

For the secondary screening, a customized library containing the 155 hits from the primary screening was distributed in several 96-well plates. Empty wells were filled with appropriate positive and negative siRNA controls. Reverse transfection was

performed as described in section 6.2.6 using PANC-1-luc as tumor cell line. Afterwards, 40 µL of TIL#1 (E:T = 25:1) or survivin-specific T cell clones (E:T = 5:1) were incubated with the siRNA transfected tumor cells for 20h (cytotoxicity setting). For the viability setting, 40 µL of CLM was added to the library in the absence of T cells. Technical duplicates were used for the experiment. Luciferase-based cytotoxicity assay was performed as in section 6.2.8.4 and cytotoxicity/viability ratios were calculated according to the formula described in section 6.2.8.4, by using siCtrl1 as negative control. The hit-list was generated by including only hits with improved T cell mediated cytotoxicity over siCtrl1 transfection, in both the TIL#1 and the survivin TCs-based screens (Cytotoxicity/viability ratio < 1). Pearson´s correlation was calculated with Microsoft Excel.

6.2.10 Real-time live cell imaging

Tumor cells were reverse transfected with several siRNA sequences as described in section 6.2.6 and subsequently challenged either with the indicated T cell source at the indicated E:T ratios or with 100 ng/mL of rHuTNF-α. Alternatively, 1 x 10^5 stable M579 knockdown or control cells (section 6.2.2) were seeded in a 96-well plate flat overnight and subsequently challenged with TIL209 (5:1). As negative controls, all experiments tumor cells were cultivated with CLM. All reactions were conducted in the presence of the YOYO-1 dye (Thermo Scientific), which was diluted 1:1000 in each well. Plates were incubated in the Incucyte ZOOM live-cell imager at 37°C and 5% CO_2 and images were acquired at the indicated time points. Data were analyzed with the Incucyte ZOOM 2016A software by creating a top-hat filter-based mask for the calculation the area of YOYO-1 incorporating cells (dead cells).

6.2.11 WST-1 assay

The WST-1 Cell Proliferation Assay (Roche) was used to measure viability of tumor cells. PANC-1 cells were reverse transfected with several siRNA sequences in a 96-well plate as described in section 6.2.6. Afterwards, 10 µL of the WST-1 reagent was added to each well and incubated for 1h at 37°C, 5% CO_2. Afterwards, t absorbance was measured at λ = 450 nm versus λ = 650 nm reference by using the Spark microplate reader (TECAN). In some cases, reverse transfected cells were stimulated

with the supernatant of polyclonally stimultated T cells for 24h before the addition of the WST-1 reagent.

6.2.12 ELISA for nuclear NF-κB detection

The NF-κB p50/p65 EZ-TFA Transcription Factor assay kit was used to measure the nuclear translocation of the p65 subunit of the NF-κB complex. Briefly, PANC-1 WT or Hela cells were reverse transfected with desired siRNAs in 6-well plate as described in section 6.2.6. Afterwards, tumor cells were stimulated either with 100 ng/mL of rHuTNF-α or with CLM for 15 or 30 min. Alternatively, PANC-1 WT cells were transfected with SIK3 overexpressing plasmid or EV as described in section 6.2.7. Tumor cells were harvested in trypsin-EDTA, washed with cold PBS and centrifuged (250 x g) for 5 min at 4°C. Cytosolic protein fraction was separated from the nuclear protein fraction as described in the assay protocol. Afterwards, the cytosolic protein fraction was discarded. The protein concentration of nuclear fractions was determined using the BCA kit according to the manufacturer's protocol. 4,5 µg of nuclear lysate were added in each well of the pre-coated NF-κB (p65 subunit) ELISA 96-well plate. The assay was performed according to the manufacturer´s instructions and absorbance was measured at λ = 450 nm, taking λ = 570 nm as reference wavelength using the Spark microplate reader (TECAN).

6.2.13 RNA sequencing

PANC-1 WT cells were reverse transfected either with siCtr1 or with siSIK3 s1 in a 6-well plate as described in 6.2.6. Afterwards, the medium was replaced with 1 mL of complete DMEM and 1 mL rHuTNF-α was added at a final concentration of 100 ng/mL. After 30 min or 4h from stimulation, tumor cells were harvested in trypsin and RNA was isolated using the RNeasy mini kit (Qiagen) according to the manufacturer´s instructions. RNA from unstimulated siRNA-transfected tumor cells was used as negative control. RNA-seq libraries were generated using the ScriptSeq Complete Kit (Illumina) according to the manufacturer's instructions. Libraries were sequenced paired-end (2 x 75bp) on a HiSeq 3000 at the Biomedical Sequencing Facility (BSF) in Vienna, Austria. Raw fastq data was quality controlled using FastQC (http://www.bioinformatics.babraham.ac.uk/projects/fastqc/) and mapped to the annotated GRCh38 assembly of the human genome using STAR (version 2.5) and the

following parameters: --alignSJoverhangMin 8 --alignSJDBoverhangMin 1 --alignMatesGapMax 1000000 --alignIntronMax 1000000 and --quantMode GeneCounts. Differentially expressed genes were analyzed using edgeR and visualized using software packages in R. Gene set enrichment analyses were done using EnrichR. Library preparation was performed by Dr. Claudia Gebhard (University of Regensburg), the bioinformatic analysis was performed by Prof. Michael Rehli (University of Regensburg).

References: STAR: PMID: 23104886: EdgeR: PMID: 19910308: EnrichR PMID: 23586463.

6.2.14 *In vivo* experiments

NOD/SCID gamma (NSG) mice were used as immunodeficient xenograft model in this study. Mice were shaved at the flank regions and subcutaneously engrafted with tumor cells. Tumor cells (shSIK3 or shCtrl M579 cells) were prepared as described in section 6.2.2. Afterwards, 3 x 10^5 tumor cells were re-suspended in 50 µL PBS, mixed with 50 µL of matrigel (Corning) and injected using 0.4 mm x 20 mm needles at day 1. Before mixing with tumor cells, matrigel was pre-diluted in PBS to reach a protein concentration of 6,4 mg/mL. shCtrl M579 cells were injected in the left flank of each mouse, whereas shSIK3 were injected in the right flank of the same mice receiving shSIK3. At day 3, 10, 17 and 24, 9 tumor-bearing mice received intravenous injection (into their tail vein) of 200 µL of TIL209 suspension at a density of 6 x 10^6 cells/mL in PBS. As a negative control, 7 tumor-bearing mice received 200 µL of PBS. After the establishment of visible tumors (day 11), mice were measured three times a week using the Vernier digital caliper. Tumor volumes were calculated using the following formula:

$$\textit{Tumor volume } (mm^2) = (Width^2 \times Length) / (\pi / 3).$$

The experiment was repeated twice using the same experimental procedure. Statistical difference was calculated using unpaired one-side Mann-Whitney U-test. Tumor and T cell injections, as well as measurements of tumor volumes, were performed by Dr. Melanie Werner-Klein (University of Regensburg).

6.2.15 Statistical evaluation

For statistical analysis, GraphPad Prism 6 software was used. If not differently stated, statistical differences between the control and the test groups were determined by using two-tailed unpaired Student's t-test. In all cases, p-value ≤ 0.05 was taken as significant, and * = $p < 0.05$, ** = $p < 0.01$.

7. Bibliography

1. Stewart, B.W., et al., *World cancer report 2014*. 2014, Lyon, FranceGeneva, Switzerland: International Agency for Research on Cancer. WHO Press. xiv, 630 pages.

2 Beebe, S.J., *Concepts of Cancer and Novel Cancer Therapy: Treating Tumors as an Aggressive Organ.* Journal of Nanomedicine & Biotherapeutic Discovery, 2014. **4**(Article e134): p. 1-3.

3. Chen, F., et al., *New horizons in tumor microenvironment biology: challenges and opportunities.* BMC Medicine, 2015. **13**(1): p. 45.

4. Augsten, M., et al., *Cancer-associated fibroblasts expressing CXCL14 rely upon NOS1-derived nitric oxide signaling for their tumor-supporting properties.* Cancer Res, 2014. **74**.

5. Branco-Price, C., et al., *Endothelial cell HIF-1 alpha and HIF-2 alpha differentially regulate metastatic success.* Cancer Cell, 2012. **21**.

6. Quail, D.F. and J.A. Joyce, *Microenvironmental regulation of tumor progression and metastasis.* Nat Med, 2013. **19**.

7. Hanahan, D. and R.A. Weinberg, *Hallmarks of Cancer: The Next Generation.* Cell, 2011. **144**(5): p. 646-674.

8. Lemmon, M.A. and J. Schlessinger, *Cell signaling by receptor tyrosine kinases.* Cell, 2010. **141**(7): p. 1117-34.

9. Witsch, E., M. Sela, and Y. Yarden, *Roles for growth factors in cancer progression.* Physiology (Bethesda), 2010. **25**(2): p. 85-101.

10. Burkhart, D.L. and J. Sage, *Cellular mechanisms of tumour suppression by the retinoblastoma gene.* Nature Reviews Cancer, 2008. **8**(9): p. 671-682.

11. Bieging, K.T., S.S. Mello, and L.D. Attardi, *Unravelling mechanisms of p53-mediated tumour suppression.* Nat Rev Cancer, 2014. **14**(5): p. 359-370.

12. Curto, M., et al., *Contact-dependent inhibition of EGFR signaling by Nf2/Merlin.* Journal of Cell Biology, 2007. **177**(5): p. 893-903.

13. Adams, J.M. and S. Cory, *The Bcl-2 apoptotic switch in cancer development and therapy.* Oncogene, 2007. **26**(9): p. 1324-37.

14. Grivennikov, S.I., F.R. Greten, and M. Karin, *Immunity, inflammation, and cancer.* Cell, 2010. **140**(6): p. 883-99.

15. Blackburn, E.H., *Telomerase and Cancer.* Kirk A. Landon - AACR Prize for Basic Cancer Research Lecture, 2005. **3**(9): p. 477-482.

16. Hanahan, D. and J. Folkman, *Patterns and emerging mechanisms of the angiogenic switch during tumorigenesis.* Cell, 1996. **86**(3): p. 353-64.

17. Vander Heiden, M.G., L.C. Cantley, and C.B. Thompson, *Understanding the Warburg effect: the metabolic requirements of cell proliferation.* Science, 2009. **324**(5930): p. 1029-33.

18. Galon, J., et al., *The continuum of cancer immunosurveillance: prognostic, predictive, and mechanistic signatures.* Immunity, 2013. **39**(1): p. 11-26.

19. Parish, C.R., *Cancer immunotherapy: the past, the present and the future.* Immunol Cell Biol, 2003. **81**(2): p. 106-13.

20. Vesely, M.D., et al., *Natural Innate and Adaptive Immunity to Cancer*

Senescence and tumour clearance is triggered by p53 restoration in murine liver carcinomas. Annual Review of Immunology, 2011. **29**(1): p. 235-271.

21. Schreiber, R.D., L.J. Old, and M.J. Smyth, *Cancer Immunoediting: Integrating Immunity's Roles in Cancer Suppression and Promotion.* Science, 2011. **331**(6024): p. 1565-1570.

22. J, G., et al., *Type, density, and location of immune cells within human colorectal tumors predict clinical outcome.* Science, 2006. **313**: p. 1960.

23. E, S., et al., *Intraepithelial CD8+ tumor-infiltrating lymphocytes and a high CD8+/regulatory T cell ratio are associated with favorable prognosis in ovarian cancer.* Proc. Natl. Acad. Sci. USA, 2005. **102**: p. 18538.

24. IS, v.H., et al., *Favorable outcome in clinically stage II melanoma patients is associated with the presence of activated tumor infiltrating T-lymphocytes and preserved MHC class I antigen expression.* Int. J. Cancer, 2008. **123**: p. 609.

25. F, P., et al., *Effector memory T cells, early metastasis, and survival in colorectal cancer.* N. Engl. J. Med., 2005. **353**: p. 2654.

26. GP, D., et al., *Cancer immunoediting: from immunosurveillance to tumor escape.* Nat. Immunol., 2002. **3**: p. 991.

27. MacEwan, D.J., *TNF ligands and receptors – a matter of life and death.* British Journal of Pharmacology, 2002. **135**(4): p. 855-875.

28. Warren, H.S. and M.J. Smyth, *NK cells and apoptosis.* Immunol Cell Biol, 1999. **77**(1): p. 64-75.

29. Algarra, I., T. Cabrera, and F. Garrido, *The HLA crossroad in tumor immunology.* Hum Immunol, 2000. **61**(1): p. 65-73.

30. Vigneron, N., *Human Tumor Antigens and Cancer Immunotherapy.* BioMed Research International, 2015. **2015**: p. 948501.

31. Chen, D.S. and I. Mellman, *Oncology meets immunology: the cancer-immunity cycle.* Immunity, 2013. **39**(1): p. 1-10.

32. Galluzzi, L., et al., *Immunogenic cell death in cancer and infectious disease.* Nat Rev Immunol, 2016. **advance online publication**.

33. Green, D.R., et al., *IMMUNOGENIC AND TOLEROGENIC CELL DEATH.* Nature reviews. Immunology, 2009. **9**(5): p. 353.

34. Lippitz, B.E., *Cytokine patterns in patients with cancer: a systematic review.* Lancet Oncol, 2013. **14**(6): p. e218-28.

35. Mellman, I., G. Coukos, and G. Dranoff, *Cancer immunotherapy comes of age.* Nature, 2011. **480**(7378): p. 480-9.

36. Bousso, P., *T-cell activation by dendritic cells in the lymph node: lessons from the movies.* Nat Rev Immunol, 2008. **8**(9): p. 675-684.

37. JA., A.-G., *Models, mechanisms and clinical evidence for cancer dormancy.* Nat. Rev. Cancer, 2007. **7**: p. 834.

38. Ranganathan, A.C., A.P. Adam, and J.A. Aguirre-Ghiso, *Opposing Roles of Mitogenic and Stress Signaling Pathways in the Induction of Cancer Dormancy.* Cell cycle (Georgetown, Tex.), 2006. **5**(16): p. 1799-1807.

39. Wikman, H., R. Vessella, and K. Pantel, *Cancer micrometastasis and tumour dormancy.* APMIS, 2008. **116**(7-8): p. 754-70.

40. Bhatia, A. and Y. Kumar, *Cancer-Immune Equilibrium: Questions Unanswered.* Cancer Microenvironment, 2011. **4**(2): p. 209-217.

41. Hakansson, L., *The capacity of the immune system to control cancer.* Eur J Cancer, 2009. **45**(12): p. 2068-70.

42. Felsher, D.W., *Tumor dormancy: death and resurrection of cancer as seen through transgenic mouse models.* Cell Cycle, 2006. **5**(16): p. 1808-11.

43. GP, D., O. LJ, and S. RD, *The three Es of cancer immunoediting.* Annu. Rev. Immunol., 2004. **22**: p. 329.

44. Mittal, D., et al., *New insights into cancer immunoediting and its three component phases — elimination, equilibrium and escape.* Current opinion in immunology, 2014. **27**: p. 16-25.

45. Bhatia, A. and Y. Kumar, *Cellular and molecular mechanisms in cancer immune escape: a comprehensive review.* Expert Review of Clinical Immunology, 2014. **10**(1): p. 41-62.

46. GP, D., O. LJ, and S. RD, *The immunobiology of cancer immunosurveillance and immunoediting.* Immunity, 2004. **21**: p. 137.

47. Pardoll, D.M., *The blockade of immune checkpoints in cancer immunotherapy.* Nat Rev Cancer, 2012. **12**(4): p. 252-64.

48. Chen, L. and D.B. Flies, *Molecular mechanisms of T cell co-stimulation and co-inhibition.* Nature reviews. Immunology, 2013. **13**(4): p. 227-242.

49. Hino, R., et al., *Tumor cell expression of programmed cell death-1 ligand 1 is a prognostic factor for malignant melanoma.* Cancer, 2010. **116**(7): p. 1757-66.

50. Song, X., et al., *Overexpression of B7-H1 correlates with malignant cell proliferation in pancreatic cancer.* Oncol Rep, 2014. **31**(3): p. 1191-8.

51. Riella, L.V., et al., *Role of the PD-1 Pathway in the Immune Response.* American journal of transplantation : official journal of the American Society of Transplantation and the American Society of Transplant Surgeons, 2012. **12**(10): p. 2575-2587.

52. Francisco, L.M., P.T. Sage, and A.H. Sharpe, *The PD-1 Pathway in Tolerance and Autoimmunity.* Immunological reviews, 2010. **236**: p. 219-242.

53. Okazaki, T., et al., *A rheostat for immune responses: the unique properties of PD-1 and their advantages for clinical application.* Nat Immunol, 2013. **14**(12): p. 1212-1218.

54. Dong, H., et al., *Tumor-associated B7-H1 promotes T-cell apoptosis: a potential mechanism of immune evasion.* Nat Med, 2002. **8**(8): p. 793-800.

55. Tivol, E.A., et al., *Loss of CTLA-4 leads to massive lymphoproliferation and fatal multiorgan tissue destruction, revealing a critical negative regulatory role of CTLA-4.* Immunity, 1995. **3**(5): p. 541-7.

56. Sansom, D.M., *CD28, CTLA-4 and their ligands: who does what and to whom?* Immunology, 2000. **101**(2): p. 169-177.

57. Kwiecien, I., et al., *Elevated regulatory T cells, surface and intracellular CTLA-4 expression and interleukin-17 in the lung cancer microenvironment in humans.* Cancer Immunology, Immunotherapy, 2017. **66**(2): p. 161-170.

58. Krummey, S.M. and M.L. Ford, *Braking Bad: Novel Mechanisms of CTLA-4 Inhibition of T Cell Responses.* American journal of transplantation : official journal of the American Society of Transplantation and the American Society of Transplant Surgeons, 2014. **14**(12): p. 2685-2690.

59. Goldberg, M.V. and C.G. Drake, *LAG-3 in Cancer Immunotherapy.* Current topics in microbiology and immunology, 2011. **344**: p. 269-278.

60. Grosso, J.F., et al., *LAG-3 regulates CD8(+) T cell accumulation and effector function in murine self- and tumor-tolerance systems.* The Journal of Clinical Investigation, 2007. **117**(11): p. 3383-3392.

61. Camisaschi, C., et al., *LAG-3 expression defines a subset of CD4(+)CD25(high)Foxp3(+) regulatory T cells that are expanded at tumor sites.* J Immunol, 2010. **184**(11): p. 6545-51.

62. Zhu, C., et al., *The Tim-3 ligand galectin-9 negatively regulates T helper type 1 immunity.* Nat Immunol, 2005. **6**(12): p. 1245-52.

63. Yan, J., et al., *Tim-3 expression defines regulatory T cells in human tumors.* PLoS One, 2013. **8**(3): p. e58006.

64. Wherry, E.J., *T cell exhaustion.* Nat Immunol, 2011. **12**(6): p. 492-9.

65. Chen, J., et al., *CEACAM6 induces epithelial-mesenchymal transition and mediates invasion and metastasis in pancreatic cancer.* Int J Oncol, 2013. **43**(3): p. 877-85.

66. Witzens-Harig, M., et al., *Tumor cells in multiple myeloma patients inhibit myeloma-reactive T cells through carcinoembryonic antigen-related cell adhesion molecule-6.* Blood, 2013. **121**(22): p. 4493-4503.

67. Nagata, S. and P. Golstein, *The Fas death factor.* Science, 1995. **267**(5203): p. 1449-56.

68. *The Fas counterattack: Fas-mediated T cell killing by colon cancer cells expressing Fas ligand.* The Journal of Experimental Medicine, 1996. **184**(3): p. 1075-1082.

69. Igney, F.H. and P.H. Krammer, *Tumor counterattack: fact or fiction?* Cancer Immunol Immunother, 2005. **54**(11): p. 1127-36.

70. Wilde, S., et al., *Human antitumor CD8+ T cells producing Th1 polycytokines show superior antigen sensitivity and tumor recognition.* J Immunol, 2012. **189**(2): p. 598-605.

71. Facciabene, A., G.T. Motz, and G. Coukos, *T-regulatory cells: key players in tumor immune escape and angiogenesis.* Cancer Res, 2012. **72**(9): p. 2162-71.

72. Protti, M.P. and L. De Monte, *Cross-talk within the tumor microenvironment mediates Th2-type inflammation in pancreatic cancer.* Oncoimmunology, 2012. **1**(1): p. 89-91.

73. Quatromoni, J.G. and E. Eruslanov, *Tumor-associated macrophages: function, phenotype, and link to prognosis in human lung cancer.* American Journal of Translational Research, 2012. **4**(4): p. 376-389.

74. Dennis, K.L., et al., *Current status of IL-10 and regulatory T-cells in cancer.* Current opinion in oncology, 2013. **25**(6): p. 637-645.

75. Hsu, P., et al., *IL-10 Potentiates Differentiation of Human Induced Regulatory T Cells via STAT3 and Foxo1.* The Journal of Immunology, 2015. **195**(8): p. 3665-3674.

76. Buer, J., et al., *Interleukin 10 Secretion and Impaired Effector Function of Major Histocompatibility Complex Class II–restricted T Cells Anergized In Vivo.* The Journal of Experimental Medicine, 1998. **187**(2): p. 177-183.

77. Ludviksson, B.R. and B. Gunnlaugsdottir, *Transforming growth factor-beta as a regulator of site-specific T-cell inflammatory response.* Scand J Immunol, 2003. **58**(2): p. 129-38.

78. Roberts, A.B. and L.M. Wakefield, *The two faces of transforming growth factor β in carcinogenesis.* Proceedings of the National Academy of Sciences of the United States of America, 2003. **100**(15): p. 8621-8623.

79. Nakashima, M., K. Sonoda, and T. Watanabe, *Inhibition of cell growth and induction of apoptotic cell death by the human tumor-associated antigen RCAS1.* Nat Med, 1999. **5**(8): p. 938-942.

80. Sonoda, K., et al., *The biological role of the unique molecule RCAS1: a bioactive marker that induces connective tissue remodeling and lymphocyte apoptosis.* Front Biosci, 2008. **13**: p. 1106-16.

81. Sonoda, K., et al., *Receptor-binding cancer antigen expressed on SiSo cells induces apoptosis via ectodomain shedding.* Experimental Cell Research, 2010. **316**(11): p. 1795-1803.

82. Calcinotto, A., et al., *Modulation of microenvironment acidity reverses anergy in human and murine tumor-infiltrating T lymphocytes.* Cancer Res, 2012. **72**(11): p. 2746-56.

83. C, U., et al., *Evidence for a tumoral immune resistance mechanism based on tryptophan degradation by indoleamine 2,3-dioxygenase.* Nat. Med., 2003. **9**: p. 1269.

84. Fallarino, F., et al., *The combined effects of tryptophan starvation and tryptophan catabolites down-regulate T cell receptor zeta-chain and induce a regulatory phenotype in naive T cells.* J Immunol, 2006. **176**(11): p. 6752-61.

85. Taylor, D.D. and C. Gercel-Taylor, *Tumour-derived exosomes and their role in cancer-associated T-cell signalling defects.* Br J Cancer, 2005. **92**(2): p. 305-11.

86. Coulie, P.G., et al., *Tumour antigens recognized by T lymphocytes: at the core of cancer immunotherapy.* Nat Rev Cancer, 2014. **14**(2): p. 135-146.

87. Matsushita, H., et al., *Cancer Exome Analysis Reveals a T Cell Dependent Mechanism of Cancer Immunoediting.* Nature, 2012. **482**(7385): p. 400-404.

88. Alexandrov, L.B., et al., *Signatures of mutational processes in human cancer.* Nature, 2013. **500**(7463): p. 415-421.

89. Vogelstein, B., et al., *Cancer Genome Landscapes.* Science, 2013. **339**(6127): p. 1546-1558.

90. Robbins, P.F., et al., *Mining Exomic Sequencing Data to Identify Mutated Antigens Recognized by Adoptively Transferred Tumor-reactive T cells.* Nature medicine, 2013. **19**(6): p. 747-752.

91. Tran, E., et al., *Cancer Immunotherapy Based on Mutation-Specific CD4+ T Cells in a Patient with Epithelial Cancer.* Science, 2014. **344**(6184): p. 641-645.

92. Wick, D.A., et al., *Surveillance of the tumor mutanome by T cells during progression from primary to recurrent ovarian cancer.* Clin Cancer Res, 2014. **20**(5): p. 1125-34.

93. Linnemann, C., et al., *High-throughput epitope discovery reveals frequent recognition of neo-antigens by CD4+ T cells in human melanoma.* Nat Med, 2015. **21**(1): p. 81-85.

94. Kontani, K., et al., *Modulation of MUC1 mucin as an escape mechanism of breast cancer cells from autologous cytotoxic T-lymphocytes.* Br J Cancer, 2001. **84**(9): p. 1258-64.

95. Campoli, M. and S. Ferrone, *HLA antigen changes in malignant cells: epigenetic mechanisms and biologic significance.* Oncogene, 2008. **27**(45): p. 5869-5885.

96. Hinrichs, C.S. and N.P. Restifo, *Reassessing target antigens for adoptive T cell therapy.* Nature biotechnology, 2013. **31**(11): p. 999-1008.

97. Soriano, C., et al., *Increased proteinase inhibitor-9 (PI-9) and reduced granzyme B in lung cancer: Mechanism for immune evasion?* Lung Cancer, 2012. **77**(1): p. 38-45.

98. Ray, M., et al., *Inhibition of Granzyme B by PI-9 protects prostate cancer cells from apoptosis.* The Prostate, 2012. **72**(8): p. 846-855.

99. Cunningham, T.D., X. Jiang, and D.J. Shapiro, *Expression of High Levels of Human Proteinase Inhibitor 9 Blocks Both Perforin/Granzyme and Fas/Fas Ligand-mediated Cytotoxicity.* Cellular immunology, 2007. **245**(1): p. 32-41.

100. Volkmann, M., et al., *Loss of CD95 expression is linked to most but not all p53 mutants in European hepatocellular carcinoma.* J Mol Med (Berl), 2001. **79**(10): p. 594-600.

101. Maeda, T., et al., *Fas gene mutation in the progression of adult T cell leukemia.* J Exp Med, 1999. **189**(7): p. 1063-71.

102. Pitti, R.M., et al., *Genomic amplification of a decoy receptor for Fas ligand in lung and colon cancer.* Nature, 1998. **396**(6712): p. 699-703.

103. Hoesel, B. and J.A. Schmid, *The complexity of NF-κB signaling in inflammation and cancer.* Molecular Cancer, 2013. **12**: p. 86-86.

104. Neri, A., et al., *B cell lymphoma-associated chromosomal translocation involves candidate oncogene lyt-10, homologous to NF-κB p50.* Cell, 1991. **67**(6): p. 1075-1087.

105. Courtois, G. and T.D. Gilmore, *Mutations in the NF-[kappa]B signaling pathway: implications for human disease.* Oncogene, 0000. **25**(51): p. 6831-6843.

106. Baud, V. and M. Karin, *Is NF-[kappa]B a good target for cancer therapy? Hopes and pitfalls.* Nat Rev Drug Discov, 2009. **8**(1): p. 33-40.

107. Ben-Neriah, Y. and M. Karin, *Inflammation meets cancer, with NF-[kappa]B as the matchmaker.* Nat Immunol, 2011. **12**(8): p. 715-723.

108. Karin, M. and A. Lin, *NF-kappaB at the crossroads of life and death.* Nat Immunol, 2002. **3**(3): p. 221-7.

109. Liu, J. and A. Lin, *Role of JNK activation in apoptosis: a double-edged sword.* Cell Res, 2005. **15**(1): p. 36-42.

110. Beg, A.A. and D. Baltimore, *An essential role for NF-kappaB in preventing TNF-alpha-induced cell death.* Science, 1996. **274**(5288): p. 782-4.

111. Yu, H., M. Kortylewski, and D. Pardoll, *Crosstalk between cancer and immune cells: role of STAT3 in the tumour microenvironment.* Nat Rev Immunol, 2007. **7**(1): p. 41-51.

112. Noh, K.H., et al., *Activation of Akt as a mechanism for tumor immune evasion.* Mol Ther, 2009. **17**(3): p. 439-47.

113. Kortylewski, M., et al., *Inhibiting Stat3 signaling in the hematopoietic system elicits multicomponent antitumor immunity.* Nat Med, 2005. **11**(12): p. 1314-21.

114. Xu, Q., et al., *Targeting Stat3 blocks both HIF-1 and VEGF expression induced by multiple oncogenic growth signaling pathways.* Oncogene, 2005. **24**(36): p. 5552-60.

115. Farkona, S., E.P. Diamandis, and I.M. Blasutig, *Cancer immunotherapy: the beginning of the end of cancer?* BMC Med, 2016. **14**: p. 73.

116. Fenoglio, D., et al., *Generation of more effective cancer vaccines.* Hum Vaccin Immunother, 2013. **9**(12): p. 2543-7.

117. Copier, J. and A. Dalgleish, *Whole-cell vaccines: A failure or a success waiting to happen?* Curr Opin Mol Ther, 2010. **12**(1): p. 14-20.

118. Palucka, K. and J. Banchereau, *Dendritic cell-based cancer therapeutic vaccines.* Immunity, 2013. **39**(1): p. 38-48.

119. Kantoff , P.W., et al., *Sipuleucel-T Immunotherapy for Castration-Resistant Prostate Cancer.* New England Journal of Medicine, 2010. **363**(5): p. 411-422.

120. Phan, G.Q. and S.A. Rosenberg, *Adoptive Cell Transfer for Patients With Metastatic Melanoma: The Potential and Promise of Cancer Immunotherapy.* Cancer Control, 2013. **20**(4): p. 289-297.

121. Hinrichs, C.S. and S.A. Rosenberg, *Exploiting the curative potential of adoptive T-cell therapy for cancer.* Immunological Reviews, 2014. **257**(1): p. 56-71.

122. Kochenderfer, J.N., et al., *Eradication of B-lineage cells and regression of lymphoma in a patient treated with autologous T cells genetically engineered to recognize CD19.* Blood, 2010. **116**(20): p. 4099-102.

123. Kakarla, S. and S. Gottschalk, *CAR T cells for solid tumors: armed and ready to go?* Cancer journal (Sudbury, Mass.), 2014. **20**(2): p. 151-155.

124. Grosso, J.F. and M.N. Jure-Kunkel, *CTLA-4 blockade in tumor models: an overview of preclinical and translational research.* Cancer Immunity, 2013. **13**: p. 5.

125. FS, H., et al., *Improved survival with ipilimumab in patients with metastatic melanoma.* N. Engl. J. Med., 2010. **363**: p. 711.

126. Shu, C.A. and N.A. Rizvi, *Into the Clinic With Nivolumab and Pembrolizumab.* Oncologist, 2016. **21**(5): p. 527-8.

127. Selby, M.J., et al., *Preclinical Development of Ipilimumab and Nivolumab Combination Immunotherapy: Mouse Tumor Models, In Vitro Functional Studies, and Cynomolgus Macaque Toxicology.* PLoS ONE, 2016. **11**(9): p. e0161779.

128. Quezada, S.A. and K.S. Peggs, *Exploiting CTLA-4, PD-1 and PD-L1 to reactivate the host immune response against cancer.* British Journal of Cancer, 2013. **108**(8): p. 1560-1565.

129. Topalian, S.L., et al., *Survival, durable tumor remission, and long-term safety in patients with advanced melanoma receiving nivolumab.* J Clin Oncol, 2014. **32**(10): p. 1020-30.

130. Sharma, P. and J.P. Allison, *Immune checkpoint targeting in cancer therapy: toward combination strategies with curative potential.* Cell, 2015. **161**(2): p. 205-14.

131. Curti, B.D., et al., *OX40 is a potent immune-stimulating target in late-stage cancer patients.* Cancer Res, 2013. **73**(24): p. 7189-98.

132. Bartkowiak, T. and M.A. Curran, *4-1BB Agonists: Multi-Potent Potentiators of Tumor Immunity.* Frontiers in Oncology, 2015. **5**: p. 117.

133. Hunter, T.B., et al., *An agonist antibody specific for CD40 induces dendritic cell maturation and promotes autologous anti-tumour T-cell responses in an in vitro mixed autologous tumour cell/lymph node cell model.* Scand J Immunol, 2007. **65**(5): p. 479-86.

134. Wolchok , J.D., et al., *Nivolumab plus Ipilimumab in Advanced Melanoma.* New England Journal of Medicine, 2013. **369**(2): p. 122-133.

135. Alexandrov, L.B., et al., *Signatures of mutational processes in human cancer.* Nature, 2013. **500**(7463): p. 415-421.

136. Schumacher, T.N. and R.D. Schreiber, *Neoantigens in cancer immunotherapy.* Science, 2015. **348**(6230): p. 69-74.

137. Liontos, M., et al., *DNA damage, tumor mutational load and their impact on immune responses against cancer.* Annals of Translational Medicine, 2016. **4**(14): p. 264.

138. Bailey, P., et al., *Exploiting the neoantigen landscape for immunotherapy of pancreatic ductal adenocarcinoma.* Sci Rep, 2016. **6**: p. 35848.

139. Kunk, P.R., et al., *From bench to bedside a comprehensive review of pancreatic cancer immunotherapy.* Journal for ImmunoTherapy of Cancer, 2016. **4**(1): p. 14.

140. Fridman, W.H., et al., *The immune contexture in human tumours: impact on clinical outcome.* Nat Rev Cancer, 2012. **12**.

141. Ino, Y., et al., *Immune cell infiltration as an indicator of the immune microenvironment of pancreatic cancer.* Br J Cancer, 2013. **108**.

142. Collins, M.A., et al., *Oncogenic Kras is required for both the initiation and maintenance of pancreatic cancer in mice.* J Clin Invest, 2012. **122**.

143. Royal, R.E., et al., *Phase 2 trial of single agent Ipilimumab (anti-CTLA-4) for locally advanced or metastatic pancreatic adenocarcinoma.* J Immunother, 2010. **33**(8): p. 828-33.

144. Jazirehi, A.R., A. Lim, and T. Dinh, *PD-1 inhibition and treatment of advanced melanoma-role of pembrolizumab.* American Journal of Cancer Research, 2016. **6**(10): p. 2117-2128.

145. Sharma, P., et al., *Primary, Adaptive, and Acquired Resistance to Cancer Immunotherapy.* Cell, 2017. **168**(4): p. 707-723.

146. Hugo, W., et al., *Genomic and Transcriptomic Features of Response to Anti-PD-1 Therapy in Metastatic Melanoma.* Cell, 2016. **165**(1): p. 35-44.

147. O'Donnell, J.S., M.J. Smyth, and M.W.L. Teng, *Acquired resistance to anti-PD1 therapy: checkmate to checkpoint blockade?* Genome Medicine, 2016. **8**: p. 111.

148. Ribas, A., et al., *Association of pembrolizumab with tumor response and survival among patients with advanced melanoma.* JAMA, 2016. **315**(15): p. 1600-1609.

149. Zaretsky, J.M., et al., *Mutations Associated with Acquired Resistance to PD-1 Blockade in Melanoma.* New England Journal of Medicine, 2016. **375**(9): p. 819-829.

150. Koyama, S., et al., *Adaptive resistance to therapeutic PD-1 blockade is associated with upregulation of alternative immune checkpoints.* Nature Communications, 2016. **7**: p. 10501.

151. Zhou, P., et al., *In vivo Discovery of Immunotherapy Targets in the Tumor Microenvironment.* Nature, 2014. **506**(7486): p. 52-57.

152. Khandelwal, N., et al., *A high-throughput RNAi screen for detection of immune-checkpoint molecules that mediate tumor resistance to cytotoxic T lymphocytes.* EMBO Mol Med, 2015. **7**(4): p. 450-63.

153. Hariharan, D., A. Saied, and H.M. Kocher, *Analysis of mortality rates for pancreatic cancer across the world.* HPB (Oxford), 2008. **10**(1): p. 58-62.

154. Paniccia, A., et al., *Immunotherapy for pancreatic ductal adenocarcinoma: an overview of clinical trials.* Chin J Cancer Res, 2015. **27**(4): p. 376-91.

155. Yang, J.C., et al., *Ipilimumab (anti-CTLA4 antibody) causes regression of metastatic renal cell cancer associated with enteritis and hypophysitis.* J Immunother, 2007. **30**(8): p. 825-30.

156. Slovin, S.F., et al., *Ipilimumab alone or in combination with radiotherapy in metastatic castration-resistant prostate cancer: results from an open-label, multicenter phase I/II study.* Ann Oncol, 2013. **24**(7): p. 1813-21.

157. Hodi, F.S., et al., *Ipilimumab plus sargramostim vs ipilimumab alone for treatment of metastatic melanoma: a randomized clinical trial.* JAMA, 2014. **312**(17): p. 1744-53.

158. Dudley, M.E., et al., *Generation of tumor-infiltrating lymphocyte cultures for use in adoptive transfer therapy for melanoma patients.* J Immunother, 2003. **26**(4): p. 332-42.

159. Crespo, J., et al., *T cell anergy, exhaustion, senescence, and stemness in the tumor microenvironment.* Curr Opin Immunol, 2013. **25**(2): p. 214-21.

160. Jiang, Y., Y. Li, and B. Zhu, *T-cell exhaustion in the tumor microenvironment.* Cell Death Dis, 2015. **6**: p. e1792.

161. Woo, S.R., et al., *Immune inhibitory molecules LAG-3 and PD-1 synergistically regulate T-cell function to promote tumoral immune escape.* Cancer Res, 2012. **72**(4): p. 917-27.

162. Fourcade, J., et al., *Upregulation of Tim-3 and PD-1 expression is associated with tumor antigen-specific CD8+ T cell dysfunction in melanoma patients.* J Exp Med, 2010. **207**(10): p. 2175-86.

163. Boutros, M. and J. Ahringer, *The art and design of genetic screens: RNA interference.* Nat Rev Genet, 2008. **9**(7): p. 554-66.

164. Ryu, K.-Y., et al., *The mouse polyubiquitin gene UbC is essential for fetal liver development, cell-cycle progression and stress tolerance.* The EMBO Journal, 2007. **26**(11): p. 2693-2706.

165. Liu, Q., et al., *Chk1 is an essential kinase that is regulated by Atr and required for the G(2)/M DNA damage checkpoint.* Genes & Development, 2000. **14**(12): p. 1448-1459.

166. van Vugt, M.A.T.M. and R.H. Medema, *Getting in and out of mitosis with Polo-like kinase-1.* 0000. **24**(17): p. 2844-2859.

167. Coutinho, P., et al., *Differential requirements for COPI transport during vertebrate early development.* Dev Cell, 2004. **7**(4): p. 547-58.

168. Gilsdorf, M., et al., *GenomeRNAi: a database for cell-based RNAi phenotypes. 2009 update.* Nucleic Acids Research, 2010. **38**(Database issue): p. D448-D452.

169. Zou, W., J.D. Wolchok, and L. Chen, *PD-L1 (B7-H1) and PD-1 pathway blockade for cancer therapy: Mechanisms, response biomarkers, and combinations.* Science Translational Medicine, 2016. **8**(328): p. 328rv4-328rv4.

170. Chen, H.Y., et al., *Galectin-3 negatively regulates TCR-mediated CD4+ T-cell activation at the immunological synapse.* Proc Natl Acad Sci U S A, 2009. **106**(34): p. 14496-501.

171. Hsu, D.K., H.Y. Chen, and F.T. Liu, *Galectin-3 regulates T-cell functions.* Immunol Rev, 2009. **230**(1): p. 114-27.

172. Slovin, S.F., et al., *Ipilimumab alone or in combination with radiotherapy in metastatic castration-resistant prostate cancer: results from an open-label, multicenter phase I/II study.* Annals of Oncology, 2013. **24**(7): p. 1813-1821.

173. Brahmer, J.R., et al., *Safety and Activity of Anti–PD-L1 Antibody in Patients with Advanced Cancer.* The New England journal of medicine, 2012. **366**(26): p. 2455-2465.

174. Topalian, S.L., et al., *Safety, Activity, and Immune Correlates of Anti–PD-1 Antibody in Cancer.* The New England journal of medicine, 2012. **366**(26): p. 2443-2454.

175. Cochaud, S., et al., *IL-17A is produced by breast cancer TILs and promotes chemoresistance and proliferation through ERK1/2.* Scientific Reports, 2013. **3**: p. 3456.

176. Kumar, S., et al., *Interleukin-1α Promotes Tumor Growth and Cachexia in MCF-7 Xenograft Model of Breast Cancer.* The American Journal of Pathology, 2003. **163**(6): p. 2531-2541.

177. Lewis, A.M., et al., *Interleukin-1 and cancer progression: the emerging role of interleukin-1 receptor antagonist as a novel therapeutic agent in cancer treatment.* J Transl Med, 2006. **4**: p. 48.

178. Ågerstam, H., et al., *Antibodies targeting human IL1RAP (IL1R3) show therapeutic effects in xenograft models of acute myeloid leukemia.* Proceedings of the National Academy of Sciences, 2015. **112**(34): p. 10786-10791.

179. Bellucci, R., et al., *Interferon-γ-induced activation of JAK1 and JAK2 suppresses tumor cell susceptibility to NK cells through upregulation of PD-L1 expression.* Oncoimmunology, 2015. **4**(6): p. e1008824.

180. Shin, G., et al., *GENT: gene expression database of normal and tumor tissues.* Cancer Inform, 2011. **10**: p. 149-57.

181. The, G.C., *The Genotype-Tissue Expression (GTEx) project.* Nature genetics, 2013. **45**(6): p. 580-585.

182. Rhodes, D.R., et al., *Oncomine 3.0: Genes, Pathways, and Networks in a Collection of 18,000 Cancer Gene Expression Profiles.* Neoplasia (New York, N.Y.), 2007. **9**(2): p. 166-180.

183. Uhlen, M., et al., *Towards a knowledge-based Human Protein Atlas.* Nat Biotechnol, 2010. **28**(12): p. 1248-50.

184. Roskoski, R., *A historical overview of protein kinases and their targeted small molecule inhibitors.* Pharmacological Research, 2015. **100**: p. 1-23.

185. Burkart, A.D., et al., *Ovastacin, a cortical granule protease, cleaves ZP2 in the zona pellucida to prevent polyspermy.* J Cell Biol, 2012. **197**(1): p. 37-44.

186. Poitras, P. and T.L. Peeters, *Motilin.* Curr Opin Endocrinol Diabetes Obes, 2008. **15**(1): p. 54-7.

187. Ma, Y., et al., *Prevalence of off-target effects in Drosophila RNA interference screens.* Nature, 2006. **443**(7109): p. 359-363.

188. Birmingham, A., et al., *3[prime] UTR seed matches, but not overall identity, are associated with RNAi off-targets.* Nat Meth, 2006. **3**(3): p. 199-204.

189. Charoenfuprasert, S., et al., *Identification of salt-inducible kinase 3 as a novel tumor antigen associated with tumorigenesis of ovarian cancer.* Oncogene, 2011. **30**(33): p. 3570-3584.

190. Chen, H., et al., *Salt-inducible kinase 3 is a novel mitotic regulator and a target for enhancing antimitotic therapeutic-mediated cell death.* Cell Death & Disease, 2014. **5**(4): p. e1177.

191. Sundberg, T.B., et al., *Small-molecule screening identifies inhibition of salt-inducible kinases as a therapeutic strategy to enhance immunoregulatory functions of dendritic cells.* Proceedings of the National Academy of Sciences of the United States of America, 2014. **111**(34): p. 12468-12473.

192. Topfer, K., et al., *Tumor evasion from T cell surveillance.* J Biomed Biotechnol, 2011. **2011**: p. 918471.

193. Vinay, D.S., et al., *Immune evasion in cancer: Mechanistic basis and therapeutic strategies.* Seminars in Cancer Biology, 2015. **35, Supplement**: p. S185-S198.

194. *Cytotoxic T lymphocyte granules are secretory lysosomes, containing both perforin and granzymes.* The Journal of Experimental Medicine, 1991. **173**(5): p. 1099-1109.

195. Liechtenstein, T., et al., *PD-L1/PD-1 Co-Stimulation, a Brake for T cell Activation and a T cell Differentiation Signal.* Journal of clinical & cellular immunology, 2012. **Suppl 12**: p. 006.

196. Karwacz, K., et al., *PD-L1 co-stimulation contributes to ligand-induced T cell receptor down-modulation on CD8(+) T cells.* EMBO Molecular Medicine, 2011. **3**(10): p. 581-592.

197. Smyth, M.J., et al., *Unlocking the secrets of cytotoxic granule proteins.* J Leukoc Biol, 2001. **70**(1): p. 18-29.

198. Groscurth, P. and L. Filgueira, *Killing Mechanisms of Cytotoxic T Lymphocytes.* Physiology, 1998. **13**(1): p. 17-21.

199. Prevost-Blondel, A., et al., *Crucial role of TNF-alpha in CD8 T cell-mediated elimination of 3LL-A9 Lewis lung carcinoma cells in vivo.* J Immunol, 2000. **164**(7): p. 3645-51.

200. Martinez-Losato, L., Anel, A., Pardo, J. , *How Do Cytotoxic Lymphocytes Kill Cancer Cells?*, in *Clin. Cancer Res.* 2015.

201. Ndebele, K., et al., *Tumor necrosis factor (TNF)-related apoptosis-inducing ligand (TRAIL) induced mitochondrial pathway to apoptosis and caspase activation is potentiated by phospholipid scramblase-3.* Apoptosis, 2008. **13**(7): p. 845-56.

202. Trapani, J.A. and M.J. Smyth, *Functional significance of the perforin/granzyme cell death pathway.* Nat Rev Immunol, 2002. **2**(10): p. 735-747.

203. van Horssen, R., T.L. Ten Hagen, and A.M. Eggermont, *TNF-alpha in cancer treatment: molecular insights, antitumor effects, and clinical utility.* Oncologist, 2006. **11**(4): p. 397-408.

204. Dace, D.S., P.W. Chen, and J.Y. Niederkorn, *CD8+ T cells circumvent immune privilege in the eye and mediate intraocular tumor rejection by a TNF-alpha-dependent mechanism.* J Immunol, 2007. **178**(10): p. 6115-22.

205. Poehlein, C.H., et al., *TNF plays an essential role in tumor regression after adoptive transfer of perforin/IFN-gamma double knockout effector T cells.* J Immunol, 2003. **170**(4): p. 2004-13.

206. Reissfelder, C., et al., *Tumor-specific cytotoxic T lymphocyte activity determines colorectal cancer patient prognosis.* J Clin Invest, 2015. **125**(2): p. 739-51.

207. Bertazza, L., Mocellin, S., *The Dual Role of Tumor Necrosis Factor (TNF) in Cancer Biology.* Curr. Med. Chem., 2010. **17**(29): p. 3337-3352.

208. Balkwill, F., *TNF-alpha in promotion and progression of cancer.* Cancer Metastasis Rev, 2006. **25**(3): p. 409-16.

209. Tse, B.W.C., K.F. Scott, and P.J. Russell, *Paradoxical Roles of Tumour Necrosis Factor-Alpha in Prostate Cancer Biology.* Prostate Cancer, 2012. **2012**: p. 8.

210. Faustman, D.L. and M. Davis, *TNF Receptor 2 and Disease: Autoimmunity and Regenerative Medicine.* Front Immunol, 2013. **4**: p. 478.

211. Lizcano, J.M., et al., *LKB1 is a master kinase that activates 13 kinases of the AMPK subfamily, including MARK/PAR-1.* EMBO J, 2004. **23**(4): p. 833-43.

212. Walkinshaw, D.R., et al., *The tumor suppressor kinase LKB1 activates the downstream kinases SIK2 and SIK3 to stimulate nuclear export of class IIa histone deacetylases.* J Biol Chem, 2013. **288**(13): p. 9345-62.

213. Wajant, H., K. Pfizenmaier, and P. Scheurich, *Tumor necrosis factor signaling.* Cell Death Differ, 0000. **10**(1): p. 45-65.

214. Wajant, H. and P. Scheurich, *TNFR1-induced activation of the classical NF-kappaB pathway.* FEBS J, 2011. **278**(6): p. 862-76.

215. Brenner, D., H. Blaser, and T.W. Mak, *Regulation of tumour necrosis factor signalling: live or let die.* Nat Rev Immunol, 2015. **15**(6): p. 362-374.

216. Tang, F., et al., *The absence of NF-kappaB-mediated inhibition of c-Jun N-terminal kinase activation contributes to tumor necrosis factor alpha-induced apoptosis.* Mol Cell Biol, 2002. **22**(24): p. 8571-9.

217. Tang, G., et al., *Inhibition of JNK activation through NF-kappaB target genes.* Nature, 2001. **414**(6861): p. 313-7.

218. Lin, A., *Activation of the JNK signaling pathway: breaking the brake on apoptosis.* Bioessays, 2003. **25**(1): p. 17-24.

219. Drabsch, Y., R.G. Robert, and T.J. Gonda, *MYB suppresses differentiation and apoptosis of human breast cancer cells.* Breast Cancer Research : BCR, 2010. **12**(4): p. R55-R55.

220. Vaillant, C., et al., *Serpine2/PN-1 Is Required for Proliferative Expansion of Pre-Neoplastic Lesions and Malignant Progression to Medulloblastoma.* PLoS ONE, 2015. **10**(4): p. e0124870.

221. Koizume, S. and Y. Miyagi, *Anti-apoptotic genes are synergistically activated in OVSAYO cells cultured under conditions of serum starvation and hypoxia.* Genomics Data, 2015. **5**: p. 129-131.

222. Choi, S., D.S. Lim, and J. Chung, *Feeding and Fasting Signals Converge on the LKB1-SIK3 Pathway to Regulate Lipid Metabolism in Drosophila.* PLoS Genet, 2015. **11**(5): p. e1005263.

223. Wang, B., et al., *A hormone-dependent module regulating energy balance.* Cell, 2011. **145**(4): p. 596-606.

224. Luan, B., et al., *Leptin-mediated increases in catecholamine signaling reduce adipose tissue inflammation via activation of macrophage HDAC4.* Cell Metab, 2014. **19**(6): p. 1058-65.

225. Page, D.B., et al., *Immune modulation in cancer with antibodies.* Annu Rev Med, 2014. **65**: p. 185-202.

226. Bu, X., K.M. Mahoney, and G.J. Freeman, *Learning from PD-1 Resistance: New Combination Strategies.* Trends in Molecular Medicine. **22**(6): p. 448-451.

227. McGranahan, N. and C. Swanton, *Biological and therapeutic impact of intratumor heterogeneity in cancer evolution.* Cancer Cell, 2015. **27**(1): p. 15-26.

228. Aglietta, M., et al., *A phase I dose escalation trial of tremelimumab (CP-675,206) in combination with gemcitabine in chemotherapy-naive patients with metastatic pancreatic cancer.* Ann Oncol, 2014. **25**(9): p. 1750-5.

229. Santoiemma, P.P. and D.J. Powell, Jr., *Tumor infiltrating lymphocytes in ovarian cancer.* Cancer Biol Ther, 2015. **16**(6): p. 807-20.

230. Rosenberg, S.A. and N.P. Restifo, *Adoptive cell transfer as personalized immunotherapy for human cancer.* Science, 2015. **348**(6230): p. 62-8.

231. Kalos, M. and Carl H. June, *Adoptive T Cell Transfer for Cancer Immunotherapy in the Era of Synthetic Biology.* Immunity. **39**(1): p. 49-60.

232. da Cunha, J.P.C., et al., *Bioinformatics construction of the human cell surfaceome.* Proceedings of the National Academy of Sciences of the United States of America, 2009. **106**(39): p. 16752-16757.

233. Bellucci, R., et al., *Interferon-gamma-induced activation of JAK1 and JAK2 suppresses tumor cell susceptibility to NK cells through upregulation of PD-L1 expression.* Oncoimmunology, 2015. **4**(6): p. e1008824.

234. Bellucci, R., et al., *Tyrosine kinase pathways modulate tumor susceptibility to natural killer cells.* J Clin Invest, 2012. **122**(7): p. 2369-83.

235. Kwilas, A.R., et al., *Immune consequences of tyrosine kinase inhibitors that synergize with cancer immunotherapy.* Cancer cell & microenvironment, 2015. **2**(1): p. e677.

236. Rivera, I.O., et al., *PD-L1/PD-1 Immunotherapy Modulates Effector T Cells Homeostasis and Function in Murine Pancreatic Cancer.* The Journal of Immunology, 2016. **196**(1 Supplement): p. 72.11-72.11.

237. Lewis-Wambi, J.S., et al., *Overexpression of CEACAM6 promotes migration and invasion of oestrogen deprived breast cancer cells.* European journal of cancer (Oxford, England : 1990), 2008. **44**(12): p. 1770-1779.

238. Duxbury, M.S., et al., *Overexpression of CEACAM6 promotes insulin-like growth factor I-induced pancreatic adenocarcinoma cellular invasiveness.* Oncogene, 2004. **23**(34): p. 5834-42.

239. Blumenthal, R.D., et al., *Expression patterns of CEACAM5 and CEACAM6 in primary and metastatic cancers.* BMC Cancer, 2007. **7**: p. 2-2.

240. Agerstam, H., et al., *IL1RAP antibodies block IL-1-induced expansion of candidate CML stem cells and mediate cell killing in xenograft models.* Blood, 2016. **128**(23): p. 2683-2693.

241. Apte, R.N., et al., *The involvement of IL-1 in tumorigenesis, tumor invasiveness, metastasis and tumor-host interactions.* Cancer Metastasis Rev, 2006. **25**(3): p. 387-408.

242. Sanmamed, M.F., et al., *Agonists of Co-stimulation in Cancer Immunotherapy Directed Against CD137, OX40, GITR, CD27, CD28, and ICOS.* Semin Oncol, 2015. **42**(4): p. 640-55.

243. Dembic, Z., *Chapter 7 - Cytokines of the Immune System: Chemokines*, in *The Cytokines of the Immune System*. 2015, Academic Press: Amsterdam. p. 241-262.

244. Dembic, Z., *Chapter 8 - Cytokines Important for Growth and/or Development of Cells of the Immune System*, in *The Cytokines of the Immune System*. 2015, Academic Press: Amsterdam. p. 263-281.

245. Landskron, G., et al., *Chronic inflammation and cytokines in the tumor microenvironment.* J Immunol Res, 2014. **2014**: p. 149185.

246. Šedý, J., V. Bekiaris, and C.F. Ware, *Tumor Necrosis Factor Superfamily in Innate Immunity and Inflammation.* Cold Spring Harbor perspectives in biology, 2014. **7**(4): p. a016279 10.1101/cshperspect.a016279.

247. Chittasupho, C., et al., *Autoimmune therapies targeting costimulation and emerging trends in multivalent therapeutics.* Therapeutic delivery, 2011. **2**(7): p. 873-889.

248. Gashaw, I., et al., *What makes a good drug target?* Drug Discovery Today, 2012. **17**: p. S24-S30.

249. Andreassi, J.L., et al., *Structure of the Ternary Complex of Phosphomevalonate Kinase — The Enzyme and its Family.* Biochemistry, 2009. **48**(27): p. 6461-6468.

250. Moutinho, M., M.J. Nunes, and E. Rodrigues, *The mevalonate pathway in neurons: It's not just about cholesterol.* Exp Cell Res, 2017.

251. Berul, C.I., et al., *DMPK dosage alterations result in atrioventricular conduction abnormalities in a mouse myotonic dystrophy model.* Journal of Clinical Investigation, 1999. **103**(4): p. R1-R7.

252. Fu, Y.H., et al., *Decreased Expression of Myotonin Protein-Kinase Messenger-Rna and Protein in Adult Form of Myotonic-Dystrophy.* Science, 1993. **260**(5105): p. 235-238.

253. Egner, U. and R.C. Hillig, *A structural biology view of target drugability.* Expert Opinion on Drug Discovery, 2008. **3**(4): p. 391-401.

254. Lazo, J.S. and E.R. Sharlow, *Drugging Undruggable Molecular Cancer Targets.* Annu Rev Pharmacol Toxicol, 2016. **56**: p. 23-40.

255. Echeverri, C.J., et al., *Minimizing the risk of reporting false positives in large-scale RNAi screens.* Nat Methods, 2006. **3**(10): p. 777-9.

256. Echeverri, C.J., et al., *Minimizing the risk of reporting false positives in large-scale RNAi screens.* Nature Methods, 2006. **3**(10): p. 777-779.

257. Sharma, S. and A. Rao, *RNAi screening: tips and techniques.* Nature immunology, 2009. **10**(8): p. 799-804.

258. Reynolds, A., et al., *Rational siRNA design for RNA interference.* Nat Biotech, 2004. **22**(3): p. 326-330.

259. Jackson, A.L. and P.S. Linsley, *Recognizing and avoiding siRNA off-target effects for target identification and therapeutic application.* Nat Rev Drug Discov, 2010. **9**(1): p. 57-67.

260. Du, W.Q., J.N. Zheng, and D.S. Pei, *The diverse oncogenic and tumor suppressor roles of salt-inducible kinase (SIK) in cancer.* Expert Opin Ther Targets, 2016. **20**(4): p. 477-85.

261. Wang, Z.N., et al., *Cloning of a novel kinase (SIK) of the SNF1/AMPK family from high salt diet-treated rat adrenal.* Febs Letters, 1999. **453**(1-2): p. 135-139.

262. Horike, N., et al., *Adipose-specific expression, phosphorylation of Ser794 in insulin receptor substrate-1, and activation in diabetic animals of salt-inducible kinase-2.* J Biol Chem, 2003. **278**(20): p. 18440-7.

263. Katoh, Y., et al., *Salt-inducible kinase (SIK) isoforms: their involvement in steroidogenesis and adipogenesis.* Mol Cell Endocrinol, 2004. **217**(1-2): p. 109-12.

264. Jaleel, M., et al., *The ubiquitin-associated domain of AMPK-related kinases regulates conformation and LKB1-mediated phosphorylation and activation.* Biochemical Journal, 2006. **394**(Pt 3): p. 545-555.

265. Mihaylova, M.M. and R.J. Shaw, *The AMP-activated protein kinase (AMPK) signaling pathway coordinates cell growth, autophagy, & metabolism.* Nature cell biology, 2011. **13**(9): p. 1016-1023.

266. Lin, X., et al., *Salt-inducible kinase is involved in the ACTH/cAMP-dependent protein kinase signaling in Y1 mouse adrenocortical tumor cells.* Mol Endocrinol, 2001. **15**(8): p. 1264-76.

267. Feldman, J.D., et al., *The salt-inducible kinase, SIK, is induced by depolarization in brain.* J Neurochem, 2000. **74**(6): p. 2227-38.

268. Ruiz, J.C., F.L. Conlon, and E.J. Robertson, *Identification of Novel Protein-Kinases Expressed in the Myocardium of the Developing Mouse Heart.* Mechanisms of Development, 1994. **48**(3): p. 153-164.

269. Uebi, T., et al., *Involvement of SIK3 in glucose and lipid homeostasis in mice.* PLoS One, 2012. **7**(5): p. e37803.

270. Wolber, L.E., et al., *Salt-inducible kinase 3, SIK3, is a new gene associated with hearing.* Human Molecular Genetics, 2014. **23**(23): p. 6407-6418.

271. Cheng, H., et al., *SIK1 couples LKB1 to p53-dependent anoikis and suppresses metastasis.* Science signaling, 2009. **2**(80): p. ra35-ra35.

272. Selvik, L.-K.M., et al., *Salt-Inducible Kinase 1 (SIK1) Is Induced by Gastrin and Inhibits Migration of Gastric Adenocarcinoma Cells.* PLoS ONE, 2014. **9**(11): p. e112485.

273. Ashour Ahmed, A., et al., *SIK2 is a centrosome kinase required for bipolar mitotic spindle formation that provides a potential target for therapy in ovarian cancer.* Cancer cell, 2010. **18**(2): p. 109-121.

274. Amin, N., et al., *LKB1 regulates polarity remodeling and adherens junction formation in the Drosophila eye.* Proc Natl Acad Sci U S A, 2009. **106**(22): p. 8941-6.

275. Guarino, M., *Epithelial-mesenchymal transition and tumour invasion.* Int J Biochem Cell Biol, 2007. **39**(12): p. 2153-60.

276. Wehr, M.C., *Salt-inducible kinases regulate growth through the Hippo signalling pathway in Drosophila.* 2013. **15**(1): p. 61-71.

277. Harvey, K.F., X. Zhang, and D.M. Thomas, *The Hippo pathway and human cancer.* Nat Rev Cancer, 2013. **13**(4): p. 246-257.

278. Halder, G. and R.L. Johnson, *Hippo signaling: growth control and beyond.* Development (Cambridge, England), 2011. **138**(1): p. 9-22.

279. von Manstein, V., et al., *Resistance of Cancer Cells to Targeted Therapies Through the Activation of Compensating Signaling Loops.* Current Signal Transduction Therapy, 2013. **8**(3): p. 193-202.

280. Kim, H., et al., *Direct Interaction of CD40 on Tumor Cells with CD40L on T Cells Increases the Proliferation of Tumor Cells by Enhancing TGF-β Production and Th17 Differentiation.* PLoS ONE, 2015. **10**(5): p. e0125742.

281. Kalliolias, G.D. and L.B. Ivashkiv, *TNF biology, pathogenic mechanisms and emerging therapeutic strategies.* Nat Rev Rheumatol, 2016. **12**(1): p. 49-62.

282. Wang, A.M., et al., *Molecular-Cloning of the Complementary-DNA for Human-Tumor Necrosis Factor.* Science, 1985. **228**(4696): p. 149-154.

283. Balkwill, F., *Tumour necrosis factor and cancer.* Nat Rev Cancer, 2009. **9**(5): p. 361-371.

284. Fajardo, L.F., et al., *Dual role of tumor necrosis factor-alpha in angiogenesis.* Am J Pathol, 1992. **140**(3): p. 539-44.

285. Watanabe, N., et al., *Toxic effect of tumor necrosis factor on tumor vasculature in mice.* Cancer Res, 1988. **48**(8): p. 2179-83.

286. Elinav, E., et al., *Inflammation-induced cancer: crosstalk between tumours, immune cells and microorganisms.* Nat Rev Cancer, 2013. **13**(11): p. 759-771.

287. Moore, R.J., et al., *Mice deficient in tumor necrosis factor-alpha are resistant to skin carcinogenesis.* Nat Med, 1999. **5**(7): p. 828-31.

288. Suganuma, M., et al., *Essential role of tumor necrosis factor alpha (TNF-alpha) in tumor promotion as revealed by TNF-alpha-deficient mice.* Cancer Research, 1999. **59**(18): p. 4516-4518.

289. Arnott, C.H., et al., *Expression of both TNF-alpha receptor subtypes is essential for optimal skin tumour development.* Oncogene, 2004. **23**(10): p. 1902-1910.

290. Popivanova, B.K., et al., *Blocking TNF-alpha in mice reduces colorectal carcinogenesis associated with chronic colitis.* J Clin Invest, 2008. **118**(2): p. 560-70.

291. Shalapour, S. and M. Karin, *Immunity, inflammation, and cancer: an eternal fight between good and evil.* J Clin Invest, 2015. **125**(9): p. 3347-55.

292. Li, J., et al., *TNF-α induces leukemic clonal evolution ex vivo in Fanconi anemia group C murine stem cells.* The Journal of Clinical Investigation, 2007. **117**(11): p. 3283-3295.

293. Yan, B., et al., *Tumor Necrosis Factor-α Is a Potent Endogenous Mutagen that Promotes Cellular Transformation.* Cancer Research, 2006. **66**(24): p. 11565-11570.

294. Komori, A., et al., *Tumor Necrosis Factor Acts as a Tumor Promoter in BALB/3T3 Cell Transformation.* Cancer Research, 1993. **53**(9): p. 1982-1985.

295. Leibovich, S.J., et al., *Macrophage-induced angiogenesis is mediated by tumour necrosis factor-[alpha].* Nature, 1987. **329**(6140): p. 630-632.

296. Sorokin, L., *The impact of the extracellular matrix on inflammation.* Nat Rev Immunol, 2010. **10**(10): p. 712-723.

297. Rossi, C.R., et al., *TNFalpha-based isolated perfusion for limb-threatening soft tissue sarcomas: state of the art and future trends.* J Immunother, 2003. **26**(4): p. 291-300.

298. Christoforidis, D., et al., *Isolated liver perfusion for non-resectable liver tumours: a review.* Eur J Surg Oncol, 2002. **28**(8): p. 875-90.

299. Madhusudan, S., et al., *Study of etanercept, a tumor necrosis factor-alpha inhibitor, in recurrent ovarian cancer.* J Clin Oncol, 2005. **23**(25): p. 5950-9.

300. Maisey, N., *Antitumor necrosis factor (TNF-a) antibodies in the treatment of renal cell cancer.* Cancer Investigation, 2007. **25**(7): p. 589-593.

301. Naude, P.J., et al., *Tumor necrosis factor receptor cross-talk.* FEBS J, 2011. **278**(6): p. 888-98.

302. Patel, K., et al., *The LKB1-salt-inducible kinase pathway functions as a key gluconeogenic suppressor in the liver.* Nat Commun, 2014. **5**: p. 4535.

303. Gan, R.Y. and H.B. Li, *Recent Progress on Liver Kinase B1 (LKB1): Expression, Regulation, Downstream Signaling and Cancer Suppressive Function.* Int J Mol Sci, 2014. **15**(9): p. 16698-718.

304. Lombardi, M.S., et al., *SIK inhibition in human myeloid cells modulates TLR and IL-1R signaling and induces an anti-inflammatory phenotype.* J Leukoc Biol, 2016. **99**(5): p. 711-21.

305. Pattison, M.J., et al., *TLR and TNF-R1 activation of the MKK3/MKK6–p38α axis in macrophages is mediated by TPL-2 kinase.* Biochemical Journal, 2016. **473**(18): p. 2845-2861.

306. Verstrepen, L., et al., *TLR-4, IL-1R and TNF-R signaling to NF-κB: variations on a common theme.* Cellular and Molecular Life Sciences, 2008. **65**(19): p. 2964-2978.

307. Rivas, M.A., et al., *TNFα acting on TNFR1 promotes breast cancer growth via p42/P44 MAPK, JNK, Akt and NF-κB-dependent pathways.* Experimental Cell Research, 2008. **314**(3): p. 509-529.

308. Battegay, E.J., et al., *TNF-alpha stimulation of fibroblast proliferation. Dependence on platelet-derived growth factor (PDGF) secretion and alteration of PDGF receptor expression.* J Immunol, 1995. **154**(11): p. 6040-7.

309. Jourdan, M., et al., *Tumor necrosis factor is a survival and proliferation factor for human myeloma cells.* European Cytokine Network, 1999. **10**(1): p. 65-70.

310. Ofengeim, D. and J. Yuan, *Regulation of RIP1 kinase signalling at the crossroads of inflammation and cell death.* Nat Rev Mol Cell Biol, 2013. **14**(11): p. 727-736.

311. McIlwain, D.R., T. Berger, and T.W. Mak, *Caspase functions in cell death and disease.* Cold Spring Harb Perspect Biol, 2013. **5**(4): p. a008656.

312. Säll, J., et al., *Salt-inducible kinase 2 and -3 are downregulated in adipose tissue from obese or insulin-resistant individuals: implications for insulin signalling and glucose uptake in human adipocytes.* Diabetologia, 2017. **60**(2): p. 314-323.

313. Bassel-Duby, R. and E.N. Olson, *Signaling pathways in skeletal muscle remodeling.* Annu Rev Biochem, 2006. **75**: p. 19-37.

314. Henriksson, E., et al., *SIK2 regulates CRTCs, HDAC4 and glucose uptake in adipocytes.* Journal of Cell Science, 2015. **128**(3): p. 472-486.

315. Chen, L.-f., et al., *Duration of Nuclear NF-κB Action Regulated by Reversible Acetylation.* Science, 2001. **293**(5535): p. 1653-1657.

316. Huang, B., et al., *Posttranslational modifications of NF-κB: another layer of regulation for NF-κB signaling pathway.* Cellular signalling, 2010. **22**(9): p. 1282-1290.

317. Chen, L.f., Y. Mu, and W.C. Greene, *Acetylation of RelA at discrete sites regulates distinct nuclear functions of NF-κB.* The EMBO Journal, 2002. **21**(23): p. 6539-6548.

318. Yong Kim, S., et al., *Salt-inducible kinases 1 and 3 negatively regulate Toll-like receptor 4-mediated signal.* Mol Endocrinol, 2013. **27**(11): p. 1958-68.

319. Sanosaka, M., et al., *Salt-inducible kinase 3 deficiency exacerbates lipopolysaccharide-induced endotoxin shock accompanied by increased levels of pro-inflammatory molecules in mice.* Immunology, 2015. **145**(2): p. 268-278.

320. Darling, N.J., et al., *Inhibition of SIK2 and SIK3 during differentiation enhances the anti-inflammatory phenotype of macrophages.* Biochemical Journal, 2017. **474**(4): p. 521-537.

321. Choi, S., W. Kim, and J. Chung, *Drosophila salt-inducible kinase (SIK) regulates starvation resistance through cAMP-response element-binding protein (CREB)-regulated transcription coactivator (CRTC).* J Biol Chem, 2011. **286**(4): p. 2658-64.

322. Clark, K., et al., *Phosphorylation of CRTC3 by the salt-inducible kinases controls the interconversion of classically activated and regulatory macrophages.* Proc Natl Acad Sci U S A, 2012. **109**(42): p. 16986-91.

323. Itoh, Y., et al., *Salt-inducible Kinase 3 Signaling Is Important for the Gluconeogenic Programs in Mouse Hepatocytes.* J Biol Chem, 2015. **290**(29): p. 17879-93.

324. Screaton, R.A., et al., *The CREB coactivator TORC2 functions as a calcium- and cAMP-sensitive coincidence detector.* Cell, 2004. **119**(1): p. 61-74.

325. Koo, S.H., et al., *The CREB coactivator TORC2 is a key regulator of fasting glucose metabolism.* Nature, 2005. **437**(7062): p. 1109-11.

326. Takemori, H., J. Kajimura, and M. Okamoto, *TORC-SIK cascade regulates CREB activity through the basic leucine zipper domain.* FEBS J, 2007. **274**(13): p. 3202-9.

327. Wen, A.Y., K.M. Sakamoto, and L.S. Miller, *The role of the transcription factor CREB in immune function.* J Immunol, 2010. **185**(11): p. 6413-9.

328. Ollivier, V., et al., *Elevated cyclic AMP inhibits NF-kappaB-mediated transcription in human monocytic cells and endothelial cells.* J Biol Chem, 1996. **271**(34): p. 20828-35.

329. Parry, G.C. and N. Mackman, *Role of cyclic AMP response element-binding protein in cyclic AMP inhibition of NF-kappaB-mediated transcription.* J Immunol, 1997. **159**(11): p. 5450-6.

330. GP, D., et al., *IFN unresponsiveness in LNCaP cells due to the lack of JAK1 gene expression.* Cancer Res., 2005. **65**: p. 3447.

331. Schonberg, K., et al., *JAK Inhibition Impairs NK Cell Function in Myeloproliferative Neoplasms.* Cancer Res, 2015. **75**(11): p. 2187-99.

332. Parampalli Yajnanarayana, S., et al., *JAK1/2 inhibition impairs T cell function in vitro and in patients with myeloproliferative neoplasms.* Br J Haematol, 2015. **169**(6): p. 824-33.

333. Kwilas, A.R., et al., *Dual effects of a targeted small-molecule inhibitor (cabozantinib) on immune-mediated killing of tumor cells and immune tumor microenvironment permissiveness when combined with a cancer vaccine.* Journal of Translational Medicine, 2014. **12**: p. 294.

334. Sundberg, T.B., et al., *Development of Chemical Probes for Investigation of Salt-Inducible Kinase Function in Vivo.* ACS Chem Biol, 2016. **11**(8): p. 2105-11.

335. MacKenzie, K.F., et al., *PGE-2 Induces Macrophage IL-10 Production and a Regulatory-like Phenotype via a Protein Kinase A–SIK–CRTC3 Pathway.* The Journal of Immunology, 2013. **190**(2): p. 565-577.

336. Niino, D., et al., *Ratio of M2 macrophage expression is closely associated with poor prognosis for Angioimmunoblastic T-cell lymphoma (AITL).* Pathol Int, 2010. **60**(4): p. 278-83.

337. Nabeshima, A., et al., *Tumour-associated macrophages correlate with poor prognosis in myxoid liposarcoma and promote cell motility and invasion via the HB-EGF-EGFR-PI3K/Akt pathways.* British Journal of Cancer, 2015. **112**(3): p. 547-555.

338. Boutros, M., L.P. Brás, and W. Huber, *Analysis of cell-based RNAi screens.* Genome Biology, 2006. **7**(7): p. R66-R66.

339. Gilbert, D.F., et al., *A novel multiplex cell viability assay for high-throughput RNAi screening.* PLoS One, 2011. **6**(12): p. e28338.

8. Abbreviations and Definitions

%	Percentage	CCR2	C-C chemokine receptor type 2
°C	Degree celsius	CCR9	C-C chemokine receptor type 9
µg	microgram	CD	Cluster of differentiation
µm	micrometer	CDC42BPA	CDC42 binding protein kinase alpha
4-1BB	TNFRSF9	cDNA	complementary DNA
^{51}Cr	Radioactive Chromium isotope 51	CEACAM6	Carcinoembryonic antigen related cell adhesion molecule 6
AB	Human serum type AB	c-FLIP	Caspase-like apoptosis regulatory protein
ACT	Adoptive cell transfer	CHK1	checkpoint kinase 1
AIDS	Acquired immunodeficiency syndrome	CLM	Complete lymphocyte medium
AKT	Protein kinase B	cm	millimeters
AMP	Adenosine Monophosphate	CMM	Complete melanoma medium
AMPK	AMP-activated protein kinases	CO2	Carbon dioxide
APC	Antigen presenting cell	COPB2	coatomer protein complex subunit beta 2
ASTL	Astacin-like metallo-endopeptidase	CRC	Colorectal cancer
ATCC	American type culture collection	CRD	Cysteine-rich domains
BCL-2	B-cell lymphoma-2	CREB	cAMP response element-binding protein
BCL-xL	B-cell lymphoma-extra large	c-Src	C-Src Tyrosine Kinase
BD	Becton Dickinson	CTG	CellTiter-Glo
bp	Base pair	CTL	Cytotoxic T lymphocyte
BSA	Bovine serum albumin	CTLA-4	Cytotoxic T lymphocyte antigen 4
Ca2+	Calcium	CTRC	CREB-regulated transcription coactivators
CAR	Chimeric antigen receptors	CXCL9	C-X-C chemokine ligand 9

CCL3	C-C chemokine ligand 3	DC	Dendritic cell
DcR3	*Decoy receptor 3*	G418	Geneticin sulfate
DKFZ	German Cancer Research Center - Heidelberg	GENT	Gene expression database of normal and tumor tissues
DMEM	Dulbecco´s modified Eagle´s medium	GFP	Green fluorescent protein
DMPK	Myotonic dystrophy protein kinase	GITR	TNFRSF18
DNA	Deoxyribonucleic acid	GM-CSF	Granulocyte macrophage colony-stimulating factor
e.g.	Latin "exempli gratia" - "for example"	GPCR	G-protein coupled receptor
E:T	Effector to target ratio	GPR31	G-protein coupled receptor 31
EDTA	Ethylenediaminetetraacetic acid	GTEx	the portal for the genotype-tissue expression
ELISA	Enzyme-linked Immunosorbent Assay	GVAX	GM-CSF-transduced autologous tumor cell vaccine
EMT	Epithelial-mesenchymal transition	h	hours
ERK1/2	extracellular signal-regulated kinases 1 and 2	HDAC4	Histone deacetylase 4
et al.	Latin "et ali" - "and others"	HEPES	4-(2-hydroxyethyl)-1-piperazineethanesulfonic acid
FACS	Fluorescence-activated cell sorting	HIV	Human immunodeficiency virus
FAM195A	Family with sequence similarity 195, member A	HLA	Human leukocyte antigen
FAS	Fas cell surface death receptor/TNFRSF6	HRP	Horseradish peroxidase
FASL	Fas ligand	HSP	Heat shock protein
FAT1	Atypical cadherin 1	HT	High-throughput
FCS	Fetal calf serum	i.e.	Latin "id est"- "that is to say"
FITC	Fluoerescein	IBD	Inflammatory bowel disease
Fluc	Firefly luciferase	ICAM-1	Intracellular Adhesion Molecule 1
FluT	Flu-antigen specific CD8+ T cells	IDO	Indoleamine 2,3-dioxygenase
Foxo1	signaling and activating the forkhead Box O1	IgG	Immunoglobulin G
g	gram	IgSF	Immunoglobulin super family

IHC	Immunohistochemistry
IL	Interleukin
IL17RA	Interleukin 17 receptor A
IL1R	Interleukin 1 receptor
IL1RAP	Interleukin 1 receptor accessory protein
IL36G	Interleukin-36 gamma
IPRES	Innate anti-PD-1 resistance signature
ITIM	Tyrosine-based inhibitory motif
JAK	Janus kinase
JNK	C-Jun N-terminal protein kinase
kb	Kilobase
kd	Knockdown
kDA	Kilodalton
KO	Knockout
L	Liter
LAG-3	Lymphocyte activation gene 3
LIMK2	LIM domain kinase 2
LKB-1	Liver kinase B1
LPS	Lipopolysaccharide
luc	luciferase
M	molar
mA	Milliampere
mAb	Monoclonal antibody
MAPK	Mitogen-activated protein kinase
MAST3	Microtubule associated serine/threonine kinase 3
MDSC	Myeloid-derived suppressor cell
mg	Milligram
MHC-I	Class I major histocompatibility molecules
MHC-II	Class II major histocompatibility molecules
MIL	Marrow infiltrating lymphocyte
min	minutes
miRNA	micro RNA
mL	milliliter
MLN	Motilin
MM	Multiple Myeloma
mm	millimeter
mRNA	Messenger RNA
MS	Multiple sclerosis
MUC1	Mucin 1
MYB	Transcriptional Activator Myb
NEAA	Non-essential amino acid
NF-κB	Nuclear factor-kappa B
NK	Natural killer
NOD	Non-obese diabetic
ns	Not significant
NSG	NOD/SCID Il2rg$^{-/-}$ gamma
nt	Nucleotide
NTSR2	Neurotensin receptor 2

OKT-3	Muronomab-CD3	qPCR	Quantitative PCR
OX40	TNFRSF4	RA	Rheumatoid arthritis
p	Phosphorylation	Rb	Retinoblastoma-associated protein
P/S	Penicillin/Streptomycin	RCAS-1	Receptor-Binding Cancer Antigen Expressed On SiSo Cells
p38	p38 mitogen activated kinase	RCI	Regensburg Center for Interventional Immunology - Regensburg
p53	Tumor protein p53	REP	Rapid expansion protocol
p65	p65 subunit of the NF-κB complex	RET	Rearranged during transfection
PAGE	Polyacrylamide gel electrophoresis	rHu	Recombinant human
PANC-1-luc	Firefly Luciferase stably-expressing PANC-1 cells	RIPK1	Receptor interacting serine/threonine kinase 1
PBMC	Peripheral blood mononuclear cell	RNA	Ribonucleic acid
PBS	Phosphate buffer saline	RNAi	RNA interference
PCR	Polymerase chain reaction	RT	Room temperature
PD-1	Programmed death 1	SCID	Severe combined immunodeficient
PDAC	Pancreatic ductal adenocarcinoma	SDS	Sodium dodecyl sulfate
PD-L1	Programmed death ligand 1	sec	Seconds
PE	Phycoerythrin	SEM	Standard error of the mean
pH	Latin "poteintia hydrogenii"	SERPINE 2	Serpin Family E Member 2
PHA	Phytohaemagglutinin	SHP-2	SH2-domain containing tyrosine phosphatase 2
PI3K	Phosphatidylinositol-4,5-bisphosphate 3-kinase	shRNA	Short hairpin RNA
PI-9	Serpin family B member 9	siCD	"Cell Death" siRNA cocktail
PLK1	polo-like kinase 1	SIK1	Salt-inducible kinase 1
PMA	Phorbol 12-myristate 13-acetate	SIK2	Salt-inducible kinase 2
PMVK	Phosphomevalonate kinase	SIK3	Salt-inducible kinase 3
PO	Pacific orange	siRNA	small interfering RNA

SNH	Sucrose-nonfermenting-1 protein kinase homology
STAT	Signal transducer and activator of transcription
TAE	Tris-Acetate-EDTA
TAM	Tumor associated macrophage
TAP	Transporter associated with antigen processing
TBS	Tris buffer saline
TCR	T cell receptor
TCs	T cells
TGF-β	Transforming growth factor beta
Th	T helper
THD	TNF homology domain
TIGIT	T cell immunoreceptor with Ig and ITIM domains
TILs	Tumor infiltrating lymphocytes
TIM-3	T cell immunoglobulin mucin 3
TKI	Tyrosine kinase inhibitor
TLR4	Toll-like receptor 4
™	Trademark
TME	Tumor microenvironment
TNFR-I	TNF receptor 1
TNFR-II	TNF receptor 2
TNFRSF	TNF receptor superfamily members
TNF-α	Tumor necrosis factor - alpha
TPA	12-O-tetradecanoylphorbol 13-acetate
TRADD	TNFR-I-associated death domain protein
TRAF2	TNF receptor associated factor 2
TRAIL	TNF-related apoptosis inducing ligand
T_{reg}	Regulatory T cells
Trp	Tryptophan
TSAs	Tumor specific antigens
U	Unit
UBC	Ubiquitin C
UV	Ultraviolet
V	Volt
VEGF	vascular endothelial growth factor
VEGFR 2	Vascular endothelial growth factor receptor 2
VISTA	V-domain Ig suppressor of T cell activation
w/v	weight/volume
WB	Western blot
X	X-fold
XIAP	X-linked inhibitor of apoptosis
α	Alpha
β	Beta
β2m	β-2 microglobulin
γ	Gamma
κ	Kappa
π	Pi